UNIVERSIDADE DE LISBOA
FACULDADE DE CIÊNCIAS
DEPARTAMENTO DE BIOLOGIA

Unveiling the role of *Burkholderia cepacia* complex small RNAs in extracellular vesicles on host-pathogen interactions

Vera Côrte-Real de Landerset da Costa Esteves

Mestrado em Microbiologia Aplicada

Dissertação orientada por:
Prof. Jorge Leitão
Prof. Mónica Cunha

2025

This Dissertation was fully performed at the Institute for Bioengineering and Biosciences of Instituto Superior Técnico under the direct co-supervision of Professor Jorge Leitão.

Professor Mónica Cunha was the internal supervisor designated in the scope of the Master's in Applied Microbiology of the Faculty of Sciences of the University of Lisbon

Acknowledgements

I would like to express my deepest gratitude to my dissertation supervisors for their guidance and support, which were essential for the completion of this work. I wish to especially thank Professor Joana Feliciano, who accompanied me throughout the entire duration of this project and whose advice and patience provided great encouragement and helped in strengthening my skills.

Abstract

The *Burkholderia cepacia* complex (Bcc) comprises a group of opportunistic bacteria known to cause life-threatening respiratory infections in cystic fibrosis (CF) patients. These pathogens exhibit high intrinsic resistance to antibiotics and possess multiple virulence factors, making infections particularly difficult to treat and their clinical outcomes highly unpredictable. To support the development of novel therapeutic strategies, further investigation into the molecular mechanisms underlying host-pathogen interactions is needed. This project addresses that need by focusing on the extracellular vesicles (EVs) produced by Bcc bacteria and the small non-coding RNAs (sRNAs) they carry. In other bacterial pathogens, EV-associated sRNAs have been shown to act as post-transcriptional regulators of gene expression with the capacity to modulate host innate immune responses and promote infection. To emulate clinically relevant conditions, optimal parameters for EV production under antibiotic-induced stress were first studied. Bioinformatic analyses were conducted to predict potential human gene targets of sRNAs identified in previous studies. Two small RNAs were selected, nc5U55 and RIT17b, which have been previously found to be expressed during biofilm formation and *B. cenocepacia* infection of *Caenorhabditis elegans*. Each sRNA was then overexpressed and analyzed through an assortment of phenotypic assays, selected based on potential target predictions in *B. cenocepacia* using TargetRNA3 and CopraRNA. Additionally, the expression of BCAS0104 and BCAL0527, two genes involved in motility, was analyzed using RT-PCR. Overexpression of RIT17b resulted in increased biofilm formation, greater susceptibility to tetracycline and ciprofloxacin, reduced motility, and potentially increased virulence. On the other hand, overexpression of nc5U55 led to reduced growth in rich medium, but not in minimal medium, reduced swimming, and greater resistance to ciprofloxacin and tetracycline. These findings were evaluated with the aim of opening the path for future research.

Keywords

Small RNAs; Extracellular vesicles; Cystic fibrosis; *Burkholderia cepacia* complex.

Resumo

As bactérias oportunistas do complexo *Burkholderia cepacia* (Bcc), associadas a infeções respiratórias graves em doentes imunocomprometidos, particularmente em pacientes com fibrose quística, apresentam uma elevada resistência intrínseca a antibióticos e uma vasta gama de fatores de virulência. No âmbito da resistência a antibióticos, destacam-se fatores como alterações estruturais nos lipopolissacáridos (LPS) presentes na membrana externa, bombas de efluxo e a produção de β-lactamases. Adicionalmente, a capacidade de formação de biofilme em células epiteliais pulmonares contribui de forma significativa para a persistência da infeção.Por outro lado, relativamente a fatores de virulência, as bactérias deste complexo são capazes de secretar enzimas extracelulares que favorecem a adesão inicial e facilitam a invasão tecidular. Os sistemas de secreção bacterianos são também capazes de auxiliar na adesão e invasão das células hospedeiras, secretando enzimas com a habilidade de modular a resposta imune do hospedeiro e promover a sobrevivência do patógeno. Outros aspetos que contribuem para a virulência correspondem à presença de LPS, que podem desencadear uma resposta inflamatória exacerbada aos serem reconhecidos por recetores pertencentes ao sistema imunitário inato, e a capacidade de motilidade, que facilita a colonização de superfícies epiteliais. Estas características dificultam significativamente o tratamento administrado em situações de infeção e contribuem para a sua imprevisibilidade, visto que estas infeções poderão em certos casos evoluir para uma complicação patológica conhecida como síndrome de cepacia, uma manifestação mais grave de doença associada a um rápido declínio da função pulmonar, pneumonia necrosante e septicemia. Em contexto clínico, existe uma grande preocupação relativamente a transmissão entre pacientes, tendo sido implementadas medidas rigorosas de isolamento e prevenção. No entanto, a possibilidade de contaminação de produtos farmacêuticos e soluções hospitalares tem sido documentada e prevalece como um potencial risco de surto nestes contextos. Deste modo, é fundamental aprofundar o conhecimento sobre os mecanismos envolvidos na infeção do hospedeiro, de forma a apoiar o desenvolvimento de novas estratégias terapêuticas. Este projeto foi concebido com esse objetivo, focando-se especialmente no estudo das vesículas extracelulares (VEs) libertadas por estas bactérias e nos pequenos RNAs não codificantes (sRNAs) que transportam. Este estudo centrado nos sRNAs associados a VEs e na sua caracterização poderá contribuir para o desenvolvimento de vacinas, por exemplo. Abordagens terapêuticas existentes dirigidas ao RNA incluem a utilização de pequenas moléculas de modo a inibir tradução bacteriana e estratégias de edição genética baseadas em CRISPR. Estas vesículas extracelulares representam uma estratégia de estrema relevância para a entrega de sRNAs às células hospedeiras. Noutros organismos patogénicos, estes sRNAs têm sido descritos como importantes reguladores pós-transcricionais da expressão génica, com potencial para modular a resposta imunitária do hospedeiro e facilitar o estabelecimento da infeção. Em relação aos sRNAs produzidos pelas bactérias pertencentes a este complexo, apenas uma pequena percentagem se encontra funcionalmente caracterizada, tendo sido demonstrada a sua capacidade de regular uma variedade de processos, incluindo vias metabólicas, com potencial impacto no crescimento bacteriano, formação de biofilme, vias de resposta ao stress, motilidade e virulência. De forma a emular circunstâncias clinicamente relevantes, foram primeiro investigadas as melhores condições para a produção de VEs em *B. cenocepacia* K56-2 induzidas por stress antibiótico. Para tal, foi realizada uma comparação entre concentrações equivalentes de ciprofloxacina, tobramicina, ceftazidima e trimetoprim relativamente às concentrações mínimas inibitórias (CIM) calculadas para os meios LB e SCFM-FeZn pH=5.5. Em particular, SCFM-FeZn corresponde a um meio desenvolvido de modo a simular o escarro produzido por pacientes com fibrose quística, representando desta forma uma estratégia direcionada à análise de condições mais semelhantes às observadas em ambiente clínico. Com base nos resultados, onde não foram observadas diferenças significativas entre os dois meios em relação à produção de VEs, LB foi identificado como o meio indicado para os ensaios seguintes tendo em conta os objetivos do projeto. Uma segunda ronda de

produção e quantificação VEs foi realizada com um estudo adicional da curva de crescimento de *B. cenocepacia*. Esta investigação teve o objetivo de efetuar uma análise mais rigorosa para a identificação das condições de maior relevância clínica e biológica, representativas de uma resposta bacteriana ativa sem a ocorrência de uma lise celular acentuada, para a produção de vesículas extracelulares para o seu posterior isolamento e estudo do seu conteúdo. Consequentemente, 1 mg/L e 0.5 mg/L após 8 e 10 horas de crescimento, respetivamente, foram consideradas as concentrações de ciprofloxacina mais adequadas. Para tobramicina, 24 mg/L após 10 h de crescimento foi selecionada como a condição ideal para a produção de VEs originadas por stress antibiótico. Foi também realizada uma pesquisa através de abordagens bioinformáticas aos possíveis alvos no genoma humano de pequenos RNAs de *B. cenocepacia* identificados em estudos prévios. Posteriormente, os resultados obtidos foram avaliados com IntaRNA com o objetivo de analisar as interações RNA-RNA entre os pequenos RNAs e seus respetivos potenciais alvos. Com base no impacto previsto durante a infeção de acordo com os resultados relativamente aos seus potenciais alvos humanos e a interação prevista através de IntaRNA, bem como na sua presença em VEs em condições clinicamente relevantes, dois pequenos RNAs, nc5U55 e RIT17b, foram selecionados para uma análise mais detalhada. O sRNA nc5U55 tinha sido previamente identificado como estando expresso durante a formação de biofilme de *B. cenocepacia*, enquanto RIT17b tinha sido previamente descrito como expresso em condições de infeção no modelo *Caenorhabditis elegans*. Relativamente à previsão dos seus alvos humanos, DNMT3a, UNKL e BICRAL foram assinalados como os alvos de nc5U55 de maior relevância, possuindo os resultados significativos face às restantes interações avaliadas por IntaRNA. RIT17b, por sua vez, apresentou um número superior de alvos, do quais PLA2G4A e PPIA foram destacados devido ao seu papel na resposta imunitária. Consequentemente, cada sRNA foi sobre-expressado e analisado para determinar como sua a sobre-expressão poderia influenciar a fisiologia bacteriana. Esta análise foi realizada de forma a obter informações preliminares sobre a potencial função destes sRNAs nas interações hospedeiro-patógeno. Foi adicionalmente realizada a previsão bioinformática dos potenciais alvos de nc5U55 e RIT17b em *B. cenocepacia* K56-2 utilizando TargetRNA3 e CopraRNA. Com base nos alvos putativos resultantes e na sua relevância funcional, foi efetuada uma variedade de ensaios fenotípicos, incluindo curvas de crescimento em meio rico (LB) e meio mínimo (M9), quantificação relativa das VEs produzidas, ensaios de biofilme, de motilidade e de virulência em *C. elegans*, e a determinação da CIM relativamente a três antibióticos: ciprofloxacina, ceftazidima e tetraciclina. Adicionalmente, a expressão de BCAS0104 e BCAL0527, dois genes envolvidos na motilidade, foi analisada através de RT-PCR. A sobre-expressão de RIT17b resultou no aumento da formação de biofilme, possivelmente levou a uma maior suscetibilidade em relação à tetraciclina e à ciprofloxacina, a uma menor motilidade e a um potencial aumento da virulência. Por outro lado, a sobre-expressão de nc5U55 culminou num crescimento reduzido em meio rico, mas não em meio mínimo, possivelmente num swimming reduzido, e resultou numa maior resistência à ciprofloxacina e à tetraciclina. Estes resultados foram avaliados com o objetivo de fornecer os fundamentos necessários para futuros projetos de investigação. Desta forma, foi proposto que nc5U55 poderia impactar o crescimento bacteriano quando sobre-expresso por regular genes envolvidos em determinadas vias metabólicas, podendo adicionalmente desempenhar um papel na resposta ao stress e na resistência a antibióticos. No caso de RIT17b, foi proposto que este pequeno RNA estaria envolvido na regulação das fases iniciais da formação de biofilme, particularmente durante a adesão inicial e durante a fase de transição para a formação de microcolónias, explicando deste modo a maior suscetibilidade a certos antibióticos.

Palavras-chave

Pequenos RNAs; Vesículas extracelulares; Fibrose quística; Complexo *Burkholderia cepacia*.

List of Figures

List of Tables

List of Supplementary Tables

List of Abbreviations

ABC – ATP-binding Cassette
AHL – Acyl homoserine lactones
ARA – Arachidonic acid
ATP – Adenosine triphosphate
BDSF – *Burkholderia* diffusible signal factor
Bcc – *Burkholderia cepacia* complex
CAZ – Ceftazidime
CF – Cystic Fibrosis
CFTR – Cystic Fibrosis transmembrane conductance regulator
CFU – Colony forming unit
CIP – Ciprofloxacin
CLSI – Clinical and Laboratory Standards Institute
Cif – CFTR inhibitory factor
DD – Disk diffusion
DEPC – Diethyl pyrocarbonate
DNA – Deoxyribonucleic acid
EMSA – Electrophoretic mobility shift assay
EOMVs – Explosive outer mebrane vesicles
EPS – Exopolysaccharides
ESCMID – European Society of Clinical Microbiology and Infectious Diseases
EUCAST – European Committee on Antimicrobial Susceptibility Testing
EVs – Extracellular vesicles
GTP – Guanosine triphosphate
HBE – Human Bronchial Epithelial
HSL – Hexanoyl-homoserine lactone
Hif – Hypoxia-inducible factor
IGR – Intergenic regions
IL – Interleukin
IM – Inner Membrane
INF – Interferon
ISEV – International Society for Extracellular Vesicles
L-Ara4N – 4-Amino-4-deoxy-L-arabinose
LB – Lysogeny broth
LPS – Lipopolysaccharide
Lpp – Lipoproteins
MAPK – Mitogen-activated protein kinase
MATE – Multidrug and toxic compound extrusion family
MFS – Major facilitator superfamily
MHB/MHA – Mueller-Hinton broth/A
MIC – Minimum inhibitory concentration
MMPs – Matrix metalloproteinases
NADPH – Nicotinamide adenine di-nucelotide phosphate
NOD – Nucleotide-binding oligomerization domain
NTA – Nanoparticle tracking analysis
OD – Optical density
OIMVs – Outer inner membrane vesicles

OM – Outer Membrane
OMPs – Outer membrane proteins
ORF - Open reading frame
OS – Oligosaccharides
PAMPs – Pathogen-associated molecular patterns
PBPs – Penicillin-binding proteins
PCR – Polymerase Chain Reaction
PIP2/PIP3 – Phosphatidylinositol(4,5)bisphosphate/Phosphatidylinositol(3,4,5)trisphosphate
PLG – Phase lock gel
PQS – Pseudomonas quinolone signal
PaAP – P. aeruginosa aminopeptidase
QRDR – Quinolone resistance-determining region
QS – Quorum sensing
RISC – RNA-induced silencing complex
RNA – Ribonucleic acid
RNAP – RNA polymerase
RND – Resistance nodulation division family
ROS – Reactive Oxygen Species
RT-qPCR – Real-time quantitive PCR
SCFM – Synthetic cystic fibrosis medium
SD – Standard deviation
SMR – Small multidrug resistance family
Sp1 – Specificity protein 1
T3SS- Type III Secretion system
TA – Toxin-antitoxin
TCA – Tricarboxylic acid
TCS – Two-component system
TEM – Transmission electron microscopy
TET – Tetracycline
TGF – Transforming growth factor
TLR – Toll-like receptor~
TNF – Tumor necrosis factor
TOB – Tobramycin
TP – Trimethoprim
WASP - Neural Wiskott-Aldrich Syndrome protein
c-di-GMP – Cyclic diguanosine monophosphate
cDNA – Complementary DNA
mRNAs – Messenger RNAs
miRNAs – Micro RNAs
sRNAs – Small non-coding RNAs
tRNA – Transfer RNA

1. Introduction

1.1 *Burkholderia cepacia* complex characteristics, epidemiology and treatment

Burkholderia cepacia complex (Bcc) is a group composed of at least 26 species of opportunistic aerobic, non-glucose fermenting, closely related Gram-negative bacilli (Matos *et al.*, 2024) that was first discovered as the cause of onion skin rot. Before 1992 (Saeed *et al.*, 2024), these bacteria were erroneously classified under the *Pseudomonas* genus and divided into different genomovars that are currently known as *Burkholderia cepacia* (genomovar I), *Burkholderia multivorans* (genomovar II), *Burkholderia cenocepacia* (genomovar III), *Burkholderia stabilis* (genomovar IV), *Burkholderia vietnamiensis* (genomovar V), *Burkholderia dolosa* (genomovar VI), *Burkholderia ambifaria* (genomovar VII), *Burkholderia anthina* (genomovar VIII), and *Burkholderia pyrrocinia* (genomovar IX) (Sfeir, 2018). All Bcc species are capable of colonizing and infecting immunocompromised individuals, with cystic fibrosis (CF) patients having been the target of great focus and research due to their notoriety as dangerous pathogens, especially in the 1980s and 1990s as a consequence of the numerous outbreaks that occurred in European and North American CF centers (Leitão *et al.*, 2017). This high risk of infection is related to the underlying pathophysiology of CF, an autosomal recessive disease caused by a mutation in the cystic fibrosis transmembrane conductance regulator (CFTR) gene. The CFTR gene, which encodes an epithelial chloride ion channel present in many tissues, can be affected by over two thousand mutations, leading to a loss of function in chloride transport. This results in an impaired secretory activity in organs such as the lungs, causing the dehydration of the airway epithelium due to the accumulation of chloride ions. The retention of excess mucus in the airways is hazardous, contributing significantly to the chronic lower airway infections that afflict CF patients and lead to a decline in lung function (Scoffone *et al*., 2017; Lord *et al*., 2020). In addition to this favorable environment for bacterial infection, Bcc possess the advantage of a wide range of virulence factors, the innate resistance to a variety of antibiotics, easy transmission as a result of direct and indirect contact between patients, as well as unpredictable clinical manifestations of the infection, all contributing to the difficulty in Bcc infection treatment (Leitão *et al*., 2017; Sfeir, 2018). *B. cenocepacia* and *B. multivorans* are the most commonly found Bcc species in infected CF patients. In particular, the genome of the *B. cenocepacia* J2315 strain was the first to become publicly available and is used as reference by most researchers in post-genomics studies (Matos *et al.*, 2024). *B. cenocepacia* J2315 possesses a large genome of approximately 8 Mb comprised of multiple replicons: chromosome 1 (3.87 Mb), featuring most housekeeping genes, chromosome 2 (3.22 Mb), megaplasmid pC3 (0.88 Mb), and plasmid pBCJ2315 (92 kb) (Holden *et al.*, 2008).

Regarding Bcc's epidemiological status, the prevalence of infections has been greatly reduced since the 1990s due to the implementation of segregation measures as well as the development of new therapies. Notably, outbreaks in CF centers were mainly caused by *B. cenocepacia* strains such as the ET12 and PHDC lineages. The limitations on person-to-person transmission brought on by the adoption of prevention strategies led to a decrease in occurrences of such dominant strains, and are likely linked to the emergence of infections caused by non-epidemic *B. cenocepacia* strains or non-clonal strains of other Bcc species besides *B. cenocepacia*, possibly arising from different environmental sources or reservoirs (Scoffone *et al*., 2017; Sousa *et al.*, 2017). In particular, nosocomial Bcc infections tend to be caused by the contamination of drug products like intravenous fluids and even medical devices (Saeed *et al*., 2024). Presently, no standard treatment strategy has been established for Bcc infection, with different therapies being administered on a case-by-case basis. This is due to a variety of factors such as the group's intrinsic antimicrobial resistance, the poor correlation of *in vitro* susceptibility data with clinical results, the absence of randomized controlled trials and the notable clinical variability of

infection, with cases ranging from asymptomatic to a life-threatening manifestation of disease known as cepacia syndrome, characterized by necrotizing pneumonia and septicemia (Scoffone *et al*., 2017; Pita *et al*., 2023). Antibiotic selection and combined therapies must take into account drug interactions and mechanisms of action, as well as length of treatment due to possible allergic reactions, risk of toxicity, blood dyscrasias, or other side effects (Lord *et al*., 2020). Current treatments have been reported to use trimethoprim-sulfamethoxazole, ceftazidime, carbapenems such as meropenem and doripenem, doxycycline, minocycline, among other antibiotics (Sfeir, 2018). Briefly, trimethoprim-sulfamethoxazole and ceftazidime's mechanisms of action are, respectively, the inhibition of bacterial synthesis of tetrahydrofolic acid (Masters *et al*., 2003), and the inhibition of cell wall synthesis (Rains et al., 1995). Although not first-in-line agents for Bcc infection treatment, both ciprofloxacin, which disrupts DNA replication by inhibiting DNA gyrase (Sanders, 1988), and tobramycin, an aminoglycoside that inhibits protein synthesis by binding to the 30S subunit of the bacterial ribosome, are frequently administered antimicrobials with antipseudomonal action for CF therapy (Schwarz *et al.*, 2022; Millar *et al.*, 2020), and have also been considered in this study.

1.2 Antimicrobial resistance of the *Burkholderia cepacia* complex

Bcc have been reported to be innately resistant to fosfomycin, polymyxins like polymyxin B and colistin, aminoglycosides, β-lactams such as amoxicillin, ampicillin, sulbactam, ticarcillin, ertapenem and piperacillin, among others (Saeed *et al.*, 2024). Many processes that confer antimicrobial resistance are at play. Gram-negative bacterial envelopes consist of a fluid phospholipid bilayer that functions as a site for energy generation and the biosynthesis of various cellular components named inner membrane (IM), the periplasm, an intermediate compartment rich in proteins that includes a thin peptidoglycan layer, and an outer membrane (OM). The OM is known to be the first line of defense against bactericidal agents (Rhodes & Schweizer, 2016), being composed of an inner leaflet containing phospholipids and an outer layer mainly constituted of lipopolysaccharides (LPS). LPS composition includes phosphorylated N-acetyl glucosamine dimeric structures bound to multiple fatty acids (lipid A) connected to core oligosaccharides (OS), with the outermost portion of the LPS being a long polysaccharide chain of repeating oligosaccharide subunits that are notably variable between different Gram-negative bacteria species called O-antigen. Proteins anchored to the OM can be mostly divided into β-barrel proteins named outer membrane proteins (OMPs) and lipoproteins (Lpp) (Kim *et al.*, 2020; Furuyama & Sircili, 2021). In response to the presence of antibiotics, LPS might suffer alterations to promote bacterial survival such as the addition of 4-amino-4-deoxy-L-arabinose (L-Ara4N), a modification that leads to a reduction in the negative charge of lipid A and a decrease in membrane permeability. The fact that in Bcc L-Ara4N is a major component of lipid A and OS is considered to be an effective contributor to its intrinsic resistance against polymyxin B, a cationic antibiotic. However, it is not considered its sole determinant (Scoffone *et al*., 2017). The alternative sigma factor RpoE, a regulator to a group of genes that encode proteins involved in extracytoplasmic stress response, is also an important factor. RpoE is hypothesized to additionally regulate *mucD*, which encodes a periplasmic protein that promotes resistance as well, though there is still no direct evidence confirming this. Furthermore, the zinc metalloproteases ZmpA and ZmpB of *B. cenocepacia* have been demonstrated to degrade antimicrobial peptides *in vitro*, yet most knock-out mutant strains revealed no increased sensitivity to the same agents (Loutet & Valvano, 2011). Kumar *et al.* (2016) assembled a pUC plasmid-based genomic expression library from *B. pseudomallei* sp. A191 and discovered five polymyxin E resistant clones, through which a two-component regulatory system responsible for the resistance was revealed, composed of a histidine kinase (*mrgS*) and its response regulator (*mrgR*). Another factor that contributes to a lower permeability of the cell envelope and thus is able to reduce antibiotic uptake by the bacterial cell are porin proteins like OmpF, OmpA, and OmpC (Rhodes & Schweizer, 2016). An

additional and important mechanism of antimicrobial resistance is efflux pump activity, strongly associated with acquired resistance of Bcc to β-lactams and aminoglycosides, as well as to quinolones, chloramphenicol and trimethoprim (Lord *et al*., 2020; Sfeir, 2018). Five families of transporters can participate in this process: the major facilitator superfamily (MFS), the ATP-binding cassette family (ABC), the small multidrug resistance family (SMR), the multidrug and toxic compound extrusion family (MATE), and lastly the resistance nodulation division family (RND), considered to be the clinically most significant (Scoffone *et al*., 2017). For instance, the RND-3 and RND-4 efflux systems contribute to the intrinsic resistance of *B. cenocepacia* J2315 to a variety of drugs, while RND-8 and RND-9 efflux systems were shown to be involved in biofilm tobramycin resistance (Buroni *et al.*, 2014). Certain Bcc strains may also possess inducible β-lactamases or dihydrofolate reductases (Lord *et al*., 2020). More precisely, in the *B. cenocepacia* J2315 genome there exist two class A (PenA and PenB) and one class D β-lactamases in chromosome 2, and one class C (AmpC), a broad-spectrum cephalosporinase, located in the megaplasmid pC3 (Holden *et al.*, 2008; Hwang & Kim, 2015), all three β-lactamase groups that have a serine active site. This is in great contrast to the *B. cenocepacia* LMG 16656 strain, in which it has been surmised that most β-lactamases are part of class B (metallo-β-lactamases) (Scoffone *et al*., 2017). Other *Burkholderia* spp. may present the Pen-like β-lactamases PenC–PenF, which share 63 to 92% identity with PenB (Poirel et al., 2008). Regarding β-lactamase inhibitors, the commercially available clavulanic acid, sulbactam and tazobactam seem to be effective against the majority of the class A group, while avibactam inhibits class C and some class D enzymes. Conversely, there are no known inhibitors that produce any effect on metallo-β-lactamases (Everaert & Coenye, 2016). Biofilm production on lung epithelial cells, with the formation of a matrix composed by exopolysaccharides (EPSs), LPS, proteins, and extracellular DNA, is another great contributor to bacterial survival in adverse environments, granting protection against the host's defenses and antibiotic activity (Sfeir, 2018; Gunardi *et al*., 2021). Persister cells may also promote the biofilm's survivability against antimicrobial agents with the downregulation of the TCA cycle and genes involved in the electron transport chain, avoiding oxidative damage due to the absence of Reactive Oxygen Species (ROS) production (Van Acker *et al.*, 2013). Bacterial persistence has been described to be regulated by an assortment of mechanisms, including the toxin-antitoxin (TA) systems, which have been shown to also inhibit cell growth and modulate processes like programmed cell death and biofilm formation (Sousa *et al.*, 2017). Furthermore, it has been revealed that, in response to unfavorable conditions like antibiotic exposure, whether *in vitro* or in the host's environment during infection, mutations can potentially accumulate in clonal lineages, increasing their antibiotic resistance (Scoffone *et al*., 2017). These mutations can impact drug targets like dihydrofolate reductases or the DNA gyrase, for example, granting resistance against trimethoprim and fluoroquinolones, respectively (Saeed *et al.*, 2024). The latter, particularly levofloxacin resistance, arises generally through mutations in the quinolone resistance-determining region (QRDR) of topoisomerase genes (Pope et al., 2007). Mutations can also reduce membrane permeability by affecting LPS structure or induce efflux pump overexpression (Nikaido & Pagès, 2011). Tseng *et al.* (2014) tested antibiotic-resistant clinical Bcc isolates for efflux pump activity and found the RND-3 efflux pump to be the most overexpressed of all RND transporters. Additionally, the mutation of BCAL1672, its regulator gene, was demonstrated to be statistically correlated with increased RND-3 expression, as well as resistance to chloramphenicol, meropenem, and levofloxacin.

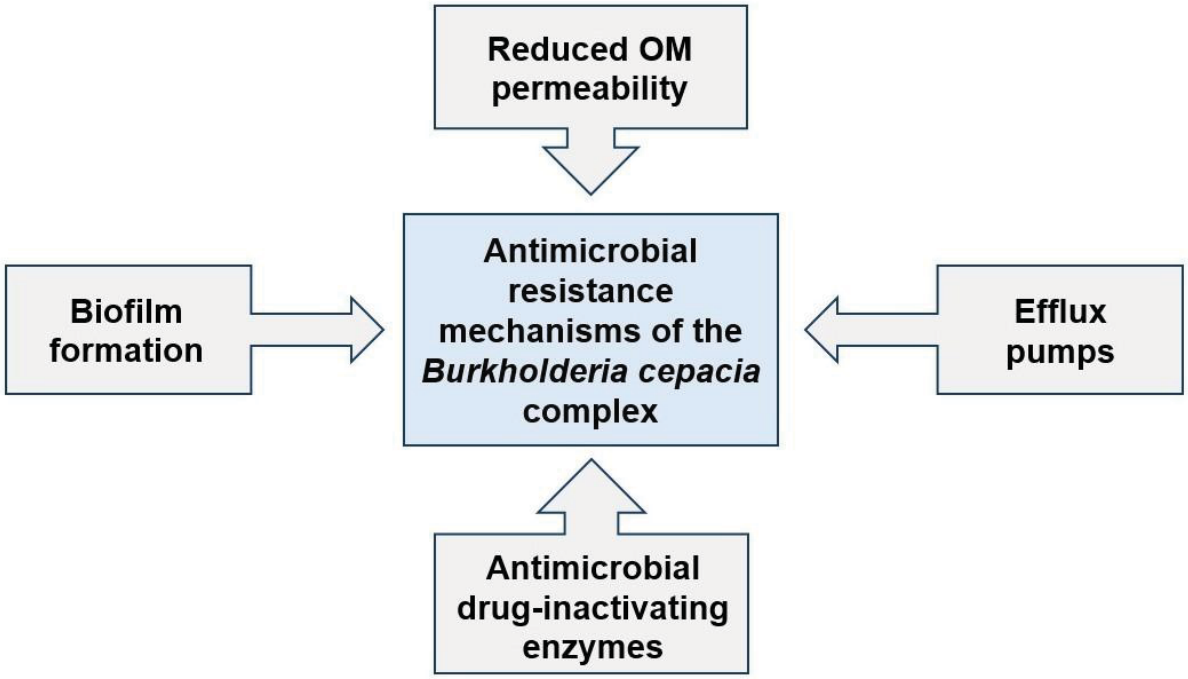

Figure 1.1: Some examples of antimicrobial resistance mechanisms found in Bcc bacteria.

There is still a considerable amount of antibiotics regarding which there is no conclusive confirmation of Bcc resistance due to inconsistent minimum inhibitory concentration (MIC) results and discrepancies between *in vitro* experimental data and clinical outcomes (Saeed *et al.*, 2024). Antibiotic susceptibility could be reduced by acidic pH and the presence of metal ions, two characteristics of CF sputum samples that are likely potentiated during infection and the consequent inflammatory response, indicating that the rich media often used in susceptibility testing might not be the most appropriate. Morales *et al.* (2023) have assessed this possibility via the use of a medium mimicking the acidic nutritional environment of CF (SCFM-FeZn), finding that, when compared with a rich medium, *B. cenocepacia* had an increased and faster growth in SCFM-FeZn and was less susceptible to many of the antibiotics that are typically used to treat Bcc infections.

1.3 Virulence factors of the *Burkholderia cepacia* complex

Although some remain poorly understood, there are many mechanisms through which Bcc bacteria are able to evade the host's immune response, enhance their survivability and aid in the colonization and establishment of infection. Enzymes secreted by Bcc are an essential contributor to the bacterium's invasion and adhesion to mucin and epithelial cells. For instance, the degradation of extracellular matrix components is mediated by serine proteases and metalloproteases, whereas lipases facilitate host invasion, although the exact molecular mechanisms underlying these processes remain unknown (Mullen *et al.*, 2007; Saeed *et al.*, 2024). Biofilm production was previously discussed as having a key role in the protection against the host's defenses and as an enabler of antibiotic resistance. Being part of the bacterial outer membrane, LPS are naturally included in biofilm composition. These can potentially cause a powerful immune reaction through the interaction between the lipid A part of its structure and certain receptor proteins of the host's innate immune system like Toll-like receptor 4, which would in turn lead to caspase-11 mediated cell death (Gunardi *et al.*, 2021). As another biofilm constituent, the EPS common to many Bcc species named cepacian has been shown to potentially aid in colonization by inhibiting neutrophil chemotaxis and ROS production *in vitro* (Suppiger *et al.*, 2013). At the moment, it has been established that quorum sensing (QS) is an important mechanism of cell-cell communication

involved in the regulation of biofilm formation. QS induction relies on the production and detection by specific receptors of signaling molecules named autoinducers that accumulate in the extracellular environment (Sousa *et al.*, 2017). Specifically, in Bcc strains the QS systems are primarily based on *N*-acyl homoserine lactones (AHLs) and BDSF (*Burkholderia* diffusible signal factor). Although AHL production tends to be strain-dependent, the CepIR QS system is conserved in all Bcc species. CepI produces mainly *N*-octanoyl-homoserine lactone (C8-HSL), an AHL that binds to CepR, which in turn positively regulates *cepI* and the *cciIR* operon that is present in many *B. cenocepacia* strains. CciI mostly synthesizes *N*-hexanoyl-homoserine lactone (C6-HSL), an AHL with high affinity for CciR, which negatively regulates *cepI* and *cepR2*, and its own expression. Confirmed to be in all known *B. cenocepacia* strains, CepR2, like CepR and CciR, is a homolog of the LuxR protein of *Vibrio fischeri*. However, unlike these other two transcriptional regulators, CepR2 is not associated with any LuxI-type inducer and can function independently of AHLs (Subramoni & Sokol, 2012). Meanwhile, the QS molecule BDSF (*cis*-2-dodecenoic acid) has been demonstrated to have antibiofilm activity via the modulation of gene expression, as observed for chitinase, a gene involved in biofilm formation (Gunardi *et al.*, 2021). BDSF is synthesized by $RpfF_{Bc}$, a homolog of the *Xanthomonas campestris* pv. *campestris* RpfF protein, and subsequently binds to the receptor protein RpfR. This binding induces an allosteric conformational change that activates RpfR's c-di-GMP phosphodiesterase activity. Consequently, degradation of cyclic diguanosine monophosphate (c-di-GMP), a second messenger that positively regulates biofilm formation, by RpfR explains the antibiofilm effects of BDSF during QS (Fazli *et al*., 2012). Besides the stated effects on biofilm formation, these QS systems have been linked, depending on the bacterial strain, to a variety of functions that promote bacterial virulence, including flagellar motility and the secretion and production of virulence factors, such as the metalloproteases ZmpA and ZmpB, siderophores, toxins, and antifungal agents (Subramoni & Sokol, 2012; Suppiger *et al.*, 2013). Similarly, signal transduction pathways composed by two-component systems (TCSs) are crucial in Bcc adaptation and pathogenesis. These systems consist of a histidine kinase that autophosphorylates in response to a signal, and a response regulator that, once phosphorylated by the histidine kinase, modulates the expression of specific target genes (Sousa *et al.*, 2017). Despite the fact that many of the approximately forty predicted TCSs in Bcc remain uncharacterized, the RqpSR system is known to induce the expression of AHLs and BDSF, implicating it in QS signaling (Schaefers, 2020). Another characterized TCS in Bcc is the EsaSR system, partly composed by the essential gene *esaR*, involved in efflux pump-related antibiotic resistance and potentially in maintaining cell envelope homeostasis (Gislason *et al.*, 2016). The oxygen-sensing FixLJ system has been identified as a global regulator of *B. dolosa* virulence and persistence in the murine pneumonia model, controlling genes related to motility and biofilm formation in response to low oxygen levels (Schaefers *et al.*, 2017). Furthermore, AtsRT has been analysed for its role in repressing QS and biofilm production, type VI-secretion system (T6SS) activity, and protease secretion (Khodai-Kalaki *et al.*, 2013). In addition to AtsRT, other hybrid TCSs such as CblTSR and BCAM0227 are involved in cable pilus gene regulation (Schaefers, 2020). The AtsRT-mediated T6SS role in Bcc pathogenesis comprises of disrupting certain immune cell processes, as is the case in *B. cepacia*-containing vacuoles by interfering with the actin cytoskeleton of macrophages and with the assembly of the reduced nicotinamide adenine di-nucelotide phosphate (NADPH) oxidase complex, along with intensifying the host's inflammatory response. This system might also potentiate T2SS activity, another important protein secretion system during infection due to its function in translocating ZmpA and ZmpB across the bacterial membrane. Lastly, both T3SS and T4SS have been presumed to contribute to the intracellular survival of *B. cenocepacia* (Leitão *et al.*, 2017). The LysR-type regulator ShvR is another modulator of T2SS, having been described to possess a multifaceted purpose that integrates some of the already mentioned cellular processes. In addition to its influence on T2SS, ShvR influences the expression of *cepIR* and *cciIR*, as well as the production of proteases and lipases, and the *afcA* and *afcC* operons, both associated with antifungal activity. As a

consequence of spanning multiple regulatory domains, ShvR exercises its influence on colony morphology, biofilm formation and virulence (O'Grady *et al.*, 2010).

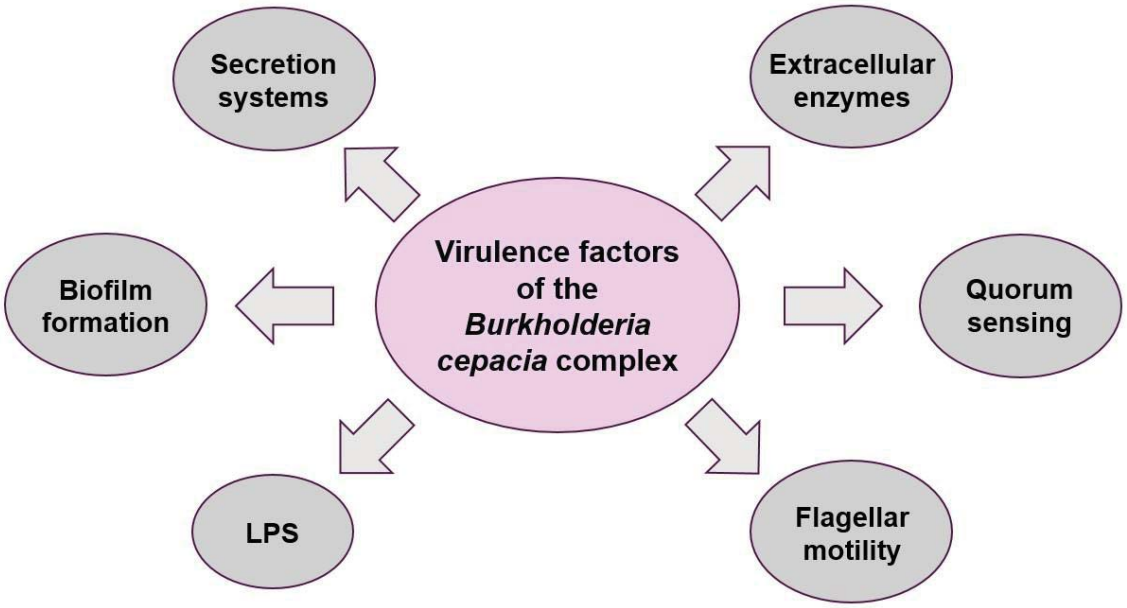

Figure 1.2: Key virulence factors of the *Burkholderia cepacia* complex.

Expanding on the subject of transcriptional regulators, twenty paralogous genes of the primary σ^{70} factor have been identified in *B. cenocepacia* J2315 (Sousa *et al.*, 2017). Many of those genes encode extracytoplasmic function (ECF) σ factors, which respond to specific environmental signals, often related to stress, resulting in the transcription of a particular set of genes by the RNA polymerase (RNAP). For example, in the case of iron limitation, the RNAP would be directed to transcribe genes linked to iron uptake, such as those encoding proteins necessary for siderophore synthesis (Grove, 2022). Other alternative σ factors have been described, such as RpoN, required for not only biofilm formation and motility, but also the prolonged bacterial survival inside macrophages (Saldías *et al.*, 2008), and RpoE, a stress response regulator similarly connected to phagolysosomal fusion delay in macrophages (Flannagan & Valvano, 2008). Small non-coding RNAs (sRNAs) also play a role in the regulation of biofilm production and overall Bcc virulence; this topic will be discussed in the following sections.

1.4 Extracellular vesicles and their relevance in infection

Considering the limited knowledge regarding the acquisition of mutations as well as other mechanisms involved in the often patient-specific adaptation and virulence of Bcc, clinical manifestations of infection remain largely unpredictable (Scoffone *et al.*, 2017). Consequently, the need for further investigation on the intra-host evolution of Bcc strains during infection remains essential. Extracellular vesicles (EVs) represent one of the factors that modulate host-pathogen interactions, having become an increasingly prominent focus of research in recent years. The term "extracellular vesicles" is attributed to membranous particles generated through blebbing of the bacterial membrane that typically range from 10 to 300 nm in diameter (Stanton, 2021). Although EVs produced by Gram-negative bacteria are usually referred to as outer membrane vesicles (OMVs), for the remainder of this work "EV" will be used as an universal term, as suggested by the International Society for Extracellular Vesicles (ISEV) (Bose *et al.*, 2020). Since these particular EVs are formed from the budding of the OM, they commonly contain OMPs, LPS and phospholipids, but may also carry peptidoglycans, periplasmic and cytoplasmic proteins, nucleic acids, ion metabolites, and signaling molecules. Depending on their function and

biogenesis, vesicles might store different cargoes (Furuyama & Sircili, 2021). Considering that specific environmental conditions will determine bacterial gene expression and EV composition, an active selection of EV cargo has been proposed. This composition likely varies according to the infection stage, though it is primarily associated with EVs produced by nonlytic methods (Lécrivain & Beckmann, 2020; Jan, 2017). The other two types of EVs generated by Gram-negative bacteria are explosive outer membrane vesicles (EOMVs), a product of explosive cell lysis triggered by a prophage endolysin, and outer inner membrane vesicles (OIMVs), containing portions of both the IM and the OM (Juodeikis & Carding, 2022). Although external stressors can induce hypervesiculation, a basal level of EVs is nonetheless inherently shed during bacterial growth (Furuyama & Sircili, 2021). The molecular basis through which this process is carried out has yet to be completely described. Still, four predominant models have been proposed to explain what causes the curvature of the membrane. The first model includes the loss or relocation of covalent linkages between the OM molecules and the peptidoglycan layer, while the second one is based on the build-up of pressure within the periplasmic space due to the accumulation of peptidoglycan fragments or misfolded proteins (Pita *et al.*, 2020). For instance, in support of the first model, it has been demonstrated that OMPs display a clustering pattern rather than being evenly distributed in the OM and migrate toward the cell poles during division. These details might indicate that vesiculation occurs between these clusters, an hypothesis further supported by the fact that OMPs are present in much lower concentrations in EVs when compared to the OM itself (Juodeikis & Carding, 2022). The third model that has been proposed is based on *Pseudomonas aeruginosa*, where vesicle formation is triggered by an increased accumulation of molecules such as B-band LPS and *Pseudomonas* quinolone signal (PQS). The fourth model attributes vesicle formation to the accumulation of phospholipids in the outer leaflet of the OM as a result of *vacJ*/*yrb* repression or deletion (Badi *et al.*, 2020). Various vesiculation mechanisms may coexist within a single bacterial strain and can be influenced by growth conditions (Juodeikis & Carding, 2022). Nevertheless, none of the proposed models fully elucidate the mechanism of nucleic acid uptake by EVs, though certain studies have linked it to the presence of OIMVs in experimental preparations (Furuyama & Sircili, 2021). EV entry into host cells can be achieved by a range of size-dependent methods, with vesicles up to 1 μm entering via micropinocytosis, while smaller vesicles being generally internalized through clathrin- and lipid raft-mediated endocytosis (Badi *et al.*, 2020). Vesicular uptake is facilitated by invasive and adhesive ligands, exemplified by the invasins IpaB, IpaC, and IpaD from *Shigella flexneri*, and the adhesins OspA and OspB from *Borrelia burgdorferi* (Jan, 2017; Tilly *et al.*, 2016). This cellular uptake can also be conditioned by other factors, such as EV membrane composition. Studies have shown that the presence or absence of the O antigen on the EV surface determined whether endocytosis was mainly lipid raft-mediated or clathrin-mediated, respectively. Furthermore, the pathogen-associated molecular patterns (PAMPs), like LPS, flagellin or nucleic acids, present on EVs can be recognized by host Toll-like receptors (TLRs) and intracellular nucleotide-binding oligomerization domain (NOD) proteins, leading to the activation of signaling pathways involved in the coordination of the innate immune response. This immune activation may also facilitate EV internalization by the host cells (Lécrivain & Beckmann, 2020; Badi *et al.*, 2020). In addition to adhesins and invasins, EVs can serve as a vehicle for the dissemination of a variety of virulence factors such as proteases, hemolysins, toxins and small RNAs, facilitating pathogenesis (Amano *et al.*, 2010). Immunomodulatory effects can also be triggered by such factors, as is the case for the effector protein BopE present in *Burkholderia pseudomallei* EVs. This type III secreted protein can activate the host GTPase Rac1, inducing downstream signaling and cytoskeletal rearrangement, which promotes bacterial invasion and intracellular survival (Stevens *et al.*, 2003). *P. aeruginosa* EVs also exploit host cell machinery, including N-WASP-mediated actin trafficking, to facilitate entry and deliver an assortment of enzymes, such as β-lactamases, alkaline phosphatases, the *P. aeruginosa* aminopeptidase (PaAP), hemolytic phospholipase C and the CFTR inhibitory factor (Cif). Cif is a protein that interferes with the cystic fibrosis transmembrane conductance regulator, reducing

chloride ion secretion and causing dehydration and mucus accumulation in the airway surface layer, which contributes to bacterial colonization. Conversely, alkaline phosphatase promotes biofilm formation, the hemolytic phospholipase C induces eukaryotic cell lysis, and PaAP aids in epithelial cell adhesion (Amano *et al.*, 2010; Juodeikis & Carding, 2022). Certain bacteria can also use EVs for offensive purposes in interbacterial competition. This can be done for nutrient acquisition, through the secretion of hydrolases or antibiotics that degrade the peptidoglycan walls of nonself strains, resulting in cell lysis (Furuyama & Sircili, 2021; Juodeikis & Carding, 2022). Notably, it has been demonstrated that *P. aeruginosa* EVs can include the T6SS, a protein secretion system that offers competitive advantages via injection of toxin proteins into other bacteria (Combo *et al.*, 2022). The hypervesiculation induced by environmental stressors, primarily resulting from explosive cell lysis due to the activation of the SOS response, offers a shield to the surviving bacterial population (Furuyama & Sircili, 2021). EV-associated virulence factors have been linked to changes in DNA methylation patterns in immune cells, along with other mechanisms that target host immune cell gene expression post-transcriptionally, as is the case for small RNAs, resulting in the downregulation of the immune response and allowing infection to persist (Charpentier *et al.*, 2023). EVs also play a crucial role in signaling and molecular delivery within microbial communities, transporting molecules such as antibiotic resistance determinants (like β-lactamases) or EPS that promote cell co-aggregation during biofilm formation. These vesicles also facilitate micronutrient acquisition and transport to bacterial cells (Jan, 2017). Although no full characterization has been attained, studies have shown that certain advantageous phenotypes, including antimicrobial resistance, can potentially be acquired via horizontal gene transfer mediated by EVs, providing an effective mechanism of gene dissemination without requiring cell-to-cell contact (Marinacci *et al.*, 2023). Additionally, they might act as decoys, sequestering antibiotics and reducing their effective concentration near bacterial cells, a process that may happen due to vesicle-associated multidrug efflux pumps, or by becoming targets of lytic phage infection (Juodeikis & Carding, 2022). For example, in *Moraxella catarrhalis*, superantigen-bearing EVs protect the pathogen by diverting the host's adaptive humoral immune response (Amano *et al.*, 2010).

Concerning Bcc, Kim *et al.* (2020) have noted that *B. cepacia* ATCC 25416 EV production was greater when under antibiotic stress conditions than when grown without antibiotics. Moreover, cytotoxicity and pro-inflammatory response levels were enhanced in host cells in response to EVs resultant from cultures grown with sub-minimum inhibitory concentrations (MICs) of ceftazidime, when compared with those obtained under other conditions. These results are consistent with previous studies indicating that environmental context strongly influences EV composition, providing evidence for the existence of a selective cargo loading into EVs. Specifically, due to the sub-lethal antibiotic concentrations, a greater amount of EVs produced by nonlytic methods could be present (Lécrivain & Beckmann, 2020; Jan, 2017), possibly indicating that the sorting mechanism could be targeted towards enhancing EV pathogenic potential.

Some recommendations have been provided by the ISEV regarding the experimental characterization of EVs, with a combination of methods such as differential centrifugation steps, ultracentrifugation, density gradients and filtration being typically used for their isolation (Charpentier *et al.*, 2023). These methods present limitations: centrifugation can lead to cell damage and unintended lysis, while filtration procedures can result in the clogging of the membrane. To minimize these issues, researchers often perform centrifugation at lower speeds or use defined media and multiple wash steps during filtration (Juodeikis & Carding, 2022). Due to the low concentration of naturally produced EVs, many researchers induce hypervesiculation through the exposure of bacteria to a large diversity of stress factors, including antibiotics (Combo *et al.*, 2022). As previously mentioned, stressful conditions affect EV composition (Jan, 2017) and lead to the copurification of nonlytic EVs with EOMVs and OIMVs, complicating

efforts to distinguish these vesicles and to accurately determine their individual functions (Juodeikis & Carding, 2022). For subsequent stages of EV analysis, microscopy-based techniques such as electron microscopy, atomic-force microscopy or super-resolution microscopy are recommended for qualitative assessments of vesicle morphology and production. Quantitative analysis can be performed using protein markers, total protein or lipid quantification, and nanoparticle tracking analysis (NTA) (Charpentier *et al.*, 2023).

1.5 Small non-coding RNAs and their role in host-pathogen interaction

Small non-coding RNAs are a heterogenous group of molecules ranging from approximately 50-450 nucleotides in length and are commonly transcribed from intergenic regions (IGR), though they may also originate from 3′UTRs and 5′UTRs (Stubben *et al.*, 2014; Sass *et al.*, 2017). These genetic elements neither encode proteins nor directly participate in protein synthesis or ribosomal function. Still, bacterial sRNAs are regarded as essential post-transcriptional regulators (Matos *et al.*, 2024) that greatly contribute to pathogenesis and environmental adaptation (Pita *et al.*, 2023). To ensure their stability and regulatory activity, many sRNAs require the assistance of RNA chaperones such as Hfq and ProQ. Unlike many prokaryotes that encode a single Hfq RNA chaperone, Bcc bacteria possess two RNA-binding proteins, Hfq and Hfq2 (Sousa *et al.*, 2017). Small RNA-mediated post-transcriptional regulation is usually achieved via complementary base-pairing with the 5'-UTR or open reading frame (ORF) of bacterial mRNAs or, in some cases, by binding to and sequestering proteins (Matos *et al.*, 2024). Within the bacterial cell, this intracellular regulation process may lead to the inhibition of translation by blocking the Shine-Dalgarno (SD) sequence and recruiting RNase E, resulting in the degradation of the transcript. Alternatively, it might disrupt secondary mRNA structures impeding ribosome access to the SD sequence, thereby activating gene expression (Choi *et al.*, 2017).

Some sRNAs secreted in host cells have the capacity to mimic or compete with host miRNAs, resulting in the suppression of particular target genes, notably those involved in immune responses (Charpentier *et al.*, 2023). Accordingly, these bacterial sRNAs have a vast influence in a variety of molecular mechanisms (Ajam-Hosseini *et al.*, 2024), being transiently expressed in response to specific environmental cues (Matos *et al.*, 2024). They participate in stress-induced regulatory pathways prompted by external stimuli, such as oxidative stress caused by ROS (Berghoff & Klug, 2012). They may also influence pathogenesis, quorum sensing, biofilm formation, and bacterial metabolism, fine-tuning nutrient acquisition and utilization (Ajam-Hosseini *et al.*, 2024). Small RNA-mediated regulation of virulence may facilitate host cell adhesion, invasion and evasion of the immune response, being therefore pivotal to the establishment of infection (Banerjee, 2025). They can also influence antibiotic resistance, as is the case with MicF, an *Escherichia coli* sRNA that inhibits *ompF* translation and induces degradation of the transcript, thereby reducing the permeability of the bacterial membrane (Delihas & Forst, 2001). Highlighting the broad impact of bacterial sRNA on diverse biological activities, Coleman *et al.* (2020) described the *P. aeruginosa* sRNA PA0805.1 as a contributor to reduced swarming, swimming, and twitching motility when overexpressed, accompanied by the downregulation of type IV pilus genes. Other genes involved in motility that also had altered expression were *algR*, *lasR*, *mvaT*, *rhlR*, and *psrA*, all regulators that have influence on virulence and quorum sensing as well. Furthermore, PA0805.1 increased adherence, cytotoxicity, and tobramycin resistance through upregulation of the multidrug efflux systems *mexXY* and *mexGHI-opmD*, as well as the protease ClpD, which is required for the motile to sessile switching and promotes biofilm dispersal and virulence. The downregulation of ExsD, a negative regulator of the T3SS, further contributed to *P. aeruginosa* cytotoxicity.

Host-pathogen interactions can be driven by sRNAs contained within EVs, which represent an important strategy for their protection and transport directly to target cells, whereupon sRNAs modulate the host's immune and metabolic function (Badi *et al.*, 2020; He *et al.*, 2023). Conversely, sRNAs have been implicated in the regulation of vesicle biogenesis. For example, Song *et al.* (2008) disclosed the existence of VrrA in *Vibrio cholerae*, a sRNA that was shown to induce EV production by negatively regulating *ompA* expression, a key factor of *V. cholerae* pathogenesis. VrrA was therefore hypothesized to contribute to stress adaptation and influence bacterial colonization. As previously mentioned, evidence supporting selective cargo loading inside EVs has been presented, a process that may be partly dictated by the dynamic extracellular environment, though it is still unknown what cellular mechanisms promote such activity (Stanton, 2021). In many studies, sRNA packaging has been associated with non-selective methods resulting from cell lysis, being identified as a consequence of bulk sequencing experiments (Lécrivain & Beckmann, 2020). However, Malabirade *et al.* (2018) have shown that in *Salmonella enterica* the RNA profile of EVs was dependent on the culture conditions, and plenty of research has validated the existence of specific loading of individual RNAs into EVs (Lécrivain & Beckmann, 2020). Furthermore, due to their size, sRNA may be able to move across the inner membrane by some undocumented mechanism. These findings suggest the existence of a complex and diverse set of sRNA inclusion processes that have yet to be completely understood (Park *et al.*, 2023). It is because of such knowledge gaps that EV-associated sRNA functional studies are also still rather limited, a predicament further amplified by the small size and low abundance of naturally produced EVs (Furuyama & Sircili, 2021). Other limitations include the potential inaccuracies of transfection experiments using individual RNAs in host cells, which often fail to consider the complexity of EV cargo, the combined effects of its diverse transcriptome, and tend to lack a broader perspective that integrates other bacterial pathways in the manipulation of the host immune response (Lécrivain & Beckmann, 2020). Computational approaches for predicting sRNA targets also have their own shortcomings, as they often produce a considerable number of false positives and cannot detect post-transcriptional regulation mechanisms beyond sequence complementarity (A. Sass *et al.*, 2017).

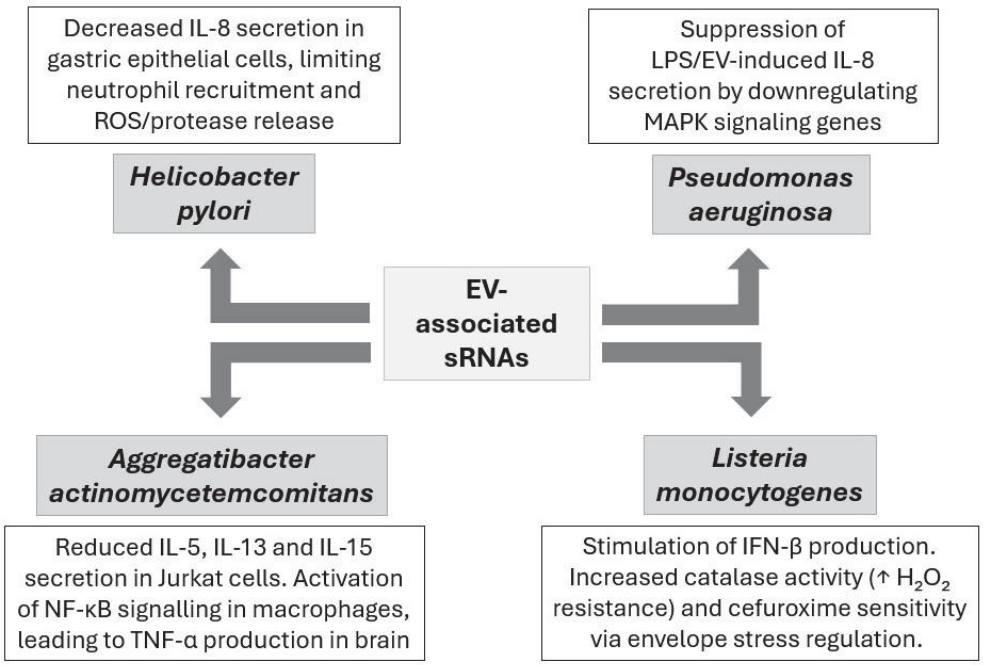

Figure 1.3: Examples of functional roles of EV-associated sRNAs found in *Helicobacter pylori*, *Pseudomonas aeruginosa*, *Aggregatibacter actinomycetemcomitans* and *Listeria monocytogenes*. This illustration highlights how small RNAs delivered via extracellular vesicles can modulate the host's immune response and create favorable conditions for bacterial survival, altering cytokine secretion, signaling pathways and stress responses.

Still, a significant number of findings regarding certain EV-associated sRNAs and their role in virulence have been attained. For instance, the transfection of three highly expressed sRNAs belonging to *Aggregatibacter actinomycetemcomitans*, *Porphyromonas gingivalis*, and *Treponema denticola* into Jurkat cells resulted in reduced secretion of IL-5, IL-13, and IL-15 (Choi, Kim, *et al.*, 2017). In another study involving *A. actinomycetemcomitans*, it was found that sRNAs transported by EVs were mostly detected by TLR-8, inducing NF-κB signaling pathways in macrophage cells that resulted in TNF-α production in the human brain. The same sRNAs were incorporated into host Ago2, a key component of the RNA-induced silencing complex (RISC), indicating a novel strategy in hijacking the host's regulatory machinery that is uncommon in other intracellular bacteria. Additionally, *A. actinomycetemcomitans* EVs were demonstrated to systemically cross the murine blood-brain barrier, suggesting a potential delivery system by which this pathogen might directly promote neuroinflammatory diseases (Han *et al.*, 2019). In *Listeria monocytogenes*, the sRNA rli32 was shown to stimulate IFN-β production, consequently creating an environment beneficial for intracellular bacterial growth. Strains overexpressing rli32 displayed increased resistance to H_2O_2 due to enhanced catalase activity, as well as increased sensitivity to the cephalosporin cefuroxime, as a result of the regulatory action of rli32 in genes associated with cell envelope stress (Frantz *et al.*, 2019). Contrarily, Zhang *et al.* (2019) identified two sRNAs (sR-2509025 and sR-989262) carried by *Helicobacter pylori* EVs that led to a decrease in IL-8 secretion by human gastric adenocarcinoma cells. This immunomodulatory effect facilitates immune evasion, seeing as IL-8 upregulation during *H. pylori* infection triggers the secretion of proteolytic enzymes and ROS by activated neutrophils recruited to the infection site. In a following study, Li *et al.* (2022) confirmed these results, observing a stronger immune reaction after mice immunization with ΔsR-989262 and ΔsR-2509025 EVs when compared to wild-type EVs. Similarly, a *P. aeruginosa* tRNA fragment (sRNA52320) was found to suppress LPS- or EV-induced IL-8 secretion by downregulating multiple genes in the MAPK signaling pathway, thus promoting the establishment of infection (Koeppen *et al.*, 2016).

1.6 Dissertation Focus

Currently, only a small percentage of Bcc sRNAs have been functionally characterized. The small RNA NcS25 has been demonstrated to repress the OM porin BCAL3473, a protein involved in nitrogen metabolism via the transport of arginine, tyrosine, tyramine, and putrescine (A. M. Sass & Coenye, 2023). Kiekens *et al.* (2018) described the sRNA NcS35 as capable of attenuating bacterial growth and metabolic rate, as well as having a negative regulatory role in cell aggregation during biofilm production, possibly having some influence in bacterial survival. RIT11b, a *B. cenocepacia* small RNA that was discovered to be downregulated during *C. elegans* infection, was additionally noted to attenuate virulence and biofilm formation, as well as promote swimming motility (Pita *et al.*, 2023). Another example is BrrF, a sRNA that is significantly upregulated in conditions of iron starvation, commonly encountered during host infection. BrrF was shown to downregulate the oxidative stress response and the TCA cycle, playing a role in the maintenance of Bcc's biological activity and homeostasis (A. M. Sass & Coenye, 2020). Considering that Bcc EVs have already been shown to induce cytotoxicity and enhance pro-inflammatory responses in host cells (Kim *et al.*, 2020), the delivery of sRNAs to host cells by EVs could facilitate immune evasion and/or in the establishment of infection. Depending on environmental conditions, these sRNAs could act as an additional immune stimulant that bacteria could exploit, as demonstrated for *A. actinomycetemcomitans* (Han *et al.*, 2019). Whether such a premise is confirmed or another regulatory mechanism is discovered, the study of the sRNAs contained within Bcc EVs and their potential roles in infection and bacterial survival may pave the way for the development of novel therapeutic approaches targeting these RNAs. Some emerging RNA-targeting strategies include the use of small molecules that would inhibit bacterial translation, CRISPR-based gene editing and

antisense oligonucleotides (ASOs) (Childs-Disney *et al.*, 2022). Furthermore, functional characterization of Bcc sRNAs could contribute to EV engineering for vaccine development, where immunosuppressive and immunostimulatory sRNAs might be excluded or used as adjuvants, respectively (Li *et al.*, 2022).

For this work, the main objective was to investigate the potential role of EV-associated small RNAs during *B. cenocepacia* infection. For this purpose, sequences of sRNAs identified in previous studies (Sass *et al.*, 2017; Pita *et al.*, 2023) were used to predict putative human targets by employing bioinformatic tools. This approach then prompted the selection of two sRNAs of interest. Seeing as EVs represent an extremely relevant strategy of sRNA delivery to host cells, the optimization of vesicle production conditions regarding the identification of clinically relevant conditions that could enhance EV production was added as a secondary purpose with the aim of facilitating future research. Although direct analysis using human cell lines would have provided insight into the biological relevance of these sRNAs in the host-pathogen interaction, this approach was not performed in this work. Instead, functional characterization of the two selected sRNAs was performed by overexpressing them in *B. cenocepacia* K56-2, followed by a variety of phenotypic assays. This experimental design resulted in an assortment of observable traits that were analyzed to establish a foundation for subsequent studies.

2. Materials and methods

2.1 Bacterial strains and growth conditions

The strains and plasmids that were used in this work are presented in **Table 2.1**. Bacterial cultures were stored in 40% (v/v) glycerol at -80ºC, then grown in Miller's LB (Lysogeny Broth) medium (NZYTech) agar (2%) plates and incubated at 37ºC for 16 to 24 h. The plates were subsequently stored under 4 ºC for future use. For genetic engineering procedures, *Escherichia coli* DH5α was used for plasmid construction and maintenance (chloramphenicol 25 µg/mL), while *B. cenocepacia* K56-2 was grown in media supplemented with chloramphenicol (200 µg/mL, NZYTech). When necessary, overnight cultures were inoculated in 3 mL of LB media supplemented with antibiotics. These were then incubated for 16 h with orbital agitation (250 rpm) at 37ºC.

Table 2.1: Strains and plasmids used in the current study.

Strain	**Description**	**Reference**
E. coli DH5α	F– φ80*lacZ*Δ M15 Δ (*lac*ZYA-*argF*) U169 *recA1 endA1 hsdR17* (rK– mK+) *phoA supE44* λ- thi–1 *gyrA*96 *relA1*	Invitrogen
B. cenocepacia K56-2	Cystic fibrosis clinical isolate (Toronto, Canada); ET12 lineage	(Darling *et al.*, 1998)
Plasmids	**Description**	**Reference**
pIN29	ori_{pBBR} Δ*mob*, Cm^r, DSRed	(Vergunst *et al.*, 2010)
pnc5U55	pIN29 overexpressing the sRNA nc5U55 from *B. cenocepacia* K56-2	This study
pRIT17b	pIN29 overexpressing the sRNA RIT17b from *B. cenocepacia* K56-2	This study

Table 2.2: Primers employed in the current study (Fw – Forward: Rv – Reverse). Sequences recognized by restriction enzymes are underlined.

Primer name	Primer Sequence (5' to 3')	Restriction site	Product Size (bp)
nc5U55_Fw	GCATCG**CATATG**CGAACGCCTGATAAA	NdeI	278
nc5U55_Rv	TAT**TCTAGA**CCGAAAAGGTGGCGGC	XbaI	
RIT17b_Fw	AGC**CATATG**GTTGTGTCCGCTGCTGTCCT	NdeI	253
RIT17b_Rv	TCG**TCTAGA**CCCGCGAGCGCTGTATTTC	XbaI	
nc5U55_RC_Fw	AGAGGAAACAGCCATCGCTT	---	902
nc5U55_RC_Rv	GACGATGCCGTTACAGATGA	---	
RIT17b_RC_Fw	TCCCGAAGGGTTTCTTGCAATCTC	---	993
RIT17b_RC_Rv	CTTTACGGGATGTTCTGGATCACG	---	
nc5U55_RTnew_Fw	CGACAAATAGCCGGATTTCAGG	---	150
nc5U55_RTnew_Rv	AAACGGTTCGATGCGGTTG	---	
RIT17b_RT_Fw	TGCTGTCCTGCACGATACAAGA	---	115
RIT17b_RT_Rv	CGCACAAGGCCCTCCTAGATAC	---	
BCAM1330_RT_Fw	GTCACGACTGACGAGAACGG	---	100
BCAM1330_RT_Rv	TCTTCTGCTGCGCACGAATC	---	
BCAS0104_RT_Fw	GATACGCAGACGCTGACGGTCA	---	107
BCAS0104_RT_Rv	GACAGTGCGCCCATCGTCTTGA	---	
BCAL0351_RT_Fw	CCCGAGCAGATCCAGAAGAC	---	105
BCAL0351_RT_Rv	GAAGCTGGTGAAGCCCTGTA	---	

Primer name	Primer Sequence (5' to 3')	Restriction site	Product Size (bp)
BCAL0527_RT_Fw	ACGCTCGAGGAAGCATGGAC	---	75
BCAL0527_RT_Rv	TGATGCTTCCGCTACCTGTTG	---	

2.2 Minimal inhibitory concentration

The minimal inhibitory concentration (MIC) of *Burkholderia cenocepacia* K56-2 was analyzed for LB broth, Mueller-Hinton broth (MHB) and SCFM-FeZn pH=5.5 (Morales *et al.*, 2023) with ciprofloxacin (CIP), ceftazidime (CAZ), tobramycin (TOB) and trimethoprim (TP) (Sigma-Aldrich™) using the microbroth dilution method, according to the to the International Standard ISO 20776-1 and EUCAST (European Committee on Antimicrobial Susceptibility Testing) recommendations. The cultures were grown without antibiotics in LB medium with shaking (250 rpm) at 37°C until the middle of the exponential phase, having started with an OD_{640} (optical density) of 0.05. The initial stock solutions of each antibiotic were prepared at concentrations that, after serial dilution and inoculation, yielded final maximum concentrations of 1024 µg/mL (for all SCFM-FeZn assays and LB-TOB and MHB–TOB conditions) or 512 µg/mL (for all other conditions). In each 96-well plate, 90 µL of growth medium was added to every well, except: the first column, which received 180 µL of each antibiotic stock solution and the last column, which was used as negative control (no bacterial inoculum) and contained 100 µL of medium. Antibiotic stock solutions were added to the first column in duplicate and serial dilutions (1:2) were performed across the plate. The second last column was used as positive control (bacterial culture without antibiotic), which led to the last 90 µL of the serial dilutions to be discarded before this column. When necessary, the bacterial suspension was adjusted to a final concentration of 5×10^6 CFU/mL, providing an inoculum of approximately 5×10^5 CFU/mL per wel. This was achieved by adding 10 µL of the final solution every well, with the exception of the control columns. The plates were incubated at 37°C for 22-24 h, after which all wells were resuspended, and turbidity was measured at 640 nm using a microplate reader. Each condition was tested in triplicate. GraphPad Prism (version 10.6.0) was then used for data analysis and MIC value determination, applying the modified Gompertz equation, as described by Lambert and Pearson (2000).

During the functional analysis of pnc5U55 and pRIT17b, the MICs for three antibiotics, tetracycline (TET), ceftazidime and ciprofloxacin (Sigma-Aldrich) were determined as just described. Overnight cultures were inoculated in 3 mL of MHB supplemented with chloramphenicol (200 µg/mL) and incubated at 37ºC with agitation. Stock solutions of CAZ (20 mg/mL) and CIP (20 mg/mL) were prepared with deionized water, whereas the stock solution of TET (25 mg/mL) was prepared with ETOH 30%. These solutions were then further diluted to obtain the final antibiotic concentrations desired in the wells of 512 mg/L, 128 mg/L, and 8 mg/L for TET, CAZ, and CIP, respectively.

2.3 *B. cenocepacia* growth under antibiotic stress

To evaluate bacterial growth and EV production, *B. cenocepacia* K56-2 was cultured in LB medium (LB 5 g/L NaCl) and SCFM-FeZn pH=5.5 with an initial OD_{640} of 0.05 at 37ºC with shaking (250 rpm). CIP, CAZ, and TOB were added separately 4 h after culture initiation, corresponding to the mid-exponential growth phase. Based on the determined MIC values for each antibiotic in both LB and SCFM-FeZn, four concentrations were tested for each condition: 0.7 x MIC, 1 x MIC, 1.4 x MIC, 2 x

MIC. The only exception was TOB SCFM-FeZn, for which only three concentrations (0.7 x MIC, 1 x MIC, 1.4 x MIC) were tested. To assess whether early antibiotic exposure or lower doses could enhance EV production, two additional conditions were tested in LB medium: 0.5 mg/L for CIP and 2 mg/L for CAZ), both added at the start of the culture growth. To further investigate the effect of increasing antibiotic pressure on vesicle production, additional TOB concentrations (6, 12, 24, 48, 96, and 134.4 mg/L) and CIP concentrations (0.25, 0.5, 1, and 2 mg/L) were tested. Samples (2 mL) were collected from each condition after 8, 10, and 24 h for relative EV quantification. Bacterial growth was monitored over 24 h by measuring optical density (OD_{640}) every 2 h up to 10 h, and again after 24 h. Control conditions included the respective medium without bacterial inoculation and bacterial cultures without antibiotic treatment.

2.4 Relative EV quantification

After sampling each condition into Eppendorf tubes (2 mL), bacterial cells were collected by centrifugation at 5000 x *g* for 15 min at 4°C. The resulting supernatants were filtered through a 0.22 µm PES sterile syringe filter (Frilabo) to remove residual cells and debris. EV quantification was performed using the lipophilic dye FM 1-43 (Invitrogen™) in a Greiner 96 well F-bottom microplate. For this purpose, a working dye solution was prepared by diluting FM 1-43 in sterile miliQ water (1:100). A volume of 10 µL of this solution was then added to 100 µL of the filtered supernatant in each well. Fluorescence was measured using a microplate reader at 485 nm excitation and 590 nm emission. Fluorescence values were corrected by subtracting the signal from corresponding medium blank. The resulting values were then normalized to the fluorescence of the positive control (*B. cenocepacia* K56-2 grown without antibiotic).

2.5 Bioinformatic sRNA target predictions

Using preliminary results from past studies, the complementary sequences of known *B. cenocepacia* EV-associated small RNAs were aligned with the human reference sequences from the NCBI Human G+T database using the algorithm BLASTN 2.16.0. The small RNAs that yielded significant alignments were then analyzed using IntaRNA version 3.4.1 (Mann *et al.*, 2017) to predict potential interactions between each sRNA and its human mRNA targets.

To predict the possible bacterial targets of the two selected small RNAs (RIT17b and nc5U55), two bioinformatic tools, TargetRNA3 and CopraRNA, were used. CopraRNA requires at least three homologous sRNA sequences from different organisms; for nc5U55, sequences from *B. cenocepacia* J2315, *B. cepacia* ATCC 25416 and *B. multivorans* were used. For RIT17b, sequences from four *B. cenocepacia* strains were included: *B. cenocepacia* J2315, FDAARGOS_734, K56-2 and NML110041. The homologous organisms were first identified using BLASTN, and the alignments were subsequently confirmed.

2.6 Primer design and optimization

In order to characterize the putative targets of RIT17b and nc5U55 in both human cells and *B. cenocepacia*, primers targeting RIT17b, nc5U55, and their respective putative target genes in *B. cenocepacia* K56-2 were designed using AmplifX version 2.1.1. Linearity and amplification efficiency were evaluated by performing qPCR with increasing concentrations of genomic DNA.

2.7 DNA cloning

To overexpress the selected sRNAs and assess their function, the cloning of the RIT17b and nc5U55 sequences was performed. As such, using the program AmplifX version 2.1.1, nested PCR amplification was performed in order to produce the RIT17b and nc5U55 fragments for cloning. This consisted in the amplification of larger genomic region flanking each sRNA (including approximately 500 bp upstream and downstream of the target sequence) using the primer pairs RIT17b_RC_Fw/RIT17b_RC_Rv and nc5U55_RC_Fw/nc5U55_RC_Rv. To obtain this larger region, the sRNA sequence was used to produce alignments for *B. cenocepacia* J2315 using the core nucleotide database (core_nt) with the algorithm BLASTN 2.16.0. The designed primers were then verified using Primer-BLAST. The resulting products were then used nc5U55_RC_Rv. The resulting products were used as templates for a second PCR using the internal primers RIT17b_Fw/ RIT17b_Rv and nc5U55_Fw/nc5U55_Rv, which introduced Ndel and Xbal restriction sites. The restriction enzymes to be employed were confirmed using NEBcutter V2.0. Plasmid (pIN29) purification from E. coli DH5α and purification of the bands collected from the agarose gel previously run to visualize the amplified fragments were performed using the Thermo Scientific™ GeneJET Plasmid Miniprep Kit and the NZYTech™ NZYGelpure kit, respectively. The amplified fragments and the pIN29 expression vector were then digested with Ndel and Xbal, purified, and ligated using T4 DNA ligase (Thermo Scientific™). For a consistent performance of both restriction enzymes, the most appropriate buffer was decided using Thermo Scientific's DoubleDigest Calculator (DoubleDigest Calculator | Thermo Fisher Scientific - US, n.d.). The ligation mixtures were transformed into E. coli DH5α competent cells by heat shock. The transformants with either RIT17b or nc5U55 were next plated onto LB agar containing chloramphenicol (25 ug/ mL), from which a selection of the successful recombinants was later performed through the identification of the loss of the DsRed marker. A colony PCR was then executed to test eight of the transformed colonies (four for nc5U55 and four for RIT17b), one positive control (PIN29 with DSRed) and one negative control (H2O). Subsequently, an agarose gel was run for further analysis, and four colonies (two for each sRNA) were selected for DNA extraction using the Thermo Scientific™ GeneJET Plasmid Miniprep Kit. Part of the purified DNA resultant of the ligation process was sent for sequencing, while the remaining DNA was used for *B. cenocepacia* K56-2 electrocompetent cell transformation (using a Bio-Rad Gene Pulser™ system) of the subsequently confirmed plasmids carrying either RIT17b or nc5U55 inserts. Once more, the transformed cells were plated on a LB agar supplemented with chloramphenicol (200 µg/mL).

2.8 RNA extraction and qRT-PCR

For total RNA extraction, bacterial cultures were grown to an OD_{640} of 0.8^{-1} (exponential phase) or 2.5^{-3} (stationary phase), mixed with STOP solution (5% water-saturated phenol, 95% ethanol), and then snap-frozen in liquid nitrogen along with the samples containing EVs. Once thawed on ice, the bacterial cells were pelleted by centrifugation (6000 g) for 10 min at 4°C. Subsequently, each sample was resuspended in 600 µl of lysozyme solution (0.5 mg/ml in Tris-EDTA 1x pH=8), treated with 60 µL of 10% SDS and incubated at 64°C for 2 min. Following that, 750 µL of acidic phenol and 66 µl of 3M NaOAc (pH 5.2) were added, and samples were incubated at 64°C for 6 min with mixing every 30 s. Samples were then centrifuged at 16 000 x *g* for 15 min at 4°C after being cooled on ice for 1 min. The resulting aqueous phase was later transferred to a Phase Lock Gel (PLG) tube in which 750 µL of chloroform were added. After another centrifugation of 15 min, the aqueous phase was recovered and mixed with 1.4 mL of a 30:1 precipitation mix (EtOH:3M NaOAc, pH 6.5). RNA was precipitated overnight at -80°C. Pelleted RNA was collected by centrifugation at 16 000 x *g* for 30 min at 4ºC and washed with 300 µL of 75% ice-cold ethanol. These pellets were air-dried and diluted in DEPC-treated water. RNA quantity and purity were assessed using a NanoDrop ND-1000 Spectrophotometer.

For DNase treatment, 40 µg of total RNA were incubated with 5 µL of DNAse I, 5 µL of DNAse buffer and 0.5 µL of SuperaseIN for 1 h at 37ºC. For further purification, acidic phenol/chloroform/isoamyl alcohol (P/C/I) was added to the DNase-digested RNAs. Isolation of the aqueous phase was achieved by centrifugation for 15 min at 16000 x *g* (4ºC). For RNA precipitation, a process that was carried out for 1 h at -80°C, the aqueous phase was transferred to a new tube, in which 375 µL of 30:1 precipitation mix (pH 6.5) were also included. RNA was then isolated by centrifugation for 30 min at 16000 x *g* (4°C). The RNA pellets were washed with 75% ethanol, air-dried and resuspended in DEPC-water. Total RNA quality was analyzed in agarose gel. NanoDrop ND-1000 Spectrophotometer was used to quantify RNA concentration.
Complementary DNA (cDNA) was synthesized from 2 µg of total RNA using NZY Reverse Transcriptase (NZYTech), the 5X Reaction Buffer that was supplied, and Random Hexamers, following the protocol provided by the manufacturers.

Quantitative PCR (qPCR) was conducted in an Applied Biosystems QuantStudio 5 Real-Time PCR System using the NZYSpeedy qPCR Green Master Mix (2x), ROX (NZYTech). Each reaction contained 100 ng of cDNA, 400 nM of each specific primer (**Table 2.2**) and the NZYSpeedy qPCR Green Master Mix. Real time PCR was performed using the following conditions: initial denaturation at 95 ºC for 2 min, followed by 40 cycles of 95 ºC for 5 seconds and 60 ºC for 30 seconds. In this process, calibration curves were generated for each pair of primers and all samples were run in two technical replicates. Relative expression was calculated with the $2^{-\Delta\Delta}$ CT method (Livak & Schmittgen, 2001) using the genes BCAM0917 and BCAL3457 as reference for normalization. Expression levels were analyzed by Two-Way ANOVA with a Tukey's multiple comparisons test using GraphPad Prism 10.6.0.

2.9 Functional analysis

A functional characterization of the two selected sRNAs (RIT17b and nc5U55) was carried out through a series of phenotypic assays. The experimental set included *B. cenocepacia* K56-2 wild type (WT), the plasmid control (pIN29), and two *B. cenocepacia* K56-2 strains carrying pnc5U55 and pRIT17b. Taking into account the possible intra-strain variability, three independent colonies from each transformed strain were selected and analyzed, in addition to the WT strain.

2.9.1 Bacterial growth curves and relative EV quantification

Overnight cultures of the four selected *B. cenocepacia* K56-2 strains were adjusted to an initial OD_{640} of 0.05 in 50 mL of fresh LB medium. Optical density was measured at 640 nm every 2 h for a period of 10 h, followed by a final measurement at 24 h. Relative EV quantification was performed on samples collected at 10h and 24h, as previously described.

In another assay, the overnight cultures were adjusted in 500 µL of sterile LB (rich medium) or M9 (minimal medium). In this process, a lidded 96-well polystyrene microtiter plate (Greiner Bio-One) was used with a volume of 150 µL in each well. A SPECTROstar Nano microplate reader (BMG Labtech) was used to carry out OD_{640} measurements every 15 min over a 48 h time period, via which the growth curves were plotted.

2.9.2 Biofilm Assays

Biofilm formation on the polystyrene surfaces was quantified using crystal violet staining, following an adapted version of a previously described methodology (O'Toole & Kolter, 1998). Bacterial cultures at an initial OD_{640} of 0.05 were inoculated in 96-well polystyrene microtiter plates (Greiner Bio-One) containing LB liquid medium. Subsequently, incubation at 37 ºC with no agitation lasted for 24 or 48 h. Adherent cells were washed with deionized water (three times) and stained with a crystal violet solution (1% wt/v). The plates were once again incubated at 37 ºC for 15 min with no agitation. Incubation was followed by another set of three washes with deionized water, and then the dissolution of the bound crystal in 190 µL of 95% EtOH. Biofilm was quantified by reading its absorbance at 590 nm with a microplate reader (SpectroStar Nano, BMG Labtech).

2.9.3 Motility tests

Swimming and swarming motility assays were performed following already established protocols (Huber *et al.*, 2001; DéZiel *et al.*, 2001). Agar plates containing 20 mL of swimming media [1% (wt/v) Tryptone, 0.5% (wt/v) NaCl, 0.3% (wt/v) Agar] or swarming media [ABC minimal media supplemented with 0.1% (wt/v) casaminoacids, and 0.4% (wt/v) agar] were spot inoculated with 5 µL of bacterial cultures with an OD_{640} of 1. The plates were incubated for 72 h, with no agitation at 37 ºC. The halos formed in each plate were then measured every 24 h. For each experiment, four plates were prepared per colony. Two independent assays were made, one for swimming motility and one for swarming motility.

2.9.4 Disk diffusion assay

A disk diffusion (DD) assay was executed to evaluate the antibiotic susceptibility of all selected colonies. Bacterial cultures were grown and adjusted to an OD_{640} of 0.2, and 100 µL of each was evenly spread onto MHA (Mueller-Hinton Agar) plates. Four sterile paper disks containing 5 µL of four distinct antibiotics (ceftazidime, ciprofloxacin, tobramycin, and tetracycline) were positioned onto the agar surface for each plate. Ten plates in total were prepared and incubated at 37 ºC for 22 h, after which the resulting zones of inhibition were measured.

2.9.5 *Caenorhabditis elegans* assay

A virulence assay was conducted using the *C. elegans* strain DH26 as the infection model. The nematodes were maintained at 20°C on NGMI plates [0.3% (wt/v) NaCl, 0.25% (wt/v) Tryptone, 1.7% (wt/v) Agar, 25 mM KH_2PO_4, 1 mM $CaCl_2$, 1mM $MgSO_4$, 5 µg/mL Cholesterol, 2 µg/mL Uracil, 50 µg/mL Nystatine] containing *E. coli* OP50 as the food source. Fresh cultures were prepared by cutting a piece of agar containing *C. elegans* with a sterile scalpel and placing it on a new plate. For the synchronization of *C. elegans*, plates containing eggs were washed with sterile distilled water, and the suspension was divided into 3 eppendorf tubes of 2 mL. To each tube, 500 µL of hypochlorite solution [4% (v/v) Sodium hypochlorite, NaOH 1,6M] was added and mixed by vortexing (up to 10 min). The eggs were recovered by centrifugation, washed and resuspended in 100 µL of sterile distilled water. The

suspension was then pipetted onto NGMI plates containing *E. coli* OP50 and incubated at 20ºC to allow synchronized development.

For the virulence assay, 35 mm diameter plates containing 4 mL of NGMII [0.3% (wt/v) NaCl, 0.35% (wt/v) Bactopeptone, 1.7% (wt/v) Agar, 25 mM KH_2PO_4, 1 mM $CaCl_2$, 1mM $MgSO_4$, 5 µg/mL Cholesterol, 2 µg/mL Uracil, 50 µg/mL Nystatine] solid medium were prepared. A volume of 50 µL of overnight cultures of the selected *B. cenocepacia* K56-2 strains and *E. coli* strains were spread onto the surface of the plates and incubated at 37 ºC with no agitation for 24 h. Except for *E. coli* and the wild type *B. cenocepacia* K56-6 (two plates for each), four NGMII plates were used for each *Burkholderia* colony, and approximately 15-20 of the synchronized L4 larvae were inoculated per plate and incubated at 25°C. Nematode survival and morphology were monitored every 24 h for four consecutive days.

3. Results and Discussion

3.1 Relative EV quantification in antibiotic-induced stress conditions

To evaluate whether medium composition had an effect on EV production, *B. cenocepacia* K56-2 was grown under different antibiotic concentrations in SCFM-FeZn and LB medium. The use of SCFM-FeZn pH=5.5 in particular was due to its distinct composition and acidic pH, as it mimics the sputum of CF patients and decreases the activity of many of the antibiotics used against *B. cenocepacia* (Morales *et al.*, 2023). As such, the minimum inhibitory concentration (MIC) regarding ciprofloxacin, ceftazidime, tobramycin and trimethoprim was initially calculated according to standard protocols. However, due to discrepancies concerning MIC values and the observed results, the original calculated values for the CAZ and TOB conditions in the LB medium were modified (**Table 3.1**). This alteration was based on the visible turbidity observed in the wells during the microplate assays, which at the time indicated an overestimation of the inhibitory threshold.

Table 3.1: *B. cenocepacia* K56-2 MIC values for LB medium and SCFM-FeZn pH=5.5. Alterations were made for the calculated values of CAZ and TOB in the LB medium (*).

	CIP (LB)	CAZ (LB) *	TOB (LB) *	TP (LB)	CIP (SCFM-FeZn)	CAZ (SCFM-FeZn)	TOB (SCFM-FeZn)	TP (SCFM-FeZn)
MIC	1.966	48	96	3.5	20.4	628.7	839.7	118.2

As displayed in **Table 3.1**, *B. cenocepacia* K56-2 was shown to be more susceptible against ciprofloxacin in all media, followed by trimethoprim, ceftazidime and then tobramycin. It is also of note that the inhibitory threshold against all antibiotics was much higher when using SCFM-FeZn pH=5.5. This serves as an illustration of how *B. cenocepacia* responds to antibiotics in a medium mimicking the acidic environment in the CF lung (Aiyer & Manos, 2022) compared to its behavior in a standard medium like LB. This may be due to the induction of antimicrobial resistance resulting from SCFM-FeZn's composition and pH, an inflicted effect on antibiotic efficacy, or a combination of both factors (Morales *et al.*, 2023). For instance, the presence of amino acids in synthetic media mimicking the CF sputum has been demonstrated to lead to differential expression of iron-regulating genes and increased biofilm growth, while mucin is a major contributor for microcolony and biofilm formation *in vivo* (Aiyer & Manos, 2022). This bacterial microcolony formation has been associated with growth in SCFM-FeZn, with an observed reduction in metabolic activity (Shukla *et al.*, 2024), a quality often correlated to

increased antimicrobial resistance (Stevanovic *et al.*, 2022). The displayed MICs for all tested antibiotics are moderately consistent with previous studies (Peeters *et al.*, 2009; Papp-Wallace *et al.*, 2020), though it should be noted that a high variability in values was still observed. The apparent inconsistency regarding MIC determination for Bcc strains has been reported before (Saiman *et al.*, 2024). Specifically, broth microdilution following CLSI methods has been shown to be reproducible for trimethoprim-sulfamethoxazole, whereas reproducibility for CAZ was shown to be below the acceptability cut-off (Jorth *et al.*, 2025). According to EUCAST guidelines, antimicrobial susceptibility testing for Bcc is not recommended due to its genetic diversity, absence of clear MIC breakpoints, the disparity between experimental data and clinical outcomes, among other factors (ESCMID - European Society of Clinical Microbiology and Infectious Diseases 2008, n.d.). As such, treatment is often administered by examining the specific conditions associated with each patient (Scoffone *et al.*, 2017). Similarly, although a higher susceptibility was detected for CIP, this may not reflect the antibiotic's effect *in vivo*, as it does not take into account the drug's ability to reach the site of infection or any possible differential gene expression caused by host factors (Van Den Driessche *et al.*, 2017). On the other hand, the observed resistance of *B. cenocepacia* against CAZ and TOB activity is mostly attributed to class A β-lactamases and low membrane permeability, respectively, though other mechanisms like efflux pump activity also play a part (Halwani *et al.*, 2007; Rhodes & Schweizer, 2016). Despite the determined MIC breakpoint for TOB, high doses of nebulized tobramycin are often administered during treatment of CF patients and have shown potential in the eradication of Bcc infections (Peeters *et al.*, 2009).

Following the methodology described by Bos *et al.* (2021), EV production was assessed through the induction of antibiotic stress using concentrations both below and above the calculated MIC value.

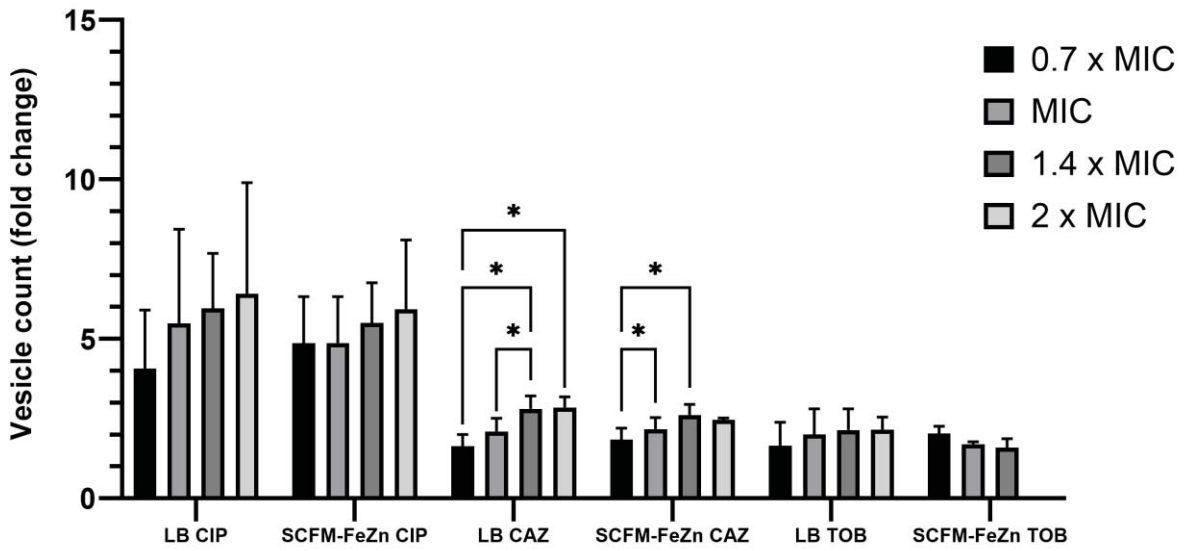

Figure 3.1: Relative EV quantification using the lipophilic dye FM 1-43 following the use of different antibiotic conditions (0.7 x MIC, 1 x MIC, 1.4 x MIC and 2 x MIC) and growth media compositions. The untreated *B. cenocepacia* K56-2 control cultured in LB medium was used as reference. Different media (LB and SCFM-FeZn pH=5.5) were compared in order to evaluate whether medium composition had an effect on EV production. No statistically significant differences were noted between LB and SCFM-FeZn for the same conditions. All data is presented as mean + SD. Statistical significance was assessed using two-way ANOVA followed by Tukey's multiple comparisons test.

Ultimately, EV production resultant of cultures grown in ciprofloxacin was the highest in both media, especially when using a concentration equivalent to the double of the calculated MIC value. By inhibiting DNA gyrase and topoisomerase IV, CIP interferes directly with DNA replication (Sanders, 1988) and induces double-strand breaks (DSBs), leading to the induction of genes involved in the SOS response (Dörr *et al.*, 2009). This is likely the cause of the observed superior EV yield, possibly also associated with a higher rate of explosive cell lysis (Furuyama & Sircili, 2021). Interestingly, EV production was the most variable when using CIP regardless of medium, which may once more be linked to the antibiotic's mechanism of action, and different responses to the induced stress could stem from the genomic plasticity characteristic of *B. cenocepacia* (Gislason *et al.*, 2017). When TOB was added to bacterial cultures, the pattern of EV yield as antibiotic concentration increased differed between media, with production reducing in SCFM-FeZn. Similarly to what can be seen for ceftazidime, the total amount of EVs originated from antibiotic stress in the "LB TOB" condition is amplified until a certain threshold (1.4 x MIC) and then stabilizes or decreases. This might mean that the bactericidal effect of an antimicrobial affects EV production after that threshold is reached, particularly since such biological activity represents a considerable energy cost to the bacterium (Roier *et al.*, 2016). Following this possibility, this suggests that SCFM-FeZn potentiates the efficacy of TOB, therefore reaching this threshold at sub-inhibitory concentrations (0.7 x MIC), which is in accordance with what Morales *et al.* (2023) described regarding the antibiotic's increased activity at an acidic pH. Ceftazidime had the second highest EV yield, likely due to its role in targeting cell wall synthesis by binding to penicillin-binding proteins (PBPs), consequently inhibiting peptidoglycan biosynthesis (Richards & Brogden, 1985). Contrastingly, when using the same protocol for trimethoprim, there was a notable lack of vesicle production, similar to the release seen in the control condition (without antibiotic), which led to its exclusion in later analyses. In the one instance where EV yield was compared between media, higher production was noted in SCFM-FeZn, contradicting what is known about the decrease of TP efficacy in acidic pH (AlRabiah *et al.*, 2018; Morales *et al.*, 2023). An attempt at optimizing EV production was made where TP concentration in LB medium was increased. However, relative quantification results remained the same, suggesting that the previously described results may be due to SCFM-FeZn's influence. The mechanism of action of this antimicrobial is tied to the inhibition of tetrahydrofolic acid synthesis (Masters *et al.*, 2003), leading to the induction of the SOS response and accumulation of ROS (Gonsalves *et al.*, 2024). Due to the minimal release of EVs, it may be that TP has a delayed effect on EV production. Alternatively, this might be caused by the antibiotic's bacteriostatic action on bacterial cultures as a consequence of the disruption of folate metabolism, as has been identified in other studies (Quinlivan *et al.*, 2000), explaining the comparably small reduction of optical density that was observed and the MIC determination results. Still, no conclusions can be drawn without more replicates or optimization of the protocol for trimethoprim.

Although SCFM-FeZn pH=5.5 mimics the CF sputum, LB medium was ultimately chosen for the following experiments due to a non-significant difference in EV yield under antibiotic stress and its practicality, making it optimal for large-scale extracellular vesicle production. However, when taking into account biological relevance, SCFM-FeZn pH=5.5 would have been a better choice. In a future study in which the cargo of *B. cenocepacia* EVs and their functionality is further analyzed, it would be ideal to compare how this aspect is influenced by different media and external stressors. As previously mentioned, SCFM-FeZn may influence antibiotic efficacy, and different vesiculation mechanisms could be triggered depending on the inflicted stress and other growth conditions (Juodeikis & Carding, 2022). Another element to consider is the generation of vesicles originating from explosive cell lysis, since active selection of EV cargo has been mostly associated with nonlytic methods of EV biogenesis (Jan, 2017). Accordingly, using supra-inhibitory antibiotic concentrations should be avoided, allowing for a

more effective EV cargo analysis, which would in turn shed some light on their potential function during Bcc infection (Furuyama & Sircili, 2021).

Future studies on EV functionality involving large-scale production, followed by proteome or transcriptome analysis, for example, would require a reliable system for EV assessment. As such, a second round of relative EV quantification with growth curve analysis was necessary to validate and identify which conditions under antibiotic stress could adequately enhance vesicle production for later EV isolation. In order to prevent explosive cell lysis to a maximal extent, CIP concentrations were changed to 0.25 mg/L, 0.5 mg/L, 1 mg/L and 2 mg/L, and a wider range of TOB concentrations was also tested in LB medium. It should be noted that TOB 6 mg/L was only tested once and that TOB 96 mg/L was only quantified one time at the 10 h time mark, meaning that variability for those cases was not validated.

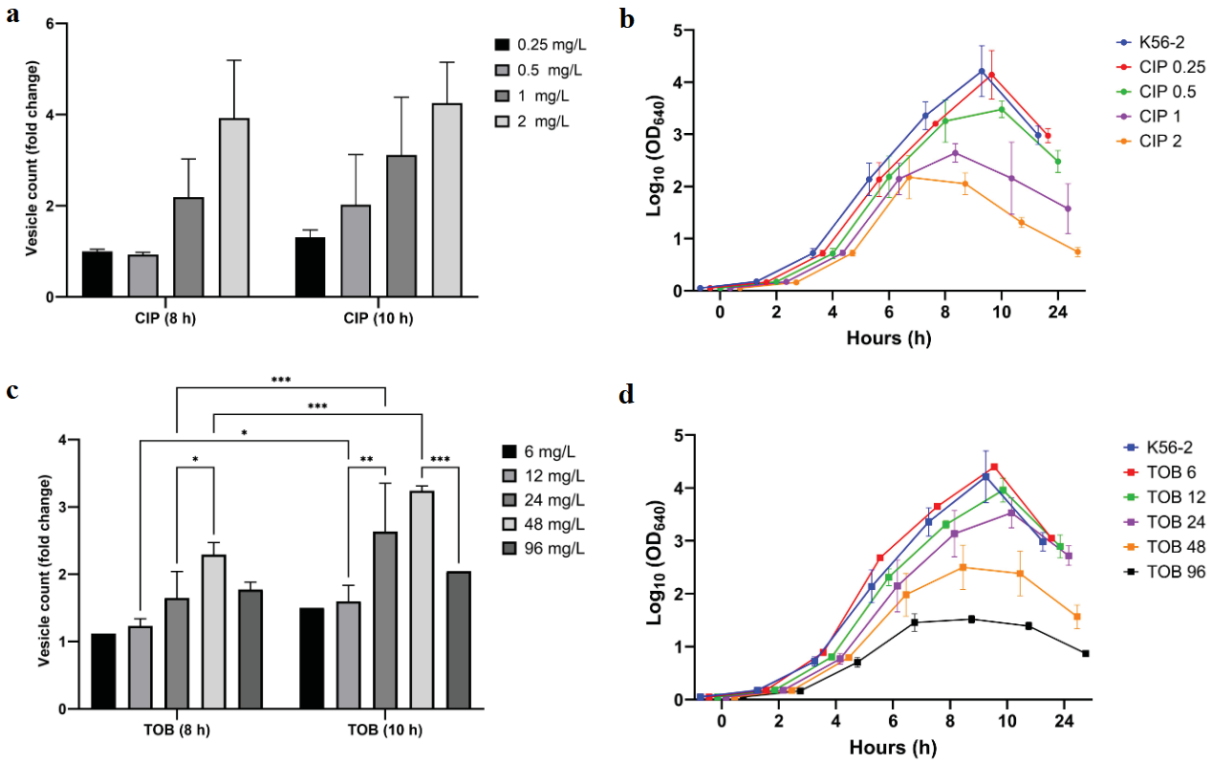

Figure 3.2: Relative EV quantification using the lipophilic dye FM 1-43 for *B. cenocepacia* K56-2 alongside bacterial growth curve analysis. For the comparative results of EV quantification, the untreated *B. cenocepacia* K56-2 control cultured in LB medium was used as reference. Growth was monitored by measuring OD_{640} every 2 h. Ciprofloxacin (CIP) and tobramycin (TOB) were added after 4 h of incubation. All data is presented as mean + SD. Statistical significance was assessed using two-way ANOVA followed by Tukey's multiple comparisons test. (A) Relative EV quantification following the use of different CIP concentrations (0.25 mg/L, 0.5 mg/L, 1 mg/L and 2 mg/L). No statistically significant differences were identified after relative quantification; (B) Growth curve of *B. cenocepacia* K56-2 under different CIP concentrations; (C) Relative EV quantification following the use of different TOB concentrations (6 mg/L, 12 mg/L, 24 mg/L, 48 mg/L and 96 mg/L). Only relevant pairwise comparisons are shown; (D) Growth curve of *B. cenocepacia* K56-2 under different TOB concentrations.

Relative quantification of extracellular vesicles revealed that CIP treatment induced a marked increase in EV release, though with considerable variability, as reflected by the standard deviations shown in **Figure 3.2**. After 8 h of incubation (4 h of exposure to the antibiotic), the two lowest sub-inhibitory CIP concentrations (0.25 and 0.5 mg/L) produced EV levels comparable to the untreated control, consistent with their similar optical density (OD) values. This suggests that, at early stages, these mild antibiotic stresses had limited impact on cell growth or vesiculation. At the same time point, the other two CIP

conditions showed a lower OD in comparison, a disparity not evident at 6 h, seemingly correlated with a superior EV release. A greater difference between the 0.25 mg/L and 0.5 mg/L conditions could be observed after another 2 h, with EV yield at 0.5 mg/L doubling in quantity while the 0.25 mg/L and 1 mg/L increased a similar proportion. By contrast, vesicle production resultant of the highest CIP concentration (2 mg/L) plateaued, and a pronounced OD decrease suggested excessive cell lysis.

At higher concentrations, cultures showed reduced OD and increased EV release, indicating that stronger antibiotic pressure enhances vesiculation, likely as a stress response. However, given that optimal vesiculation should reflect active bacterial response rather than extensive lysis, 2 mg/L was the first condition to be excluded. Despite the lack of identification methods that would help discern between vesicle types, there was a reduction in OD as early as 4 h after the addition of ciprofloxacin, likely caused by cell lysis, whereas other conditions still demonstrated growth. Similarly, the same applies at 10 h for CIP 1 mg/L but not for the other two lower concentrations. Considering that CIP 0.25 mg/L exhibited an almost identical growth pattern to the condition without antibiotic, producing an equivalent amount of vesicles at 10 h, it could be concluded that 0.25 mg/L did not impose any significant stress to the bacterial cultures. Overall, 0.5 mg/L at 10 h and 1 mg/L at 8 h were identified as the most suitable conditions for enhanced EV production under CIP stress.

Regarding the TOB conditions, EV yield varied substantially among the different tested concentrations. Although vesicle production increased with concentration when comparing 67.2 mg/L and 96 mg/L in the prior assay, the previously mentioned threshold of EV yield was reached much earlier this time at 48 mg/L, which was the condition that produced the highest quantity of extracellular vesicles. These discrepancies might have been caused by experimental errors such as some variation in the timing of measurement or inaccuracies when weighting the antibiotics. Alternatively, the observed increase between 67.2 mg/L and 96 mg/L may not become significant when performing bulk EV production. It is important to highlight that the disparity between 48 mg/L and 96 mg/L in this assay was only statistically significant at 10 h. In order to select the most ideal condition, the same reasoning as in the CIP conditions was adopted. Comparably to what was observed at 10 h for CIP 1 mg/L, TOB 48 mg/L had a slight decrease in OD at the 10 h time mark, whereas in TOB 24 mg/L growth was still detected. Seeing as TOB 24 mg/L at 10 h had the second highest EV yield, it might be the best condition for EV production when under antibiotic stress inflicted by tobramycin.

Considering that EV cargo may vary depending on the type of antibiotic stress, its concentration, and the duration of exposure, further analysis is necessary to characterize the produced EVs and to distinguish between lytic and non-lytic EV populations, as these differ morphologically and in cargo composition (Zavan *et al.*, 2023). The study of lytic EVs is also highly relevant in the context of chronic infection, particularly in cystic fibrosis, where antibiotic therapy is often long-term and recurrent. Lytic EVs, typically enriched in DNA, are associated with horizontal gene transfer and the potential dissemination of antibiotic resistance (Baeza *et al.*, 2021; Marinacci *et al.*, 2023) Interestingly, Zavan *et al*. (2023) reported no significant variation in RNA quantity between nonlytic EVs and those produced by explosive cell lysis in *P. aeruginosa*. This comparable RNA content underscores the importance of future RNA sequencing to explore their regulatory potential, as well as the relevance of both EV types to the overall objective of this study.

Although CAZ could not be reliably assessed in the second assay of relative EV quantification due to technical issues, its inclusion in future experiments remains important. Previous findings have shown that CAZ-induced EVs can enhance cytotoxicity and pro-inflammatory responses in host epithelial cells (Kim *et al.*, 2020), suggesting that CAZ exposure may significantly modulate EV function and content.

It is also important to acknowledge the inherent limitations of the present *in vitro* assays, which do not account for host immune interactions, biofilm formation, or other physiological factors influencing EV production *in vivo*. Nevertheless, these experiments were instrumental in defining suitable antibiotic concentrations for large-scale EV isolation and in establishing the framework for downstream RNA cargo characterization. Due to practical constraints related to the isolation and purification of sufficient EV quantities from all tested conditions, RNA sequencing could only be performed on a limited set of samples. This preliminary data included RNA extracted from EVs produced under conditions of explosive cell lysis at higher CIP concentrations, as well as from EVs generated under early exposure to lower doses of CIP and CAZ. Despite the limited dataset, the identified sRNAs were considered alongside sequences from previously reported studies (Sass *et al.*, 2017; Pita *et al.*, 2023), providing valuable guidance for the next stage of the experimental work.

3.2 Predicted human gene targets of *B. cenocepacia* small RNAs secreted via EVs

As previously mentioned, predictions of potential human targets of EV-associated small RNAs identified in preliminary experiments, including sRNAs previously described under infection-relevant conditions (Sass *et al.*, 2017; Pita *et al.*, 2023). Using BLASTN, the complementary sequences of a total of 298 sRNAs were aligned against the NCBI human reference sequences within the Human G+T database. Of these, only 14 produced significant alignments, which were subsequently analyzed with IntaRNA to further investigate potential RNA-RNA interactions between the small RNAs and their potential targets. Based on the predicted strength via IntaRNA and the biological relevance of these interactions, two small RNAs (nc5U55 and RIT17b) were selected for further research, as experimental validation of their predicted targets would be essential. This selection was based on their predicted impact during infection and whether the sRNAs had been found in EVs in clinically relevant conditions, having been guided by previous studies in which EV-associated sRNAs were reported to modulate host immune responses, promoting bacterial persistence and virulence. For instance, *P. aeruginosa* secretes EVs containing sRNA-52320, a tRNA fragment that suppresses IL-8 secretion by targeting several genes within the LPS-stimulated MAPK signaling pathway, like MAP2K2, MAP2K3, MAP2K4, MAP3K7 and PIK3R2, thereby facilitating chronic lung infection (Koeppen *et al.*, 2016). Similarly, small RNAs from *L. monocytogenes* and *H. pylori* have been shown to stimulate IFN-β production in bone marrow-derived macrophages and to reduce LPS-stimulated IL-8 secretion by human gastric adenocarcinoma cells in culture, respectively (Frantz *et al.*, 2019; Zhang *et al.*, 2019). RIT17b and nc5U55 were previously identified in preliminary experiments to be EV-associated sRNAs expressed during *B. cenocepacia* infection of *C. elegans* and biofilm formation, respectively (Pita *et al.*, 2023).

The *Burkholderia cenocepacia* small RNA nc5U55 was predicted to target DNA (cytosine-5)-methyltransferase 3A (DNMT3a) which, along with DNMT3b, is a de novo methyltransferase responsible for the addition of methyl groups to unmethylated cytosines. Together with DNMT3b, DNMT3a mediates DNA methylation by modifying cytosine residues within CpG dinucleotides, leading to transcriptional repression and consequently influencing cytokine gene expression in T helper cell subsets (Gamper *et al.*, 2009; Yu *et al.*, 2011). Loss of DNMT3a has been shown to increase allergic inflammation and IL-13 production (Yu *et al.*, 2011), while its recruitment by CREMα during $CD4^+$ T-cell differentiation affects chromatin remodeling of *IL2* and *IL17A*, key cytokines in immune activation and inflammation (Chen & Kolls, 2017; Mittelstaedt *et al.*, 2021). In the event that nc5U55 downregulates DNMT3a post-transcriptionally, this could destabilize T-cell gene expression, promoting dysregulated cytokine production and leading to an increased inflammatory or dysregulated immune reaction. Montague *et al.* (2024) have also found that loss of DNMT3a in fibroblasts disrupts proper

wound healing and TGF-β signaling, affecting epithelial homeostasis. Shmarina *et al.* (2024) reported that Bcc infected patients exhibited elevated TNF-α and reduced IL-17F levels in sputum samples, along with decreased plasma concentrations of TGFβ1 and IL-10, which could potentially be indirectly affected by host epigenetic and transcriptional regulatory mechanisms.

Nevertheless, nc5U55 was the only sRNA that aligned with both transcript and genomic sequences. The resulting alignments corresponded to various isoforms of BICRA like chromatin remodeling complex associated protein (BICRAL) and to transcript variant X14 of unk like zinc finger (UNKL). While neither of these predicted targets has been directly linked to immune modulation, both are predicted to participate in gene regulatory processes. *BICRAL* is expressed in neutrophils (Sjöstedt *et al.*, 2020), suggesting a possible role in innate immunity. UNKL may influence Rac signaling pathways (UNKL Unk Like Zinc Finger [Homo Sapiens (Human)], n.d.), in which small GTPases (Rac1, Rac2, RhoG) regulate growth factor, cytokine expression and ROS production. Rac1 transcription regulation is performed through the activation of transcription factor NF-kB, which in turn leads to the activation of proinflammatory cytokine transcription (Lee *et al.*, 2021) like TNF-α, the cytokine that, as mentioned, has a high level of expression in Bcc infected patients (Shmarina *et al.* 2024). NF-kB, Jun N-terminal kinases (JNKs), and p38 mitogen-activated protein kinases (MAPKs) activation by Rac1 also results in the promotion of activator protein-1 (AP1) transcription factors. Through the suppression of NF-kB activation by Rac1 and ROS production, Rac2 is able to regulate IL-1β expression, in addition to also being highly relevant in chemotaxis and phagocytosis in hematopoietic cells. Both Rac1 and Rac2 are necessary for neutrophil recruitment into the lung tissue. Lastly, the most recently found member of this GTPase family, RhoG, is known to provoke lamellipodia and filopodia formation in fibroblasts (Lee et al., 2021). UNKL can also can promote the ubiquitination of SWI/SNF-related matrix-associated actin-dependent regulator of chromatin subfamily D member 2 (SMARCD2) (UNKL Unk Like Zinc Finger [Homo Sapiens (Human)], n.d.), which is a vital factor in controlling myelopoiesis (Witzel et al., 2017) as well as possibly being involved in transcriptional regulation by means of chromatin remodeling (UniProt, n.d.-b). Furthermore, when analyzing RNA-RNA interactions between nc5U55 and UNKL, BICRAL and DNMT3a, the three interaction predictions exhibited an extremely low level of hybridization energy, which is often regarded as criteria for a good result in IntaRNA for small RNAs (Busch *et al.*, 2008).

The second selected *B. cenocepacia* sRNA, RIT17b, exhibited a broader range of predicted targets, including the cytosolic phospholipase A_2 group IVα (PLA2G4A) and peptidyl-prolyl cis-trans isomerase a (PPIA). Current studies inform the existence of different PLA_2 isoforms, of which expression is influenced by varying pathogenic stimulation. These enzymes have distinct group designations, with RIT17b possibly targeting a subtype belonging to group IV, $cPLA_2α$ (PLA2G4A). Through the hydrolyzation of membrane phospholipids, an activity that is stimulated in case of a pathogenic encounter, PLA_2 is able to release free fatty acids such as arachidonic acid (ARA; 20:4), docosahexaenoic acid (C22:6) and oleic acid (C18:1). With the increase of free ARA levels, there is a promotion of eicosanoid production, a class of lipid hormones with immunomodulatory activity that participates in inflammatory signaling (Dabral & Van Den Bogaart, 2021). The most significant isozyme involved in this process is $cPLA_2α$, which is particularly selective in regards to glycerophospholipids with ARA in the sn-2 position (Hirabayashi *et al.*, 2004). Notably, it is also the only PLA_2 form to possess MAPK phosphorylation sites, having therefore increased induction in case of infection. This is assisted through the regulation carried out by transcriptional factors like NF-kB, c-Jun, Krüppel-like factor, hypoxia-inducible factor (Hif), and specificity protein 1 (Sp1) (Dabral & Van Den Bogaart, 2021). PLA2G4A has been shown to be particularly expressed in eosinophils and different types of monocytes and dendritic cells (Sjöstedt *et al.*, 2020). In the case of PPIA, this intracellular protein is

crucial for protein folding and trafficking. As it is able to act as a molecular scaffold as well, PPIA contributes to a diverse number of functions. During an inflammatory response, it can also be secreted due to the stimuli produced by ROS generation, among other contributors (Xie *et al.*, 2019), having an important role in leukocyte chemotaxis due to its signaling cascade resulting in extracellular signal-regulated kinase activation (Yurchenko *et al.*, 2002). Aside from this fact, PPIA also exerts its proinflammatory activity on vascular smooth muscle cells (VSMCs) and endothelial cells (ECs), activates MAPK such as ERK1/2, JNK, and p38, and stimulates IkB-α phosphorylation and NF-kB activation. Additionally, it induces EC apoptosis *in vitro*, as well as the expression of matrix metalloproteinases (MMPs) and adhesion molecules (Xie *et al.*, 2019). On account of their functions, should RIT17b impact the expression of any of these proteins, it may be able to directly modulate the host's innate immune response, potentially reducing inflammation and assisting in the establishment of infection and bacterial persistence. Furthermore, other predicted targets of RIT17b such as TBC1 domain family member 13 (TBC1D13) and NEDD4 binding protein 2 (N4BP2) have been discovered to be expressed in immune cells (Sjöstedt *et al.*, 2020), possibly having an indirect role in immunity and thus plausibly benefiting bacterial virulence in the case of post-transcriptional regulation by the sRNA.

Table 3.2: Predicted human gene targets of *B. cenocepacia* small RNAs nc5U55 and RIT17b, potentially secreted through extracellular vesicles. This table lists the human mRNA targets computationally predicted for *Burkholderia cenocepacia* sRNAs identified in EVs. EV-associated small RNAs were aligned with the NCBI human reference sequences within the Human G+T database using the algorithm BLASTN 2.16.0. The small RNAs that revealed any results were then analyzed using IntaRNA version 3.4.1 to explore the interactions between each sRNA and its human mRNA target. Expression of the predicted target genes in human cells was demonstrated by Sjöstedt *et al.* (2020).

sRNA	Alignment	Official Symbol	GeneID	Features	Expression (Tissue profile; Tissue specificity/expression cluster; Single cell type specificity/expression cluster)
nc5U55	*Homo sapiens* unk like zinc finger (UNKL), misc_RNA and mRNA	UNKL	64718	Unk like zinc finger: transcript variant X14, misc_RNA (XR_007064901.1); transcript variant X12, mRNA (XM_047434490.1)	Cytoplasmic and membranous expression in several different tissue types; localized to the cytosol. Low tissue specificity. Cell type enhanced: Oocytes.
	Homo sapiens BICRA like chromatin remodeling complex associated protein (BICRAL), misc_RNA and mRNA	BICRAL	23506	BICRA like chromatin remodeling complex associated protein: transcript variant X7, misc_RNA (XR_007059228.1); transcript variant X6, mRNA (XM_047418547.1); variant X5, mRNA (XM_047418545.1); variant X4 (XM_047418544.1); variant X3 (XM_047418543.1); variant X2 (XM_047418542.1); variant 1 (NM_001318819.2).	General nuclear expression with additional cytoplasmic expression in several tissues. Low tissue specificity. Cell type enhanced: oligodendrocytes, inhibitory neurons, excitatory neurons, microglial cells.
	Homo sapiens chromosome 16	UNKL	64718	Unk like zinc finger: isoform x1 (XM_011522610.2)	Cytoplasmic and membranous expression in several different tissue types; localized to the cytosol. Low tissue specificity. Cell type enhanced: Oocytes.

sRNA	Alignment	Official Symbol	GeneID	Features	Expression (Tissue profile; Tissue specificity/expression cluster; Single cell type specificity/expression cluster)
nc5U55	*Homo sapiens* chromosome 2	DNMT3A	1788	DNA methyltransferase 3 alpha: DNA (cytosine-5) - methyltransferase 3A isoform c (NM_001320892.2)	Ubiquitous nuclear expression, localized to the nucleoplasm. Low tissue specificity. Single cell type group enriched: cardiomyocytes, rod photoreceptor cells.
		DTNB	1838	Dystrobrevin beta: isoform 28 (NM_001351394.2)	Cytoplasmic and membranous expression in several tissues.
	Homo sapiens chromosome 6	BICRAL	23506	BICRA like chromatin remodeling complex associated protein	General nuclear expression with additional cytoplasmic expression in several tissues. Low tissue specificity. Cell type enhanced: oligodendrocytes, inhibitory neurons, excitatory neurons, microglial cells). Low immune cell specificity; **immune cells expression cluster: neutrophils.**
RIT17b	*Homo sapiens* chromosome 1	PLA2G4A	5321	Phospholipase A2 group IVA	General cytoplasmic expression, most abundant in parathyroid gland and seminal vesicle tissues. Cell type enhanced: microglial cells, basal prostatic cells, secretory cells; Cell type enriched: fibroblasts (adrenal gland, kidney, pituitary gland, thyroid gland) and mitotic cells (skin). Immune cell specificity: group enriched - **intermediate monocyte, eosinophil, myeloid DC, classical monocyte, non-classical monocyte, plasmacytoid DC.**
		BRINP3	339479	BMP/retinoic acid-inducible neural-specific protein 3 isoform 1 precursor (NM_199051.3)	Cytoplasmic expression in several tissues. Tissue enhanced: brain and intestine. Cell type enhanced: oligodendrocyte precursor cells, excitatory neurons, astrocytes, inhibitory neurons.
		POGZ	23126	Pogo transposable element derived with ZNF domain: isoform 1 (NM_015100.4)	General nuclear expression; localized to the nucleoplasm and basal body, cytosol. Low tissue specificity: neuronal. Cell type enhanced: oligodendrocytes.
	Homo sapiens chromosome 2	TDRD15	100129278	Tudor domain-containing protein 15 (NM_001306137.2)	Tissue enriched: Testis. Cell type enhanced: spermatocytes, late spermatids, spermatogonia, early spermatids.
		KLHL29	114818	Kelch-like protein 29 (NM_052920.2)	Cytoplasmic expression in most tissues. Low tissue specificity. Cell type group enriched: excitatory neurons, inhibitory neurons.
	Homo sapiens chromosome 4	N4BP2	55728	NEDD4 binding protein 2 isoform x3 (XM_047415953.1)	General cytoplasmic expression. Tissue enhanced: lymphoid tissue; expression cluster: **thymus (adaptive immune response)**. Cell type enhanced: dendritic cells (antigen presentation).

sRNA	Alignment	Official Symbol	GeneID	Features	Expression (Tissue profile; Tissue specificity/expression cluster; Single cell type specificity/expression cluster)
RIT17b	*Homo sapiens* chromosome 7	PPIA	5478	Peptidylprolyl isomerase A: peptidyl-prolyl cis-trans isomerase a isoform x1 (XM_047420536.1)	Cytoplasmic expression in most tissues. Low tissue specificity. Low cell type specificity. Secreted to blood.
		H2AZ2	94239	H2A.Z variant histone 2: isoform 2 (NM_138635.3)	Ubiquitous nuclear expression. Low tissue specificity. Cell type enhanced: early spermatids; Immune cell expression cluster: eosinophils (protein ubiquitination).
	Homo sapiens chromosome 9	TBC1D13	54662	TBC1 domain family member 13 isoform x2 (XM_005252060.3)	Cytoplasmic and nuclear expression in all cells. Low tissue specificity. Cell type enhanced: oligodendrocytes; expression cluster: **langerhans cells (innate immune response)**. Immune cells specificity: I**mmune cell enhanced (basophil)**.
		ENDOG	2021	Endonuclease g mitochondrial precursor (NM_004435.2)	General cytoplasmic expression. Tissue enhanced: skeletal muscle. Cell type enhanced: late spermatids, ciliated cells.
	Homo sapiens chromosome 19	ZNF709	163051	Zinc finger protein 709 (NM_152601.4)	Localized to the nucleoplasm. Tissue enriched: testis; tissue expression cluster: spermatids (flagellum assembly). Cell type enhanced: early spermatids, late spermatids, oligodendrocyte precursor cells, inhibitory neurons, excitatory neurons.
		ZNF564	163050	Zinc finger protein 564 (NM_144976.4)	Localized to the Golgi apparatus. Low tissue specificity: kidney and intestine. Cell type enhanced: microglial cells, oligodendrocyte precursor cells.
	Homo sapiens chromosome X	ARX	170302	Aristaless related homeobox, protein arx (NM_139058.3)	Tissue group enriched: ovary, skeletal muscle. Cell type enhanced: leydig cells, ovarian stromal cells, peritubular cells, inhibitory neurons, enteroendocrine cells.
		MAGEB18	286514	MAGE family member B18: melanoma-associated antigen b18 (NM_173699.4)	Nuclear expression in seminiferous ducts. Cell type enriched: spermatocytes. Cell line expression cluster: Myeloma - Immunoglobulins.

Another sRNA, nc5U65, was initially considered for this study but was ultimately excluded from further analysis due to primer design constraints caused by its small size. This sRNA was predicted to target phosphatidylinositol 4,5-bisphosphate 3-kinase catalytic subunit gamma (PI3Kγ), a kinase that belongs to a family of heterodimeric enzymes that convert phosphatidylinositol(4,5)bisphosphate (PIP2) to phosphatidylinositol(3,4,5)trisphosphate (PIP3) at the cell membranes. PI3Kγ plays a pivotal role in immune regulation, being essential for controlling inflammatory cytokine release in macrophages, as well as for myeloid cell chemotaxis and activation (Lanahan *et al.*, 2022) and lung dendritic cell (DC) development (Nobs *et al.*, 2015). With its function being context-dependent, PI3Kγ can lead to either the suppression or the enhancement of the inflammatory responses (Lanahan *et al.*, 2022). However, previous studies have indicated that reduced PI3Kγ expression may impair innate host defense mechanisms in the lung, thereby favouring lower respiratory tract infections (Maus *et al.*, 2007).

3.3 Functional analysis of RIT17b and nc5U55

Following the *in silico* prediction of potential human targets, the next logical step would be to confirm the presence of these sRNAs within EVs and experimentally assess their functional impact by modulating their expression and testing their delivery to human cell lines. As an initial approach, this study focused on the bacterial side of this interaction by overexpressing the sRNAs nc5U55 and RIT17b in *B. cenocepacia* K56-2. As such, derivative pIN29 plasmid overexpressing nc5U55 (pnc5U55) or RIT17b (pRIT17b) under the control of the strong tac promoter were constructed and transformed in *B. cenocepacia* K56-2. Bacterial cells carrying the empty pIN29 vector were used as controls. The resulting strains were analyzed to determine how sRNA overexpression influences bacterial physiology and to provide preliminary insights into their potential roles in host-pathogen interactions. In parallel, possible *B. cenocepacia* targets of these sRNAs were also predicted using TargetRNA3 and CopraRNA to better understand their regulatory network within the bacterium. Of the resulting putative targets, a number was selected based on functional relevance and/or reliability, seeing as some predictions were shared between programs (**Supplementary Table 5.1** and **Supplementary Table 5.2**).

3.3.1 Bacterial growth and relative EV quantification

To compare bacterial growth among the different constructs, cultures were grown in LB-rich medium for 24 h, under the same conditions used for EV production. As shown in **Figure 3.3**, no significant differences in growth were observed, though pRIT17b exhibited a very slight increase in growth at the 10 h time point. Regarding EV yield, there was no significant difference detected when performing relative quantification. Notably, both pnc5U55 and pRIT17b produced less extracellular vesicles than pIN29 at 10 h.

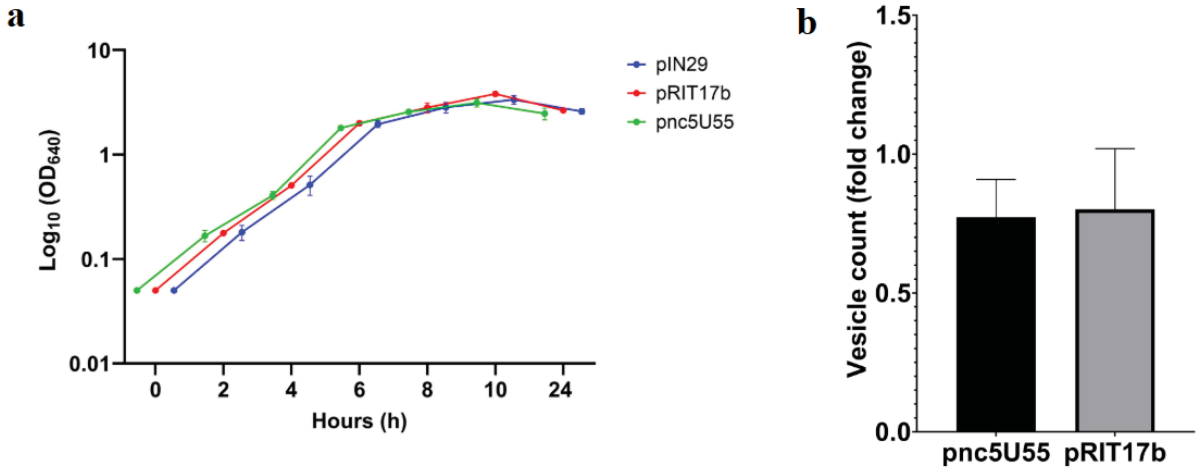

Figure 3.3: Bacterial growth curves of pIN29, pRIT17b and pnc5U55 (A), and the respective relative EV quantification after 10 h of growth in LB medium using FM 1-43 (B). The control strain pIN29 was used as reference for normalization during EV quantification. Growth was monitored by measuring OD_{640} every 2 h. All data is presented as mean + SD. Statistical significance for the growth curves and relative quantification was assessed using two-way ANOVA followed by Tukey's multiple comparisons test and an unpaired t-test with Welch's correction, respectively. No statistically significant differences were identified in either test.

To further characterize the effects of sRNA overexpression, additional growth curves were performed in a microplate reader over 48 hours in both rich medium (LB) and minimal medium (M9). In LB, the wild-type (WT) strain exhibited slightly higher growth than the pIN29-derived constructs, suggesting

that plasmid carriage may impose a modest metabolic burden. While pRIT17b and pIN29 showed comparable behavior, pnc5U55 displayed significantly lower growth, possibly indicating that nc5U55 represses genes involved in nutrient uptake or other metabolic processes. In this rich medium, pnc5U55 began showing statistically significant differences compared to pIN29 at 8 h and to WT at 10 h. After 12 h since the initiation of growth, all groups were statistically distinct from one another, with the exception of pRIT17b and pIN29. Conversely, no significant differences were observed among strains grown in M9 minimal medium (except for pnc5U55 and pRIT17b at 42 h), although WT growth was initially higher during the first 12 h and declined after 36 h, suggesting different adaptive responses to nutrient limitation. This initial behavior might reflect similar circumstances to what happens in LB medium, in which differences in growth may be caused by a potential metabolic burden resulting from the presence of pIN29. By the end of the 48 h period, the decrease in growth might indicate that WT is less suitable at long-term nutrient stress adaptation when compared with pIN29, pnc5U55 and pRIT17b. Seeing as pRIT17b and pnc5U55 resulted in a similar growth curve to pIN29, the presence of pIN29 is likely the most important contributor to the altered metabolic response rather than the overexpression of either sRNA. Interestingly, while RIT17b appeared to not majorly affect growth in either condition, pnc5U55 lacked the distinctly attenuated growth that was observed in LB medium. This suggests that the post-transcriptional targets of nc5U55 may be less relevant in a potential alternative metabolic pathway adopted in the altered conditions. Alternatively, as predicted by the theory of proteome partition, nc5U55 may be involved in the reallocation of proteomic resources from growth to stress response (Scott *et al.*, 2010). Considering that nc5U55 is being overexpressed in pnc5U55, this trade-off may occur even in a rich medium such as LB, resulting in the observed attenuated growth, whereas in M9 this effect appears to become neutral due to the nutrient stress caused by the minimal medium.

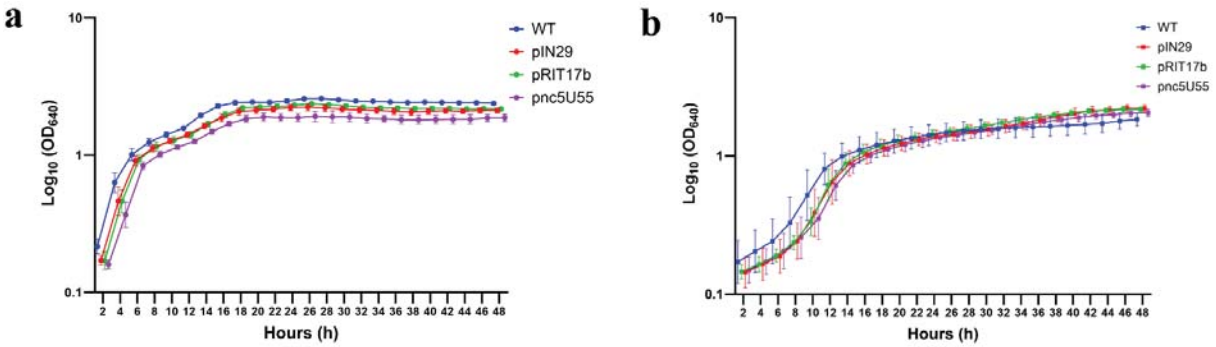

Figure 3.4: Bacterial growth curves of pIN29, pRIT17b, and pnc5U55 over a 48 h time period in (A) LB rich medium and (B) M9 minimal medium. Optical density (OD_{640}) measurements were taken every 15 min over a 48 h time period. All data is presented as mean + SD. Statistical significance was assessed using two-way ANOVA followed by Tukey's multiple comparisons test.

Some of the potential targets of nc5U55 predicted using TargetRNA3 and CopraRNA (**Supplementary Table 5.1** and **Supplementary Table 5.2**) have been documented to be related to metabolism and stress response. The BDSF-regulated gene *phbB* (BCAM0296) encodes an acetoacetyl-CoA reductase, possessing therefore a metabolic function (McCarthy *et al.*, 2010). Many other targets are predictably involved in metabolism and nutrient uptake. For instance, BCAL2953 is a putative prephenate dehydrogenase that participates in the tyrosine biosynthetic process (Shabalin et al., 2019), and BCAM1977 is a permease involved in amino acid transport which might contribute to homeostasis and detoxification, aside from its metabolic role (Jung *et al.*, 2006). Other targets are directly involved in the regulation of stress responses, such as BCAS0634, a putative NRAMP (Natural resistance-associated macrophage proteins) manganese transporter, and SigJ (BCAM1259), a RNA polymerase sigma factor. Specifically, *sigJ* is a *rpoS* homolog, a specialized sigma factor that promotes stress resistance in

bacterial cells (Battesti *et al.*, 2010), that is highly upregulated in response to low oxygen in *B. cenocepacia* H111 (Pessi *et al.*, 2013). BCAS0634 plays a role in intracellular stress, possibly promoting virulence (Holden *et al.*, 2008). Manganese transport contributes to bacterial survival in macrophages and defense against ROS. It is controlled by a variety of regulators, including Fur, a protein involved in iron homeostasis (Papp-Wallace & Maguire, 2006). The small RNA nc5U55 might also target a Fur protein (BCAL2812), which is also regulated by BDSF (McCarthy *et al.*, 2010). There were other transcriptional regulators among the predicted targets that could play a part in the in metabolism and the modulation of certain stress responses, such as BCAL0066, belonging to the AraC family and a regulator of an ethanolamine operon (Gallegos *et al.*, 1997; Lardi *et al.*, 2015), and BCAL1735, a likely regulator of sulfur metabolism from the LuxR superfamily (Van Kessel *et al.*, 2014; Lochowska *et al.*, 2011). Excluding the ones involved in metabolism and transcription regulation, the repression of other detected targets could also likely cause the observed attenuated growth, as is the case for RpmH (BCAL0423a), a ribosomal protein, and the DNA helicase RecG (BCAL3302). Additionally, depending on which stress response pathways are regulated and whether nc5U55 reallocates resources for such a purpose, EV production when this sRNA is overexpressed could be reduced, seeing as the process is closely linked to the bacterial stress response.

3.3.2 Biofilm and motility assays

Biofilm production, a key factor in *B. cenocepacia* virulence and persistence during infection (Gunardi *et al.*, 2021), was quantified after 24 and 48 h in 96-well polystyrene microtiter plates using crystal violet staining. Following the measurement at 24 h, no significant differences in biofilm formation were observed among the strains. By contrast, a significant increase in biofilm production was detected at 48 h for pRIT17b. Consistent with previous assays performed with wild-type *B. cenocepacia* K56-2 in the laboratory (results not shown), WT displayed a lower capability in this context, whereas pIN29 and pnc5U55 showed similar results. The nearly identical biofilm production between these two constructs suggests that the increase relative to WT is likely due to the presence of pIN29 plasmid rather than the overexpression of nc5U55. On the other hand, the higher biofilm yield observed for pRIT17b may result directly from the overexpression of RIT17b.

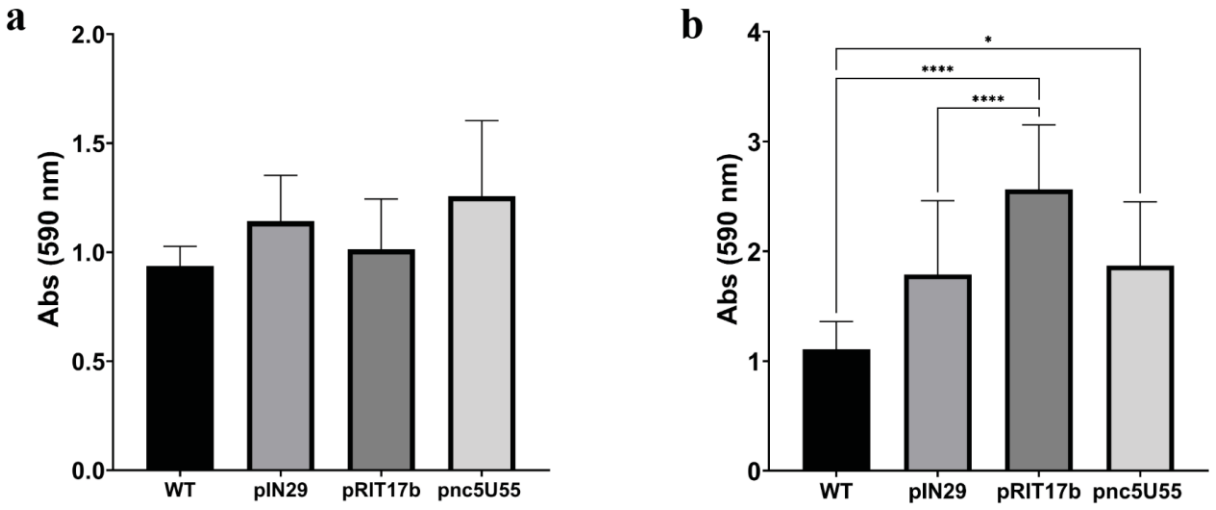

Figure 3.5: Biofilm formation results of WT, pIN29, pRIT17b, and pnc5U55 after (A) 24 h and (B) 48 h. All data is presented as mean + SD. Statistical significance was assessed using two-way ANOVA followed by Tukey's multiple comparisons test, in which a significant increase in biofilm production by pRIT17b was detected at 48 h. Pairwise comparisons between pRIT17b and pnc5U55 were not included.

Another great promoter of *B. cenocepacia* virulence is flagellar motility, which is tightly regulated by quorum sensing (Subramoni & Sokol, 2012). Bcc motility is mediated by a single polar flagellum, which functions as an adhesin and promotes both inflammatory responses as well as epithelial cell invasion. Unlike *P. aeruginosa*, studies have shown that Bcc bacteria can retain this phenotype during chronic infection instead of converting to nonmotile, a feature thought to contribute to its ability to cause septicaemia (Zlosnik *et al.*, 2014, Drevinek & Mahenthiralingam, 2010). While swimming motility involves the rotation of the polar flagellum in liquid or soft environments, the swarming occurs on moist, semisolid surfaces and involves coordinated movement, cell elongation and hyperflagellation (Morin *et al.*, 2022). Swarming also requires surfactants to reduce surface tension, whereas swimming is dependent on chemotaxis (Wadhwa & Berg, 2021). Particularly, biosurfactant production in *B. cenocepacia* is potentially controlled by the cepIR QS system (Malott *et al.*, 2005).

Although both motility assays were performed only once and should be repeated to confirm reproducibility, four plates were prepared for each of the three colonies selected per strain, taking into account potential phenotypic variability. In the swimming assay, both pnc5U55 and pRIT17b showed reduced motility compared with the controls. While the lack of replication prevents definitive conclusions, the similarity between pIN29 and WT suggests that pIN29 plasmid insertion alone did not affect swimming, and that reduced motility may instead result from nc5U55 and RIT17b overexpression. In the swarming assay, pIN29 and pnc5U55 showed similar and comparatively higher motility than the other strains, suggesting that RIT17b may negatively influence the swarming motility. Interestingly, in contrast to what was observed in the swimming assay, the presence of pIN29 appeared to enhance swarming relative to WT. Although nc5U55 overexpression did not significantly reduce swarming, its expression appeared to differentially affect the two types of motility, potentially reflecting distinct regulatory pathways involved in these behaviors.

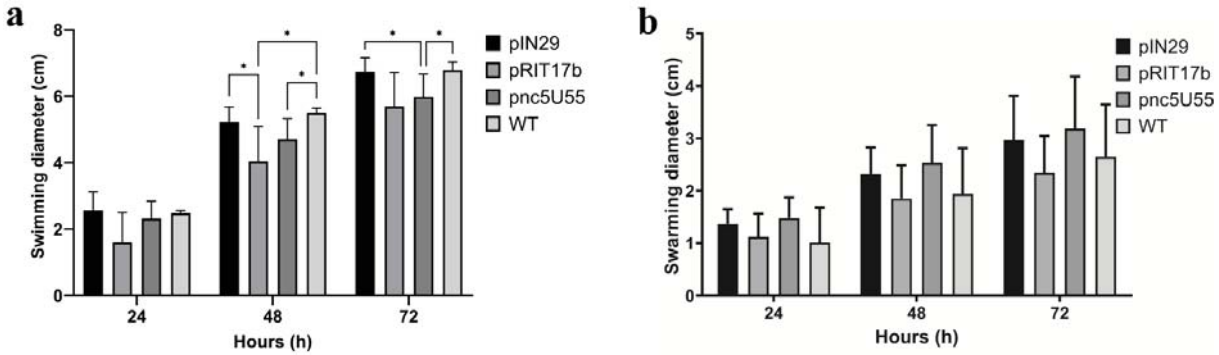

Figure 3.6: Motility assay results for WT, pIN29, pRIT17b, and pnc5U55. All data is presented as mean + SD. Statistical significance was assessed using two-way ANOVA followed by Tukey's multiple comparisons test. Pairwise comparisons between pRIT17b and pnc5U55 were excluded. (A) Swimming motility assay results. Both pnc5U55 and pRIT17b displayed reduced swimming, with significant differences relative to pIN29 at 48 h and 72 h, respectively; (B) Swarming motility assay results. Only RIT17b overexpression appeared to impact swarming, although not in a statistically significant manner.

As previously mentioned, biofilm formation plays a crucial role in the persistence of infection as well as increased resistance to antimicrobial compounds and is regulated by QS (Suppiger *et al.*, 2013). In Bcc bacteria, QS systems are generally based on AHLs, such as the CepIR and CciIR systems, and BDSF, which exhibits antibiofilm activity by binding to RpfR, thus inducing the degradation of c-di-GMP (Subramoni & Sokol, 2012; Fazli *et al.*, 2012). Several putative targets of RIT17b may be related to biofilm formation (**Supplementary Table 5.1** and **Supplementary Table 5.2**), including BCAM1330, a putative polysaccharide export protein; BCAM0581, a diffusible factor synthase A (DsfA); and BCAL3122, the glycosyltransferase WbiF. BCAM1330 has been found to be upregulated during chronic lung infection (O'Grady, 2011), consistent with the known importance of biofilms in this

context (Suppiger *et al.*, 2013). BCAM1330 belongs to a cluster (BCAM1330–BCAM1341) that was regarded as crucial for flow-chamber biofilm formation. The product encoded by this cluster is a biofilm matrix exopolysaccharide that contributes to the structural stability of the biofilm, with BCAM1330 in particular being responsible for the exportation of the resulting polysaccharide. This mechanism is regulated by c-di-GMP through the binding of BCAM1349 to the promoter region of two genes of this cluster, one of them being BCAM1330 (Fazli *et al.*, 2012). BCAM0581, also known as $RpfF_{Bc}$ in *B. cenocepacia* J2315, encodes a bifunctional crotonase (with dehydratase and thioesterase activity) that synthetises BDSF (Suppiger *et al.*, 2013). Were RIT17b to repress BCAM0581, BDSF levels would likely decrease, leading to higher intracellular c-di-GMP levels that are usually associated with increased biofilm production and reduced motility. However, deletion of BCAM0581 has been shown to reduce growth in minimal medium, cellular ATP levels, biofilm formation, motility, proteolytic activity, and virulence in infection models such as *C. elegans* and zebrafish (Deng *et al.*, 2009; Deng *et al.*, 2010). Since RIT17b overexpression did not inhibit growth and instead increased biofilm formation, it is unlikely that this sRNA affects BCAM0581 expression. Regarding BCAL3122 (*wbiF*), this gene encodes a glycosyltransferase associated with the synthesis of the O antigen in LPS (Holden *et al.*, 2008). Although direct data on the effect of *wbiF* in *B. cenocepacia* is limited, LPS are known contributors to biofilm structure and pathogenesis (Sfeir, 2018; Gunardi *et al.*, 2021). *B. glumae* wbiF mutants displayed no significant phenotypic alterations in stress tolerance, motility, or virulence (Lee *et al.*, 2019), possibly due to compensatory mechanisms. Conversely, Saldías *et al.* (2009) reported that the O-antigen of *B. cenocepacia* hindered adhesion to abiotic surfaces and bronchial epithelial cells. Therefore, if RIT17b downregulates wbiF expression, the resulting reduction in O-antigen synthesis could enhance surface attachment and biofilm formation. Certain members of the TetR family have been described as repressors of biofilm production in some species, including *Staphylococcus aureus* and *Vibrio vulnificus* (Ramos *et al.*, 2005). Although BCAL1182, a TetR-family protein potentially targeted by RIT17b, has not yet been functionally characterized, its role in biofilm formation in *B. cenocepacia* remains uncertain, as is the case for several transcriptional regulators listed in **Supplementary Table 5.1** and **Supplementary Table 5.2**. A similar rationale applies to BCAM0133, a LuxR transcriptional factor, as this type of regulators is often involved in QS and modulation of motility and biofilm production (Y. Zhang *et al.*, 2024). In fact, CepR, CciR, and CepR2, QS regulators in *B. cenocepacia*, are homologs to the LuxR protein of *V. fischeri* (Subramoni & Sokol, 2012).

Bacteria often transition from a planktonic to a sessile state as an adaptive strategy, during which motility genes are downregulated in favor of biofilm-associated genes (Dressaire *et al.*, 2015). RIT17b may participate in this regulatory shift, either by directly influencing flagellar gene expression or by modulating QS-regulated pathways. Supporting this possibility, three of its predicted targets, BCAL0526, BCAL0140, and BCAS0104, encode structural flagellar components FliE, FlhB, and FliD2, respectively (Holden *et al.*, 2008). A RT-PCR was performed to assess the influence of RIT17b and nc5U55 overexpression on the expression of BCAS0104 and BCAL0527 (**Figure 3.7C,D**). As two genes involved in flagellar motility, both had been originally highlighted, among other virulence-related genes, as biologically relevant targets to be further assessed. Ultimately, in future studies, other targets addressed in this work as potential causes for the observed results during functional analysis should also be considered in light of the need for further analysis. Two reference genes, BCAM0917 and BCAL3457, were selected for RT-PCR normalization based on their stable expression across the tested conditions and lack of computationally predicted interactions with RIT17b and nc5U55. First, both sRNAs were confirmed to be significantly overexpressed in their respective constructs (**Figure 3.7A,B**). None of the calculated differences in BCAS0104 and BCAL0527 expression between strains were statistically significant. Interestingly, BCAL0527, which encodes a flagellar component located downstream of *fliE* and was not among the predicted targets of RIT17b, showed reduced expression in

pRIT17b. Although not statistically significant, this trend suggests that RIT17b may indirectly influence BCAL0527 regulation. Other RIT17b targets may also influence motility. For instance, RIT17b was predicted to target BCAL0399, encoding an anthranilate synthase component I (TrpE) involved in tryptophan biosynthesis, was reported to impact swimming motility and its deletion mutants exhibited significantly reduced swimming (Paszti *et al.,* 2025). Similarly, Rep (BCAL0079), a DNA helicase, has been linked to swimming and swarming motility in *E. coli*, although its role in *B. cenocepacia* has yet to be validated (Girgis *et al.*, 2007; Vandenbussche *et al.*, 2020).

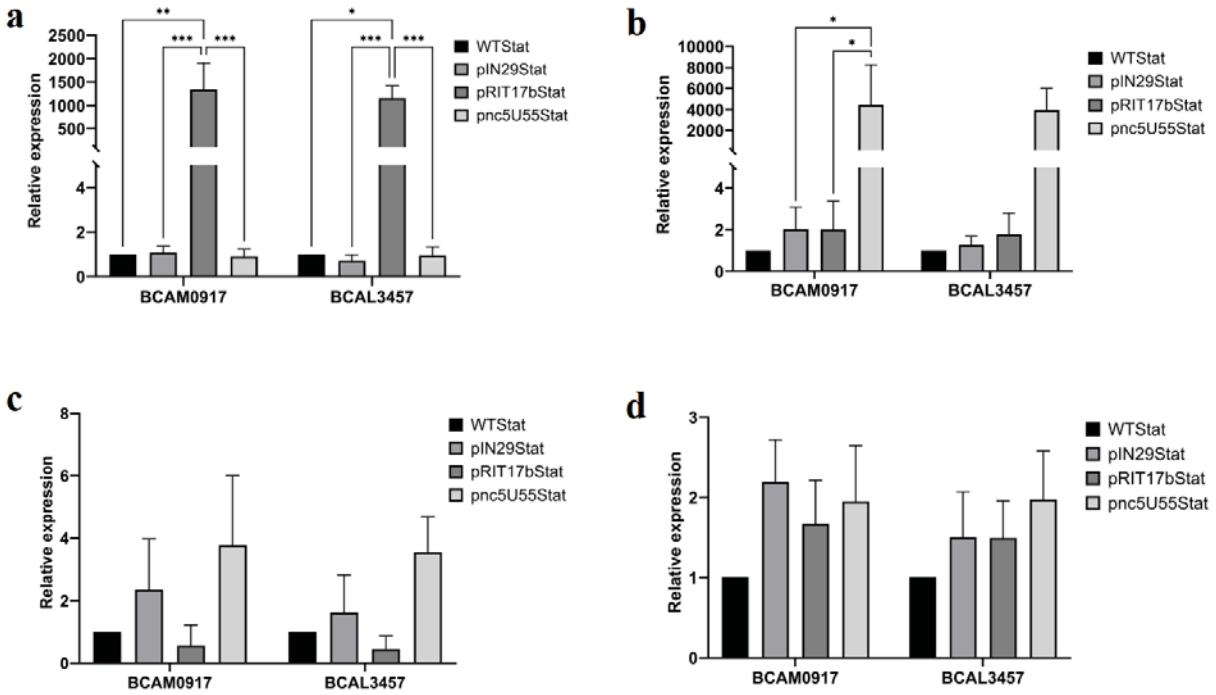

Figure 3.7: RT-PCR results using the genes BCAM0917 and BCAL3457 as reference for normalization. WT, pIN29, pRIT17b and pnc5U55 samples were collected during stationary phase. Two genes (BCAL0527 and BCAS0104) involved in flagellar motility were analyzed. All data is presented as mean + SD. Statistical significance was assessed using two-way ANOVA followed by Tukey's multiple comparisons test. (A) Confirmation of RIT17b overexpression in pRIT17b; (B) Confirmation of nc5U55 overexpression in pnc5U55; (C) Assessment of BCAL0527 expression in WT, pIN29, pRIT17b and pnc5U55. No statistically significant differences were identified; (D) Assessment of BCAS0104 expression in WT, pIN29, pRIT17b and pnc5U55. No statistically significant differences were identified.

Regarding nc5U55, the results suggest a specific role in regulating swimming in particular, having no notable effect on swarming motility. In addition to BCAL0140 and BCAS0104, two other putative targets, BCAL0563 and BCAL0527, encode flagellar components (FlgA and FliS). In **Figure 3.7C**, BCAL0527 appears more highly expressed in pnc5U55, though not significantly, while BCAS0104 expression showed minimal variation among constructs (**Figure 3.7D**). Despite the slight increase in expression of one flagellar gene, swimming motility was reduced, suggesting that nc5U55 may regulate other genes influencing this phenotype. In particular, nc5U55 may negatively regulate *cheA* (BCAL0129), reducing the amount of this histidine kinase essential for flagellum-mediated chemotaxis (Oppy *et al.*, 2019). As swimming motility depends on chemotaxis, any decrease in CheA would impair the signaling cascade that controls flagellar rotation. In E. coli, phosphorylated CheY interacts with FliM to promote clockwise flagellar rotation, whereas downregulation of *cheA* would favor counterclockwise rotation, leading to a "biased random walk" (Muok *et al.*, 2020; Wadhwa & Berg, 2021) and potentially explaining the reduced swimming observed in pnc5U55. Although less plausible, the absence of a swarming phenotype could be linked to nc5U55's potential role in stress response. In *B. glumae*, nutrient stress conditions result in a reduced growth rate and trigger QS-mediated rhamnolipid (biosurfactant)

production, reallocating cellular resources toward survival and surface expansion strategies such as swarming (Nickzad & Déziel, 2016). However, *B. glumae* is a plant pathogen with distinct regulatory mechanisms, and biosurfactant regulation in *B. cenocepacia* remains to be fully elucidated.

3.3.3 MIC determination

To adress the possibility that the selected sRNAs could be involved in the regulation of antibiotic susceptibility, a disk diffusion (DD) assay was first performed to verify whether overexpressing RIT17b or nc5U55 had an effect on CAZ, CIP, TOB, or TET susceptibility. This decision was based mainly on the target prediction results that included resistance-associated genes such as BCAM2186, BCAL1081, BCAM0731, and BCAS0289, as demonstrated in **Supplementary Table 5.1** and **Supplementary Table 5.2**. The assay results were predominantly inconclusive. Tobramycin did not result in an inhibition zone, whereas ciprofloxacin and ceftazidime did not cause notable differences between strains. For tetracycline, pIN29 and pnc5U55, while with similar results to each other, had a marginally smaller inhibition zone when compared to WT. This contrasted with pRIT17b, which appeared to be more susceptible to the antibiotic. The results of this assay initially prompted the testing of TET using the microbroth dilution method, which supported the notion that RIT17b may regulate the expression of genes related to TET resistance.

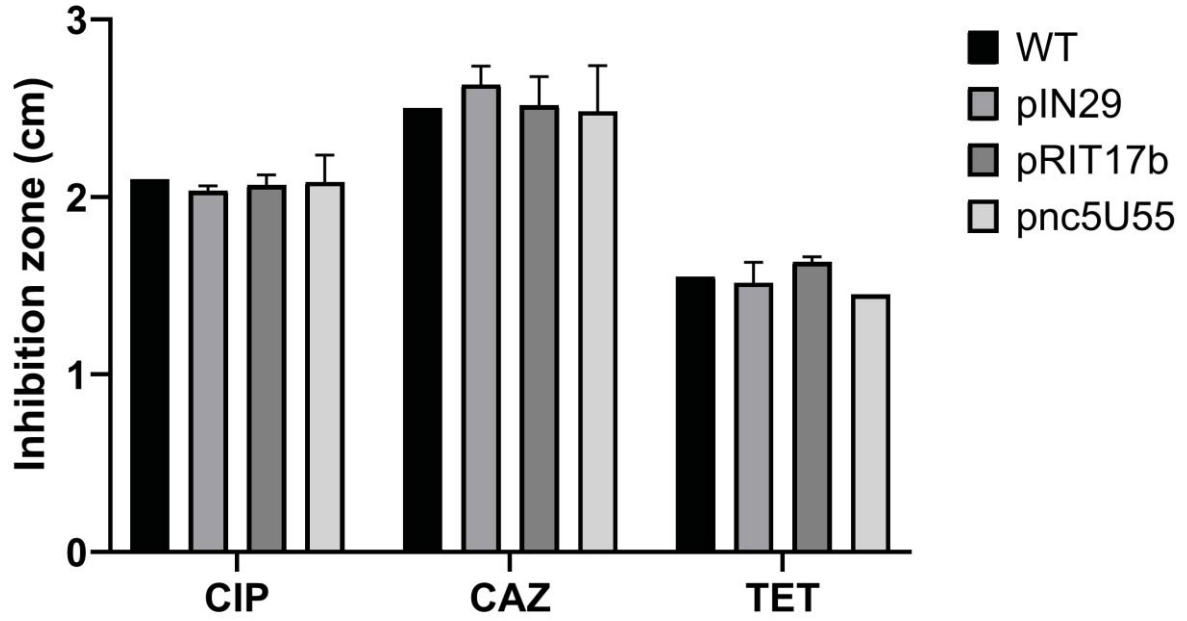

Figure 3.8: Disk diffusion assay results regarding CAZ, CIP and TET susceptibility of WT, pIN29, pRIT17b and pnc5U55. WT is represented by a single sample. All data is presented as mean + SD. Statistical significance was assessed using two-way ANOVA followed by Tukey's multiple comparisons test. Pairwise comparisons between pRIT17b and pnc5U55 were excluded. No statistically significant differences were detected.

Contrary to the DD test results, pIN29 was more susceptible to TET than WT, while pnc5U55 was significantly more resistant than pIN29, indicating that the sRNA may have a role in TET resistance. The variation in susceptibility between pIN29 and pRIT17b was not statistically significant. However, this does not exclude the possibility of RIT17b partially influencing resistance, considering that Bcc resistance to many antibiotics is multi-factorial, contributors of which include low OM permeability and efflux pumps, among others (Scoffone *et al.*, 2017; Lord *et al.*, 2020). The lack of agreement between

these two methods of antimicrobial susceptibility determination (DD assay and broth microdilution) has been denoted in EUCAST guidelines, with emphasis on the fact that DD is particularly not recommended for Bcc bacteria (ESCMID - European Society of Clinical Microbiology and Infectious Diseases 2008, n.d.). This inconsistency across the two assays was noticeable during CIP and CAZ susceptibility testing as well. Although not statistically significant, pRIT17b and nc5U55 also had higher and lower susceptibility to CIP than pIN29, respectively. This further supports the possibility of the two sRNAs playing opposite parts in the regulation of antibacterial resistance (at least against CIP and TET). Conversely, resistance to CAZ appears to decrease with the insertion of the pIN29 plasmid, with WT being demonstrated as the least susceptible of all strains, though not in a statistically significant manner.

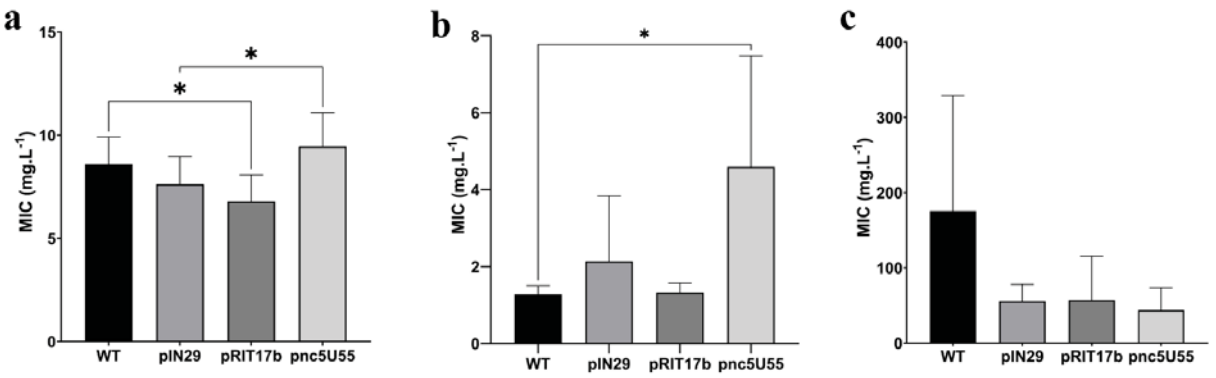

Figure 3.9: MIC determination results for tetracycline, ciprofloxacin and ceftazidime in WT, pIN29, pRIT17b and pnc5U55. All data is presented as mean + SD. Statistical significance was assessed using one-way ANOVA followed by Tukey's multiple comparisons test. (A) TET susceptibility results. The control pIN29 was found to be significantly more susceptible than pnc5U55, while WT was significantly less susceptible than pRIT17b; (B) CIP susceptibility results. WT was found to be significantly more susceptible than pnc5U55; (C) CAZ susceptibility results. No statistically significant differences were identified.

There was a partial increase in CIP and TET susceptibility for pRIT17b, in which certain components of efflux systems could have had their expression modulated, including the multidrug resistance protein MdtA (BCAL1081), a RND-6 efflux transporter (Coenye *et al.*, 2011), and a macrolide-specific efflux system protein (BCAM2186). Other than these, an ATP-binding protein (BCAM2350) and a substrate-binding protein (BCAM1973) belonging to ABC transporters, commonly known to promote multi-drug resistance (Akhtar & Turner, 2022), were also listed. Alternatively, this sRNA might regulate BCAL3473, a gene encoding a putative outer membrane porin, BCAS0768 of the AraC family, which has been identified as a regulator of a RND-2 efflux pump (Scoffone *et al.*, 2021), or BCAL2812, a Fur transcriptional regulator and possible promoter of multi-drug resistance (McCarthy *et al.*, 2010). BCAL3473 has been previously identified to be constitutively downregulated by the *B. cenocepacia* small RNA NcS25 (A. M. Sass & Coenye, 2023). Given the context of increased susceptibility to TET and CIP, RIT17b may upregulate BCAL3473 expression, resulting in increased permeability of the OM and antibiotic influx. On the other hand, RIT17b overexpression could result in the repression of MdtA and the RND-2 efflux pump regulated by BCAS0768, which have been shown to contribute to reduced fluoroquinolone susceptibility. RND-2 efflux systems also promote tetracycline resistance (Scoffone *et al.*, 2021). RIT17b was also predicted to target other transcriptional regulators aside from BCAS0768 that could potentially impact antibiotic susceptibility, among them being the TetR protein BCAL1182, seeing as this family of repressors has been denoted to play a role in multi-drug resistance as well (Ramos *et al.*, 2005). Furthermore, RIT17b and nc5U55 could target BCAL2693. Though not much is known about its function, LysR-type proteins can be linked to antibiotic resistance (Fu *et al.*, 2019). Another LysR protein within the same species is BCAM2554, a potential paralog gene and a RND efflux pump regulator that is located upstream from the ceoB cluster (BCAM2549-2552), which promotes

resistance to certain antibiotics, including ciprofloxacin (Tseng *et al.*, 2014; Gamberi *et al.*, 2013). As previously stated, nc5U55 may be linked to stress response regulation through a variety of processes, which in turn could assist in promoting antimicrobial resistance. A connection between the regulation of other stress responses and efflux pump systems has been made in other studies (Brand *et al.*, 2025), with the activation of *P. aeruginosa* RND efflux pumps in iron-limiting conditions as an example (Drevinek *et al.*, 2008). Additionally, this small RNA shares other targets with RIT17b, particularly BCAL2812 and BCAM2186, possibly leading to their upregulation rather than repression. Other than those, it may also regulate BCAS0289, a MFS efflux transporter involved in antibiotic resistance, and BCAM2035, a putative glycosyltransferase that has been denoted as being part of a potential surface polysaccharides biosynthetic cluster, likely related to LPS and capsular polysaccharide synthesis (Holden *et al.*, 2008). Additionally, it may repress BCAM0731, a regulatory protein from the MarR family. MarR proteins function as repressors of the *mar* operon, which is induced by environmental signals such as compounds like tetracycline. When this action is inactivated, the operon is constitutively expressed, culminating in porin repression and the positive regulation of cytoprotective enzymes and efflux pump synthesis (Alekshun & Levy, 1999). As stated before, LPS composition has been linked to antibiotic resistance in Bcc, whether it be through acquired mutations or key structural components such as L-Ara4N. These residues in particular confer resistance to cationic compounds such as polymyxins by reducing the anionic charge of the bacterial envelope (Vinion-Dubiel & Goldberg, 2003). The sRNA nc5U55 could also regulate two distinct ATP binding proteins and a putative permease (BCAM2017, BCAS0340, and BCAM2528), components of ABC transporters and potential promoters of resistance (Akhtar & Turner, 2022).

3.3.4 *Caenorhabditis elegans* assay

An assay using *C. elegans* was performed with the intention of analyzing the effect of the selected sRNAs on *B. cenocepacia* virulence given the identification of multiple predicted targets with the potential to impact this functional category. Among them are flagellar genes and those related to antimicrobial resistance, which will generally not be discussed as they have already been analysed in prior sections. Other potential targets will be explored in further detail, including those related to bacterial secretion systems as well as those found to be differently regulated in the context of infection. This particular infection model was selected due to its simplicity, broad usage in Bcc studies, as well as the great percentage of human homologous genes that exist in *C. elegans* (Pita *et al.*, 2023). Ortholist2 (W. Kim *et al.*, 2018) was then used in order to inspect whether any of the potential human targets had any orthologs in *C. elegans* (**Supplementary Table 5.5**). Interestingly, RIT17b targets resulted in a higher number of matches than nc5U55. Some of the identified orthologs matched with targets that had already been discussed as possible participants in the modulation of the host's immune response, with UNKL and PPIA representing the most significant examples. These findings were used as an additional justification for the execution of this assay.

During the initial days of observation, no particular differences in behavior or development were observed between nematodes. However, contrary to the expected outcome, the *C. elegans* used in the assay generated offspring despite possessing a genetic mutation that, under standard conditions, would prevent reproductive activity. This could be explained by a possible reversion of the mutation, or alternatively by an experimental error such as the inability to maintain the incubation temperature at 25 °C, thereby favoring *C. elegans* reproduction. Although the experiment did not occur as intended, the outcome was nevertheless recorded due to some results being worthy of mention. As can be seen in **Figure 3.10C**, pnc5U55 did not exhibit any substantial effect on the nematodes, which in turn carried

out their reproductive cycle similarly to what was observed with the WT. Albeit not as evident in the pictures, the *C. elegans* present in the WT generally produced a greater amount of progeny. Interestingly, pIN29 had a significantly smaller number of offspring, with a mixed population of larger nematodes similar to the ones found in WT and pnc5U55 plates and thinner nematodes like most of the population belonging to the pRIT17b conditions. In fact, pRIT17b also resulted in the lowest quantity of descendants, indicating that there might have been a greater impact on the *C. elegans* physiological state with a subsequent adaptive stress response to infection, as has been documented before (Bollen *et al.*, 2023).

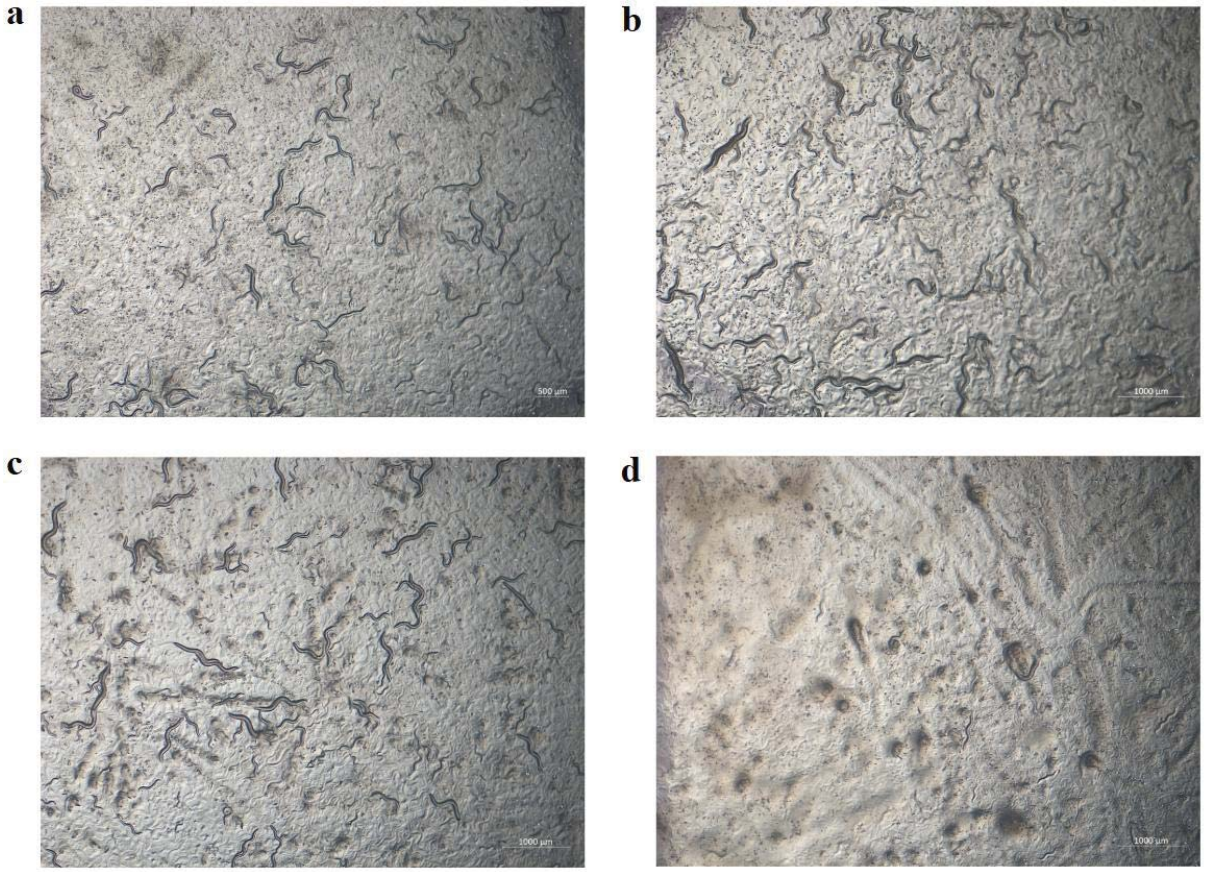

Figure 3.10: Results of the assay performed on *C. elegans* following the infection of (A) WT, (B) pIN29, (C) pnc5U55 and (D) pRIT17b. WT and pnc5U55 displayed similar results, while pRIT17b infection appeared to impact the physiological state of *C. elegans* the most, leading to the production fewer offspring.

Since the reproduction-deficient *C. elegans* strain produced an innumerable amount of progeny, only relative differences between conditions could be inferred. Nonetheless, certain arguments can be cautiously presented to justify these results based on the premise that nc5U55 and RIT17b may potentially repress and upregulate virulence promoting genes in *B. cenocepacia*, respectively. RIT17b was predicted to target a variety of genes that may promote bacterial virulence, among them BCAM1330, which is induced during chronic lung infection (O'Grady, 2011) and may be upregulated in pRIT17b. Other genes that have already been addressed in another context and that might be involved in virulence are BCAM1973, BCAL3473, BCAL3122, and BCAL0399. The substrate-binding protein BCAM1973 was shown to be downregulated during infection in *C. elegans* (Pita *et al.*, 2023), a fact that is in line with what was surmised in the prior section, seeing as RIT17b might cause a partial increase in antibiotic susceptibility by negatively regulating ABC transporter activity. BCAL3473 was also found to be induced in chronic lung infection (O'Grady, 2011), having been previously predicted to be

upregulated as a result of RIT17b overexpression. Presumably, the upregulation of an important protein in nitrogen metabolism (A. M. Sass & Coenye, 2023) could also promote virulence, especially in the absence of antibiotics. The LPS of Bcc bacteria are able to induce strong immune reactions in the host through the lipid A portion of the molecule (Gunardi et al., 2021). Certain strains from the ET12 lineage like J2315 do not possess the O antigen, highlighting its unessential role in virulence (Loutet & Valvano, 2010). On the other hand, it has been proposed that this aspect may contribute to their increased invasiveness (Saldías *et al.*, 2009), meaning that the downregulation of the glycosyltransferase BCAL3122 may not only result in increased biofilm production but also promote virulence. Furthermore, O antigen biosynthesis has been denoted to attenuate virulence in *C. elegans* (Pita *et al.*, 2023). BCAL0399 was formerly discussed as a possible contributor to the reduced swimming motility that was observed. Although not related to *C. elegans* infection, this gene has been investigated as a potential promoter of *B. cenocepacia* H111 fitness in the *Galleria mellonella* and *ex vivo* pig lung (EVPL) models due to tryptophan synthesis being a vital process in *P. aeruginosa* virulence. In their experiment, Paszti *et al.* (2025) only detected significantly attenuated killing in the *G. mellonella* model, though it was noted that BCAL0399 is in the same operon as BCAL0398, an essential fitness gene in both models. Other two core fitness determinants that were identified are also included in the potential target list of RIT17b: BCAL0667, involved in biotin synthesis, and BCAL1927, an aminotransferase that is also upregulated during infection in *C. elegans* (Pita *et al.*, 2023). It is currently unknown if BCAL0399 and BCAL0667 could have any impact during infection in *C. elegans*. The putative target BCAM0459, a cysteine desulfurase, was another gene revealed to be induced during chronic lung infection (O'Grady, 2011), possibly benefitting the bacterium through protection against oxidative stress and even promotion of pathogenesis, aside from other housekeeping functions. It should be said that this housekeeping role is fundamentally linked to the importance of cysteine desulfurases in Fe-S cluster biosynthesis, which will in turn become cofactors to multiple enzymes (Das *et al.*, 2021). RIT17b could also upregulate a protein of the T6SS (BCAL0351), a secretion system involved in the actin rearrangement of macrophages, the induction of the host's inflammatory response, as well as indirectly contributing to Bcc survival by facilitating the secretion of T2SS effectors, among other functions (Leitão et al., 2017). Despite not having been directly validated in *B. cenocepacia*, T6SS effectors and structural components have been shown to be contributors of virulence toward C. elegans in other bacteria (Khan *et al.*, 2023; Yang *et al.*, 2022). A paralogous gene of the primary σ^{70} factor was predicted as a target of the sRNA as well. EcfD (BCAL2360) is expressed under iron-limiting conditions, which are often associated with host infection, regulating siderophore production and thus assisting in bacterial survival. This gene was also found to be upregulated during *B. cenocepacia* infection in *C. elegans* (Pita *et al.*, 2023). OrbE (BCAL1695) was a putative target shared by both sRNAs that is also associated with iron acquisition, more specifically with the transmembrane transport of siderophores, possessing similar characteristics to ABC transporters (Thomas, 2007). There were other predicted targets that were found to be upregulated during infection in *C. elegans* but have yet to be extensively characterized (Pita *et al.*, 2023). Of these, BCAL2984, a family C26 cysteine peptidase, BCAL0375, a glutamyl-tRNA reductase, and BCAL0042, a multifunctional enzyme, could have an indirect influence on virulence by exercising a more metabolism-related function that would contribute to bacterial survival. In contrast, the putative lipoprotein BCAL0200 might promote adhesion or be involved in the modulation of the host's immune response during infection (Nakayama *et al.*, 2012), especially since it is described as an extracellular protein in the *Burkholderia* Genome Database (Winsor *et al.*, 2008). Some of the potential regulatory targets of nc5U55 that are upregulated in the context of infection in *C. elegans* have already been mentioned, including BCAL0423a and BCAL3302, previously speculated to be repressed in rich medium, contributing to the attenuated growth that was observed, and BCAM0731, also presumed to be possibly downregulated by nc5U55 due to the higher resistance of pnc5U55 to TET. Certain MarR family proteins have also been denoted to be regulators of virulence-related genes in Bcc species by

sensing host-derived signals (Gupta *et al.*, 2018). Aside from the synthesis of the O antigen, it has been noted that certain genes implicated in QS, as well as stress responses and nutrient uptake can also lead to reduced virulence in *C. elegans* (Pita *et al.*, 2023). All of these processes could plausibly be linked to the regulatory action of nc5U55, particularly in the case of a reallocation of resources in order to prioritize survival. Other virulence-associated targets were predicted, among them BCAM2140, a membrane transporter, in addition to BCAM2045 and BCAM2050, two BDSF-regulated T3SS proteins (McCarthy *et al.*, 2010). BCAM2140 is a QS-regulated gene that is part of a cluster encoding a T1SS involved in biofilm formation (Inhülsen *et al.*, 2012). Considering the minimal effect of nc5U55 in biofilm production, it is unlikely that this sRNA significantly influences this gene's expression. On the other hand, the T3SS has been predicted to promote the intracellular survival of *B. cenocepacia* (Leitão *et al.*, 2017) as well as being a key determinant in Bcc pathogenesis and possibly involved in the evasion of the host's immune system (Tomich *et al.*, 2003). Particularly, BcscK (BCAM2050) has been found to have increased expression in bloodstream bacterial isolates, further drawing a connection between the T3SS and bacterial protection against host defense mechanisms (Kalferstova *et al.*, 2015). Within the predicted target list are also envelope-associated proteins such as a putative OmpA/MotB family outer membrane protein (BCAM2255). OmpA is a porin that is essential for membrane integrity and defense against osmotic stress (Zhou *et al.*, 2023). Its downregulation is often associated with higher envelope stress, leading to increased EV production in bacteria like *Vibrio cholerae* (Song *et al.*, 2008), as well as lower membrane permeability and higher susceptibility to certain antibiotics (Zhou *et al.*, 2023). On the other hand, OmpA overexpression can be connected to infection (Sánchez-Encinales *et al.*, 2017), seeing as this type of porins has been found to play a role in the virulence of many pathogens, including *B. cenocepacia* (S. A. Sousa *et al.*, 2016). Given that nc5U55 elicited no increase in EV yield, antimicrobial susceptibility or virulence in the performed assays, it is unlikely that BCAM2255 is being regulated by the small RNA.

4. Final Remarks

To summarize, RIT17b overexpression was shown to possibly enhance biofilm formation, tetracycline and ciprofloxacin susceptibility, and potentially increase virulence, as well as reduce motility. The outcome of the performed phenotypic assays led to the conclusion that the regulatory action of RIT17b could possibly be linked to the promotion of pathogenesis through virulence-related strategies such as biofilm formation. In fact, increased biofilm production was the most significant distinction of pRIT17b and may be the primary effect of its post-transcriptional regulation. As was discussed earlier, during the switch to a sessile lifestyle, motility-associated genes can be repressed in favor of the activation of biofilm pathways (Dressaire *et al.*, 2015), as was seen to be the case with the partial downregulation of BCAL0527, a gene not included in the putative target list of the sRNA. It could additionally be that, by potentially being predisposed toward biofilm formation, pRIT17b is more susceptible to certain antimicrobial drugs when in a planktonic state. For instance, Gu *et al.* (2019) found that *E. coli* RP437 exhibited increased susceptibility to antibiotics in comparison to planktonic cells during the earlier stages of biofilm formation, particularly during initial adhesion and during the transition stage to microcolony formation. At the time when irreversible attachment to a surface takes place, there is often the previously described switch to a nonmotile lifestyle which demands distinct regulation pathways with a strategic reallocation of cellular resources. It is only after those initial stages of cell-cell interactions, when there is an active production of the biofilm matrix that protects the bacterial cells, that antibiotic susceptibility lowers. The formed biofilm would then possess other defense strategies against antimicrobial compounds other than a physical barrier that reduces their penetration, among them being the stratification of metabolic activity, the formation of persister cells and the upregulation

of resistance-associated genes (Azeem *et al.*, 2025). On the other hand, pnc5U55 demonstrated reduced growth in rich medium (LB) but not minimal medium (M9), attenuated swimming motility but not swarming, and enhanced resistance against ciprofloxacin and tetracycline. Lastly, nc5U55 may also cause lower virulence, though it is not certain. From these results, it was proposed that this sRNA may play a role in stress response and antibiotic resistance, possibly resulting in a shift of metabolic investment toward survival under stress when overexpressed. Alternatively, there are other *B. cenocepacia* sRNAs that have been identified to impact bacterial growth. For example, A. M. Sass *et al.* (2019) discovered that the overexpression of NcS27 caused decreased growth on substrates such as phenylalanine, tyrosine, glycerol and galactose, and that the regulation of genes involved in those metabolic pathways could result in growth inhibition on rich media. However, this inhibition did not occur in minimal media supplemented with other individual carbon compounds, which could be another potential justification for the observed behavior of pnc5U55 in M9. To further assess the impact of this sRNA, additional assays involving other stress response pathways or the analysis of metabolic function, such as carbon source utilization, could have been performed.

Regarding EV production and relative quantification results, many questions were still left unanswered. As was mentioned, it would be ideal in future studies to perform RNA-seq following EV isolation, specifically with the intention of comparing how different conditions, from the inflicted stress to the media used during the assay, affect vesiculation and the incorporation of EV cargo. An additional aspect involving relative EV quantification during the phenotypic tests of pRIT17b and pnc5U55 that was not analyzed would be whether EV production would change under antibiotic stress. Presumably, this change would be relatively consistent with the reported results. Also concerning the phenotypic assays that were performed on pnc5U55 and pRIT17b, it would be essential to repeat the experiments to ensure reliability and reproducibility. For future studies, experimentally verifying if the selected sRNAs and their human targets truly interact would be crucial as well. To this effect, an electrophoretic mobility shift assay (EMSA) could be performed to analyze RNA-RNA interactions *in vitro* (Bak *et al.*, 2014), though this may not completely reflect the *in vivo* conditions in which this process might occur. Alternatively, this interaction could be surveyed through sRNA reporters, using epithelial cell lines in place of *in vivo* infection models. It could also be relevant to compare the expression of predicted targets of interest by performing RT-PCR after the interaction with the sRNAs or after the delivery of EVs isolated from pRIT17b or pnc5U55. For other alternatives that could mimic more rigorously the environment where infection takes place, it has been expressed that it is quite challenging to accurately develop *ex vivo* models of chronic Bcc infections in the CF lung that are also consistent among each other in regard to conserved virulence determinants (Zlosnik *et al.*, 2014). *In vivo* experiments could be conducted as well on a mouse infection model by transfecting HBE (Human Bronchial Epithelial) cells with RIT17b or nc5U55, similarly to what was achieved by Koeppen *et al.* (2016) with sRNA-52320.

5. References

Aiyer, A., & Manos, J. (2022). The use of artificial sputum media to enhance investigation and subsequent treatment of cystic fibrosis bacterial infections. Microorganisms, 10(7), 1269. https://doi.org/10.3390/microorganisms10071269

Ajam-Hosseini, M., Akhoondi, F., Parvini, F., & Fahimi, H. (2024). Gram-negative bacterial sRNAs encapsulated in OMVs: an emerging class of therapeutic targets in diseases. Frontiers in Cellular and Infection Microbiology, 13. https://doi.org/10.3389/fcimb.2023.1305510

Akhtar, A. A., & Turner, D. P. (2022). The role of bacterial ATP-binding cassette (ABC) transporters in pathogenesis and virulence: Therapeutic and vaccine potential. Microbial Pathogenesis, 171, 105734. https://doi.org/10.1016/j.micpath.2022.105734

Alekshun, M. N., & Levy, S. B. (1999). The mar regulon: multiple resistance to antibiotics and other toxic chemicals. Trends in Microbiology, 7(10), 410–413. https://doi.org/10.1016/s0966-842x(99)01589-9

AlRabiah, H., Allwood, J. W., Correa, E., Xu, Y., & Goodacre, R. (2018). pH plays a role in the mode of action of trimethoprim on *Escherichia coli*. PLoS ONE, 13(7), e0200272. https://doi.org/10.1371/journal.pone.0200272

Amano, A., Takeuchi, H., & Furuta, N. (2010). Outer membrane vesicles function as offensive weapons in host–parasite interactions. Microbes and Infection, 12(11), 791–798. https://doi.org/10.1016/j.micinf.2010.05.008

Azeem, K., Fatima, S., Ali, A., Ubaid, A., Husain, F. M., & Abid, M. (2025). Biochemistry of Bacterial Biofilm: Insights into Antibiotic Resistance Mechanisms and Therapeutic Intervention. Life, 15(1), 49. https://doi.org/10.3390/life15010049

Badi, S. A., Bruno, S. P., Moshiri, A., Tarashi, S., Siadat, S. D., & Masotti, A. (2020). Small RNAs in outer membrane vesicles and their function in Host-Microbe interactions. Frontiers in Microbiology, 11. https://doi.org/10.3389/fmicb.2020.01209

Baeza, N., Delgado, L., Comas, J., & Mercade, E. (2021). Phage-Mediated Explosive Cell Lysis Induces the Formation of a Different Type of O-IMV in *Shewanella vesiculosa* M7T. Frontiers in Microbiology, 12. https://doi.org/10.3389/fmicb.2021.713669

Bak, G., Han, K., Kim, K., & Lee, Y. (2014). Electrophoretic mobility shift assay of RNA–RNA complexes. Methods in Molecular Biology, 153–163. https://doi.org/10.1007/978-1-4939-1896-6_12

Banerjee, R. (2025). Tiny but mighty: small RNAs—The micromanagers of bacterial survival, virulence, and Host–Pathogen interactions. Non-Coding RNA, 11(3), 36. https://doi.org/10.3390/ncrna11030036

Battesti, A., Majdalani, N., & Gottesman, S. (2010). The RpoS-Mediated General Stress Response in *Escherichia coli*. Annual Review of Microbiology, 65(1), 189–213. https://doi.org/10.1146/annurev-micro-090110-102946

Berghoff, B., Klug, G. (2012). Small RNAs with a Role in the Oxidative Stress Response of Bacteria. In: Regulatory RNAs in Prokaryotes. Springer, Vienna. https://doi.org/10.1007/978-3-7091-0218-3_1

BICRAL BICRA like chromatin remodeling complex associated protein. (2025, February 8). NCBI. https://www.ncbi.nlm.nih.gov/gtr/genes/23506/

Bollen, D. P., Reddy, K. C., Lascarez-Lagunas, L. I., Kim, D. H., & Colaiácovo, M. P. (2023). Germline mitotic quiescence and cell death are induced in *Caenorhabditis elegans* by exposure to pathogenic *Pseudomonas aeruginosa*. Genetics, 226(1). https://doi.org/10.1093/genetics/iyad197

Bos, J., Cisneros, L. H., & Mazel, D. (2021). Real-time tracking of bacterial membrane vesicles reveals enhanced membrane traffic upon antibiotic exposure. Science Advances, 7(4). https://doi.org/10.1126/sciadv.abd1033

Bose, S., Aggarwal, S., Singh, D. V., & Acharya, N. (2020). Extracellular vesicles: An emerging platform in gram-positive bacteria. Microbial Cell, 7(12), 312–322. https://doi.org/10.15698/mic2020.12.737

Brand, C., Newton-Foot, M., Grobbelaar, M., & Whitelaw, A. (2025). Antibiotic-induced stress responses in Gram-negative bacteria and their role in antibiotic resistance. Journal of Antimicrobial Chemotherapy. https://doi.org/10.1093/jac/dkaf068

Buroni, S., Matthijs, N., Spadaro, F., Van Acker, H., Scoffone, V. C., Pasca, M. R., Riccardi, G., & Coenye, T. (2014). Differential Roles of RND Efflux Pumps in Antimicrobial Drug Resistance of Sessile and Planktonic *Burkholderia cenocepacia* Cells. Antimicrobial Agents and Chemotherapy, 58(12), 7424–7429. https://doi.org/10.1128/aac.03800-14

Busch, A., Richter, A. S., & Backofen, R. (2008). IntaRNA: efficient prediction of bacterial sRNA targets incorporating target site accessibility and seed regions. Bioinformatics, 24(24), 2849–2856. https://doi.org/10.1093/bioinformatics/btn544

Charpentier, L. A., Dolben, E. F., Hendricks, M. R., Hogan, D. A., Bomberger, J. M., & Stanton, B. A. (2023). Bacterial outer membrane vesicles and immune modulation of the host. Membranes, 13(9), 752. https://doi.org/10.3390/membranes13090752

Chen, K., & Kolls, J. K. (2017). InterLuekin-17A (IL17A). Gene, 614, 8–14. https://doi.org/10.1016/j.gene.2017.01.016

Childs-Disney, J. L., Yang, X., Gibaut, Q. M. R., Tong, Y., Batey, R. T., & Disney, M. D. (2022). Targeting RNA structures with small molecules. Nature Reviews Drug Discovery, 21(10), 736–762. https://doi.org/10.1038/s41573-022-00521-4

Choi, J., Kim, S., Hong, S., & Lee, H. (2017). Secretable small RNAs via outer membrane vesicles in periodontal pathogens. Journal of Dental Research, 96(4), 458–466. https://doi.org/10.1177/0022034516685071

Choi, J., Um, J., Cho, J., & Lee, H. (2017). Tiny RNAs and their voyage via extracellular vesicles: Secretion of bacterial small RNA and eukaryotic microRNA. Experimental Biology and Medicine, 242(15), 1475–1481. https://doi.org/10.1177/1535370217723166

Coenye, T., Van Acker, H., Peeters, E., Sass, A., Buroni, S., Riccardi, G., & Mahenthiralingam, E. (2011). Molecular Mechanisms of Chlorhexidine Tolerance in *Burkholderia cenocepacia* Biofilms. Antimicrobial Agents and Chemotherapy, 55(5), 1912–1919. https://doi.org/10.1128/aac.01571-10

Coleman, S. R., Smith, M. L., Spicer, V., Lao, Y., Mookherjee, N., & Hancock, R. E. W. (2020). Overexpression of the Small RNA PA0805.1 in *Pseudomonas aeruginosa* Modulates the Expression of a Large Set of Genes and Proteins, Resulting in Altered Motility, Cytotoxicity, and Tobramycin Resistance. mSystems, 5(3). https://doi.org/10.1128/msystems.00204-20

Combo, S., Mendes, S., Nielsen, K. M., Da Silva, G. J., & Domingues, S. (2022). The Discovery of the Role of Outer Membrane Vesicles against Bacteria. Biomedicines, 10(10), 2399. https://doi.org/10.3390/biomedicines10102399

Dabral, D., & Van Den Bogaart, G. (2021). The roles of phospholipase A2 in phagocytes. Frontiers in Cell and Developmental Biology, 9. https://doi.org/10.3389/fcell.2021.673502

Darling, P., Chan, M., Cox, A. D., & Sokol, P. A. (1998). Siderophore Production by Cystic Fibrosis Isolates of *Burkholderia cepacia*. Infection and Immunity, 66(2), 874–877. https://doi.org/10.1128/iai.66.2.874-877.1998

Das, M., Dewan, A., Shee, S., & Singh, A. (2021). The multifaceted bacterial cysteine desulfurases: from metabolism to pathogenesis. Antioxidants, 10(7), 997. https://doi.org/10.3390/antiox10070997

De Palma, F. D. E., Raia, V., Kroemer, G., & Maiuri, M. C. (2020). The multifaceted roles of MicroRNAs in cystic fibrosis. Diagnostics, 10(12), 1102. https://doi.org/10.3390/diagnostics10121102

Delihas, N., & Forst, S. (2001). MicF : an antisense RNA gene involved in response of *Escherichia coli* to global stress factors 1 Edited by D. Draper. Journal of Molecular Biology, 313(1), 1–12. https://doi.org/10.1006/jmbi.2001.5029

Deng, Y., Boon, C., Eberl, L., & Zhang, L. (2009). Differential modulation of *Burkholderia cenocepacia* Virulence and energy metabolism by the Quorum-Sensing Signal BDSF and its synthase. Journal of Bacteriology, 191(23), 7270–7278. https://doi.org/10.1128/jb.00681-09

Deng, Y., Wu, J., Eberl, L., & Zhang, L. (2010). Structural and Functional Characterization of Diffusible Signal Factor Family Quorum-Sensing Signals Produced by Members of the *Burkholderia cepacia* Complex. Applied and Environmental Microbiology, 76(14), 4675–4683. https://doi.org/10.1128/aem.00480-10

DéZiel, E., Comeau, Y., & Villemur, R. (2001). Initiation of Biofilm Formation by *Pseudomonas aeruginosa* 57RP Correlates with Emergence of Hyperpiliated and Highly Adherent Phenotypic Variants Deficient in Swimming, Swarming, and Twitching Motilities. Journal of Bacteriology, 183(4), 1195–1204. https://doi.org/10.1128/jb.183.4.1195-1204.2001

Dörr, T., Lewis, K., & Vulić, M. (2009). SOS Response Induces Persistence to Fluoroquinolones in *Escherichia coli*. PLoS Genetics, 5(12), e1000760. https://doi.org/10.1371/journal.pgen.1000760

DoubleDigest Calculator | Thermo Fisher Scientific - US. (n.d.). https://www.thermofisher.com/pt/en/home/brands/thermo-scientific/molecular-biology/thermo-scientific-restriction-modifying-enzymes/restriction-enzymes-thermo-scientific/double-digest-calculator-thermo-scientific.html

Dressaire, C., Moreira, R. N., Barahona, S., De Matos, A. P. A., & Arraiano, C. M. (2015). BOLA is a transcriptional switch that turns off motility and turns on biofilm development. mBio, 6(1). https://doi.org/10.1128/mbio.02352-14

Drevinek, P., Holden, M. T., Ge, Z., Jones, A. M., Ketchell, I., Gill, R. T., & Mahenthiralingam, E. (2008). Gene expression changes linked to antimicrobial resistance, oxidative stress, iron depletion and retained motility are observed when *Burkholderia cenocepacia* grows in cystic fibrosis sputum. BMC Infectious Diseases, 8(1). https://doi.org/10.1186/1471-2334-8-121

ESCMID - European Society of Clinical Microbiology and Infectious Diseases 2008. (n.d.). eucast: Guidance Documents. https://www.eucast.org/eucastguidancedocuments

Everaert, A., & Coenye, T. (2016). Effect of β-Lactamase inhibitors on in vitro activity of β-Lactam antibiotics against *Burkholderia cepacia* complex species. Antimicrobial Resistance and Infection Control, 5(1). https://doi.org/10.1186/s13756-016-0142-3

Fazli, M., McCarthy, Y., Givskov, M., Ryan, R. P., & Tolker-Nielsen, T. (2012). The exopolysaccharide gene cluster Bcam1330–Bcam1341 is involved in *Burkholderia cenocepacia* biofilm formation, and its expression is regulated by c-di-GMP and Bcam1349. MicrobiologyOpen, 2(1), 105–122. https://doi.org/10.1002/mbo3.61

Flannagan, R. S., & Valvano, M. A. (2008). *Burkholderia cenocepacia* requires RpoE for growth under stress conditions and delay of phagolysosomal fusion in macrophages. Microbiology, 154(2), 643–653. https://doi.org/10.1099/mic.0.2007/013714-0

Frantz, R., Teubner, L., Schultze, T., La Pietra, L., Müller, C., Gwozdzinski, K., Pillich, H., Hain, T., Weber-Gerlach, M., Panagiotidis, G., Mostafa, A., Weber, F., Rohde, M., Pleschka, S.,

Chakraborty, T., & Mraheil, M. A. (2019). The secRNome of *Listeria monocytogenes* Harbors Small Noncoding RNAs That Are Potent Inducers of Beta Interferon. mBio, 10(5). https://doi.org/10.1128/mbio.01223-19

Fu, Y., Cai, Q., Wang, Y., Li, W., Yu, J., Yang, G., Lin, W., & Lin, X. (2019). Four LysR-type transcriptional regulator family proteins (LTTRs) involved in antibiotic resistance in *Aeromonas hydrophila*. World Journal of Microbiology and Biotechnology, 35(8). https://doi.org/10.1007/s11274-019-2700-3

Furuyama, N., & Sircili, M. P. (2021). Outer Membrane vesicles (OMVs) produced by Gram-Negative bacteria: structure, functions, biogenesis, and vaccine application. BioMed Research International, 2021, 1–16. https://doi.org/10.1155/2021/1490732

Gallegos, M. T., Schleif, R., Bairoch, A., Hofmann, K., & Ramos, J. L. (1997). Arac/XylS family of transcriptional regulators. Microbiology and Molecular Biology Reviews, 61(4), 393–410. https://doi.org/10.1128/mmbr.61.4.393-410.1997

Gamberi, T., Gamberi, T., Magherini, F., Citti, L., Buroni, S., Bazzini, S., Udine, C., Perrin, E., Modesti, A., Fani, R., Rocchiccioli, S., & Papaleo, M. C. (2013). RND-4 efflux transporter gene deletion in *Burkholderia cenocepacia* J2315: a proteomic analysis. Journal of Proteome Science and Computational Biology, 2(1), 1. https://doi.org/10.7243/2050-2273-2-1

Gamper, C. J., Agoston, A. T., Nelson, W. G., & Powell, J. D. (2009). Identification of DNA methyltransferase 3A as a T Cell Receptor-Induced regulator of TH1 and TH2 differentiation. The Journal of Immunology, 183(4), 2267–2276. https://doi.org/10.4049/jimmunol.0802960

Girgis, H. S., Liu, Y., Ryu, W. S., & Tavazoie, S. (2007). A comprehensive genetic characterization of bacterial motility. PLoS Genetics, 3(9), e154. https://doi.org/10.1371/journal.pgen.0030154

Gislason, A. S., Choy, M., Bloodworth, R. a. M., Qu, W., Stietz, M. S., Li, X., Zhang, C., & Cardona, S. T. (2016). Competitive Growth Enhances Conditional Growth Mutant Sensitivity to Antibiotics and Exposes a Two-Component System as an Emerging Antibacterial Target in *Burkholderia cenocepacia*. Antimicrobial Agents and Chemotherapy, 61(1). https://doi.org/10.1128/aac.00790-16

Gislason, A. S., Turner, K., Domaratzki, M., & Cardona, S. T. (2017). Comparative analysis of the *Burkholderia cenocepacia* K56-2 essential genome reveals cell envelope functions that are uniquely required for survival in species of the genus *Burkholderia*. Microbial Genomics, 3(11). https://doi.org/10.1099/mgen.0.000140

Gonsalves, L. J., Tran, A., Gardiner, T., Freeman, T., Dutta, A., Miller, C. J., McNamara, S., Waalkes, A., Long, D. R., Salipante, S. J., Hoffman, L. R., & Wolter, D. J. (2024). Mechanisms of *Staphylococcus aureus* survival of trimethoprim-sulfamethoxazole-induced thymineless death. mBio, 15(11). https://doi.org/10.1128/mbio.01634-24

Grove, A. (2022). Extracytoplasmic function sigma factors governing production of the primary siderophores in pathogenic *Burkholderia* species. Frontiers in Microbiology, 13. https://doi.org/10.3389/fmicb.2022.851011

Gu, H., Lee, S. W., Carnicelli, J., Jiang, Z., & Ren, D. (2019). Antibiotic Susceptibility of *Escherichia coli* Cells during Early-Stage Biofilm Formation. Journal of Bacteriology, 201(18). https://doi.org/10.1128/jb.00034-19

Gunardi, W. D., Timotius, K. H., Natasha, A., & Evriarti, P. R. (2021). Biofilm Targeting Strategy in the Eradication of *Burkholderia* Infections: A Mini-Review. The Open Microbiology Journal, 15(1), 51–57. https://doi.org/10.2174/1874285802115010051

Gupta, A., Pande, A., Sabrin, A., Thapa, S. S., Gioe, B. W., & Grove, A. (2018). MarR Family Transcription Factors from *Burkholderia* Species: Hidden Clues to Control of Virulence-Associated Genes. Microbiology and Molecular Biology Reviews, 83(1). https://doi.org/10.1128/mmbr.00039-18

Halwani, M., Mugabe, C., Azghani, A. O., Lafrenie, R. M., Kumar, A., & Omri, A. (2007). Bactericidal efficacy of liposomal aminoglycosides against *Burkholderia cenocepacia*. Journal of Antimicrobial Chemotherapy, 60(4), 760–769. https://doi.org/10.1093/jac/dkm289

Han, E., Choi, S., Lee, Y., Park, J., Hong, S., & Lee, H. (2019). Extracellular RNAs in periodontopathogenic outer membrane vesicles promote TNF-α production in human macrophages and cross the blood-brain barrier in mice. The FASEB Journal, 33(12), 13412–13422. https://doi.org/10.1096/fj.201901575r

He, M., Yin, S., Huang, X., Li, Y., Li, B., Gong, T., & Liu, Q. (2023). Insights into the regulatory role of bacterial sncRNA and its extracellular delivery via OMVs. Applied Microbiology and Biotechnology, 108(1). https://doi.org/10.1007/s00253-023-12855-z

Hirabayashi, T., Murayama, T., & Shimizu, T. (2004). Regulatory mechanism and physiological role of cytosolic phospholipase A2. Biological and Pharmaceutical Bulletin, 27(8), 1168–1173. https://doi.org/10.1248/bpb.27.1168

Holden, M. T. G., Seth-Smith, H. M. B., Crossman, L. C., Sebaihia, M., Bentley, S. D., Cerdeño-TáRraga, A. M., Thomson, N. R., Bason, N., Quail, M. A., Sharp, S., Cherevach, I., Churcher, C., Goodhead, I., Hauser, H., Holroyd, N., Mungall, K., Scott, P., Walker, D., White, B., . . . Parkhill, J. (2008). The Genome of *Burkholderia cenocepacia* J2315, an Epidemic Pathogen of Cystic Fibrosis Patients. Journal of Bacteriology, 191(1), 261–277. https://doi.org/10.1128/jb.01230-08

Huber, B., Riedel, K., Hentzer, M., Heydorn, A., Gotschlich, A., Givskov, M., Molin, S., & Eberl, L. (2001). The cep quorum-sensing system of *Burkholderia cepacia* H111 controls biofilm formation and swarming motility. Microbiology, 147(9), 2517–2528. https://doi.org/10.1099/00221287-147-9-2517

Hwang, J., & Kim, H. S. (2015). Cell Wall Recycling-Linked Coregulation of AmpC and PenB β-Lactamases through ampD Mutations in *Burkholderia cenocepacia*. Antimicrobial Agents and Chemotherapy, 59(12), 7602–7610. https://doi.org/10.1128/aac.01068-15

Inhülsen, S., Aguilar, C., Schmid, N., Suppiger, A., Riedel, K., & Eberl, L. (2012). Identification of functions linking quorum sensing with biofilm formation in *Burkholderia cenocepacia* H111. MicrobiologyOpen, 1(2), 225–242. https://doi.org/10.1002/mbo3.24

Jan, A. T. (2017). Outer Membrane Vesicles (OMVs) of gram-negative bacteria: a perspective update. Frontiers in Microbiology, 8. https://doi.org/10.3389/fmicb.2017.01053

Jorth, P., Manuel, C., McLemore, T., Humphries, R. M., Cole, N. C., Schuetz, A. N., Garica, D., Maldonado, M., Rivero, N., Galdino, A. C. M., Celedonio, D., LiPuma, J. J., Green, D. A., Zlosnik, J. E. A., Traczewski, M., & Huse, H. K. (2025). Evaluation of antimicrobial susceptibility testing methods for *Burkholderia cepacia* complex isolates from people with and without cystic fibrosis. Journal of Clinical Microbiology. https://doi.org/10.1128/jcm.01480-24

Jung, H., Pirch, T., & Hilger, D. (2006). Secondary transport of amino acids in prokaryotes. The Journal of Membrane Biology, 213(2), 119–133. https://doi.org/10.1007/s00232-006-0880-x

Juodeikis, R., & Carding, S. R. (2022). Outer membrane vesicles: biogenesis, functions, and issues. Microbiology and Molecular Biology Reviews, 86(4). https://doi.org/10.1128/mmbr.00032-22

Kalferstova, L., Kolar, M., Fila, L., Vavrova, J., & Drevinek, P. (2015). Gene Expression Profiling of *Burkholderia cenocepacia* at the Time of Cepacia Syndrome: Loss of Motility as a Marker of Poor Prognosis? Journal of Clinical Microbiology, 53(5), 1515–1522. https://doi.org/10.1128/jcm.03605-14

Khan, S., Marathe, S. A., & Jha, P. N. (2023). Characterizing the type 6 secretion system (T6SS) of E. cloacae SBP-8 and its role in pathogenesis and bacterial competition. Microbial Pathogenesis, 183, 106268. https://doi.org/10.1016/j.micpath.2023.106268

Kiekens, S., Sass, A., Van Nieuwerburgh, F., Deforce, D., & Coenye, T. (2018). The Small RNA ncS35 Regulates Growth in *Burkholderia cenocepacia* J2315. mSphere, 3(1). https://doi.org/10.1128/msphere.00579-17

Kim, S. Y., Kim, M. H., Son, J. H., Kim, S. I., Yun, S. H., Kim, K., Kim, S., Shin, M., & Lee, J. C. (2020). Outer membrane vesicles produced by *Burkholderia cepacia* cultured with subinhibitory concentrations of ceftazidime enhance pro-inflammatory responses. Virulence, 11(1), 995–1005. https://doi.org/10.1080/21505594.2020.1802193

Koeppen, K., Hampton, T. H., Jarek, M., Scharfe, M., Gerber, S. A., Mielcarz, D. W., Demers, E. G., Dolben, E. L., Hammond, J. H., Hogan, D. A., & Stanton, B. A. (2016). A Novel Mechanism of Host-Pathogen Interaction through sRNA in Bacterial Outer Membrane Vesicles. PLoS Pathogens, 12(6), e1005672. https://doi.org/10.1371/journal.ppat.1005672

Kumar, M., Gupta, A., Sahoo, R. K., Jena, J., Debata, N. K., & Subudhi, E. (2016). Functional genome screening to elucidate the colistin resistance mechanism. Scientific Reports, 6(1). https://doi.org/10.1038/srep23156

Lambert, R., & Pearson, J. (2000). Susceptibility testing: accurate and reproducible minimum inhibitory concentration (MIC) and non-inhibitory concentration (NIC) values. Journal of Applied Microbiology, 88(5), 784–790. https://doi.org/10.1046/j.1365-2672.2000.01017.x

Lanahan, S. M., Wymann, M. P., & Lucas, C. L. (2022). The role of PI3Kγ in the immune system: new insights and translational implications. Nature Reviews. Immunology, 22(11), 687–700. https://doi.org/10.1038/s41577-022-00701-8

Lardi, M., Aguilar, C., Pedrioli, A., Omasits, U., Suppiger, A., Cárcamo-Oyarce, G., Schmid, N., Ahrens, C. H., Eberl, L., & Pessi, G. (2015). σ 54 -Dependent Response to Nitrogen Limitation and Virulence in *Burkholderia cenocepacia* Strain H111. Applied and Environmental Microbiology, 81(12), 4077–4089. https://doi.org/10.1128/aem.00694-15

Lécrivain, A., & Beckmann, B. M. (2020). Bacterial RNA in extracellular vesicles: A new regulator of host-pathogen interactions? Biochimica Et Biophysica Acta (BBA) - Gene Regulatory Mechanisms, 1863(7), 194519. https://doi.org/10.1016/j.bbagrm.2020.194519

Lee, C. F., Carley, R. E., Butler, C. A., & Morrison, A. R. (2021). RAC GTPASe Signaling in Immune-Mediated Mechanisms of Atherosclerosis. Cells, 10(11), 2808. https://doi.org/10.3390/cells10112808

Lee, C., Mannaa, M., Kim, N., Kim, J., Choi, Y., Kim, S. H., Jung, B., Lee, H., Lee, J., & Seo, Y. (2019). Stress Tolerance and Virulence-Related Roles of Lipopolysaccharide in *Burkholderia glumae*. The Plant Pathology Journal, 35(5), 445–458. https://doi.org/10.5423/ppj.oa.04.2019.0124

Leitão, J. H., Feliciano, J. R., Sousa, S. A., Pita, T., & Guerreiro, S. I. (2017). *Burkholderia cepacia* Complex Infections Among Cystic Fibrosis Patients: Perspectives and Challenges. In InTech eBooks. https://doi.org/10.5772/67712

Li, B., Xu, Y., Xu, T., Guo, Z., Xu, Q., Li, Y., Zeng, L., Huang, X., & Liu, Q. (2022). Disruption of sncRNA Improves the Protective Efficacy of Outer Membrane Vesicles against *Helicobacter pylori* Infection in a Mouse Model. Infection and Immunity, 90(8). https://doi.org/10.1128/iai.00267-22

Livak, K. J., & Schmittgen, T. D. (2001). Analysis of relative gene expression data using Real-Time Quantitative PCR and the 2−ΔΔCT method. Methods, 25(4), 402–408. https://doi.org/10.1006/meth.2001.1262

Lochowska, A., Iwanicka-Nowicka, R., Zielak, A., Modelewska, A., Thomas, M. S., & Hryniewicz, M. M. (2011). Regulation of Sulfur Assimilation Pathways in *Burkholderia cenocepacia* through Control of Genes by the SsuR Transcription Factor. Journal of Bacteriology, 193(8), 1843–1853. https://doi.org/10.1128/jb.00483-10

Lord, R., Jones, A. M., & Horsley, A. (2020). Antibiotic treatment for *Burkholderia cepacia* complex in people with cystic fibrosis experiencing a pulmonary exacerbation. Cochrane Library, 2020(4). https://doi.org/10.1002/14651858.cd009529.pub4

Loutet, S. A., & Valvano, M. A. (2010). A Decade of *Burkholderia cenocepacia* Virulence Determinant Research. Infection and Immunity, 78(10), 4088–4100. https://doi.org/10.1128/iai.00212-10

Loutet, S. A., & Valvano, M. A. (2011). Extreme antimicrobial peptide and polymyxin B resistance in the genus *Burkholderia*. Frontiers in Cellular and Infection Microbiology, 1. https://doi.org/10.3389/fcimb.2011.00006

Malabirade, A., Habier, J., Heintz-Buschart, A., May, P., Godet, J., Halder, R., Etheridge, A., Galas, D., Wilmes, P., & Fritz, J. V. (2018). The RNA Complement of Outer Membrane Vesicles From *Salmonella enterica* Serovar *Typhimurium* Under Distinct Culture Conditions. Frontiers in Microbiology, 9. https://doi.org/10.3389/fmicb.2018.02015

Mann, M., Wright, P. R., & Backofen, R. (2017). IntaRNA 2.0: enhanced and customizable prediction of RNA–RNA interactions. Nucleic Acids Research, 45(W1), W435–W439. https://doi.org/10.1093/nar/gkx279

Marinacci, B., Krzyżek, P., Pellegrini, B., Turacchio, G., & Grande, R. (2023). Latest update on outer membrane vesicles and their role in horizontal gene transfer: A Mini-Review. Membranes, 13(11), 860. https://doi.org/10.3390/membranes13110860

Masters, P. A., O'Bryan, T. A., Zurlo, J., Miller, D. Q., & Joshi, N. (2003). Trimethoprim-Sulfamethoxazole revisited. Archives of Internal Medicine, 163(4), 402. https://doi.org/10.1001/archinte.163.4.402

Matos, G. R., Feliciano, J. R., & Leitão, J. H. (2024). Non-coding regulatory sRNAs from bacteria of the *Burkholderia cepacia* complex. Applied Microbiology and Biotechnology, 108(1). https://doi.org/10.1007/s00253-024-13121-6

Maus, U. A., Backi, M., Winter, C., Srivastava, M., Schwarz, M. K., Rückle, T., Paton, J. C., Briles, D., Mack, M., Welte, T., Maus, R., Bohle, R. M., Seeger, W., Rommel, C., Hirsch, E., Lohmeyer, J., & Preissner, K. T. (2007). Importance of Phosphoinositide 3-Kinase γ in the Host Defense against Pneumococcal Infection. American Journal of Respiratory and Critical Care Medicine, 175(9), 958–966. https://doi.org/10.1164/rccm.200610-1533oc

McCarthy, Y., Yang, L., Twomey, K. B., Sass, A., Tolker-Nielsen, T., Mahenthiralingam, E., Dow, J. M., & Ryan, R. P. (2010). A sensor kinase recognizing the cell-cell signal BDSF (cis-2-dodecenoic acid) regulates virulence in *Burkholderia cenocepacia*. Molecular Microbiology, 77(5), 1220–1236. https://doi.org/10.1111/j.1365-2958.2010.07285.x

Millar, B. C., McCaughan, J., Rendall, J. C., & Moore, J. E. (2020). Delafloxacin—A novel fluoroquinolone for the treatment of ciprofloxacin-resistant *Pseudomonas aeruginosa* in patients with cystic fibrosis. The Clinical Respiratory Journal, 15(1), 116–120. https://doi.org/10.1111/crj.13262

Mittelstaedt, N. N., Becker, A. L., De Freitas, D. N., Zanin, R. F., Stein, R. T., & De Souza, A. P. D. (2021). DNA methylation and immune memory response. Cells, 10(11), 2943. https://doi.org/10.3390/cells10112943

Montague, J., Rosenstiel, P., & Escudero-Hernández, C. (2024). P094 Lack of DNA methyltransferase DNMT3A in fibroblasts impairs cell growth and wound healing. Journal of Crohn S and Colitis, 18(Supplement_1), i369. https://doi.org/10.1093/ecco-jcc/jjad212.0224

Morales, L. D., Av-Gay, Y., & Murphy, M. E. P. (2023). Acidic pH modulates *Burkholderia cenocepacia* antimicrobial susceptibility in the cystic fibrosis nutritional environment. Microbiology Spectrum, 11(6). https://doi.org/10.1128/spectrum.02731-23

Morin, C., Landry, M., Groleau, M., & Déziel, E. (2022). Surface Motility Favors Codependent Interaction between *Pseudomonas aeruginosa* and *Burkholderia cenocepacia*. mSphere, 7(4). https://doi.org/10.1128/msphere.00153-22

Muok, A. R., Briegel, A., & Crane, B. R. (2020). Regulation of the chemotaxis histidine kinase CheA: A structural perspective. Biochimica et Biophysica Acta (BBA) - Biomembranes, 1862(1), 183030. https://doi.org/10.1016/j.bbamem.2019.183030

Nakayama, H., Kurokawa, K., & Lee, B. L. (2012). Lipoproteins in bacteria: structures and biosynthetic pathways. FEBS Journal, 279(23), 4247–4268. https://doi.org/10.1111/febs.12041

Nickzad, A., & Déziel, E. (2016). Adaptive Significance of Quorum Sensing-Dependent Regulation of Rhamnolipids by Integration of Growth Rate in *Burkholderia glumae*: A Trade-Off between Survival and Efficiency. Frontiers in Microbiology, 7. https://doi.org/10.3389/fmicb.2016.01215

Nikaido, H., & Pagès, J. (2011). Broad-specificity efflux pumps and their role in multidrug resistance of Gram-negative bacteria. FEMS Microbiology Reviews, 36(2), 340–363. https://doi.org/10.1111/j.1574-6976.2011.00290.x

Nobs, S. P., Schneider, C., Dietrich, M. G., Brocker, T., Rolink, A., Hirsch, E., & Kopf, M. (2015). PI3-Kinase-Γ has a distinct and essential role in Lung-Specific dendritic cell development. Immunity, 43(4), 674–689. https://doi.org/10.1016/j.immuni.2015.09.006

O'Grady, E. (2011). *Burkholderia cenocepacia* differential gene expression during host–pathogen interactions and adaptation to the host environment. Frontiers in Cellular and Infection Microbiology, 1. https://doi.org/10.3389/fcimb.2011.00015

O'Grady, E. P., Nguyen, D. T., Weisskopf, L., Eberl, L., & Sokol, P. A. (2010). The *Burkholderia cenocepacia* LysR-Type Transcriptional Regulator ShvR Influences Expression of Quorum-Sensing, Protease, Type II Secretion, and afc Genes. Journal of Bacteriology, 193(1), 163–176. https://doi.org/10.1128/jb.00852-10

O'Toole, G. A., & Kolter, R. (1998). Initiation of biofilm formation in *Pseudomonas fluorescens* WCS365 proceeds via multiple, convergent signalling pathways: a genetic analysis. Molecular Microbiology, 28(3), 449–461. https://doi.org/10.1046/j.1365-2958.1998.00797.x

Oppy C.C., Jebeli L., Kuba M., Oates C. V., Strugnell R., Edgington-Mitchell L.E., Valvano M.A., Hartland E. L., Newton H. J., Scott N. E. (2019). Loss of O-Linked Protein Glycosylation in *Burkholderia cenocepacia* Impairs Biofilm Formation and Siderophore Activity and Alters Transcriptional Regulators. mSphere4:10.1128/msphere.00660-19. https://doi.org/10.1128/msphere.00660-19

Papp-Wallace, K. M., & Maguire, M. E. (2006). Manganese transport and the role of manganese in virulence. Annual Review of Microbiology, 60(1), 187–209. https://doi.org/10.1146/annurev.micro.60.080805.142149

Papp-Wallace, K. M., Shapiro, A. B., Becka, S. A., Zeiser, E. T., LiPuma, J. J., Lane, D. J., Panchal, R. G., Mueller, J. P., O'Donnell, J. P., & Miller, A. A. (2020). In Vitro Antibacterial Activity and In Vivo Efficacy of Sulbactam-Durlobactam against Pathogenic *Burkholderia* Species. Antimicrobial Agents and Chemotherapy, 65(3). https://doi.org/10.1128/aac.01930-20

Park, J. H., Song, S., Kim, S., Kim, M., & Kim, K. (2023). Optimizing Conditions for the Production of Bacterial Extracellular Vesicles of *Vibrio vulnificus* and Analysis of the Inner Small RNA Compositions. Journal of Microbiology and Biotechnology, 34(1), 29–38. https://doi.org/10.4014/jmb.2310.10002

Paszti, S., Gualdi, S., Torres, M., Augusto, L., Harrison, F., & Eberl, L. (2025). Unraveling *Burkholderia cenocepacia* H111 fitness determinants using two animal models. mSystems. https://doi.org/10.1128/msystems.01354-24

Peeters, E., Nelis, H. J., & Coenye, T. (2009). In vitro activity of ceftazidime, ciprofloxacin, meropenem, minocycline, tobramycin and trimethoprim/sulfamethoxazole against planktonic and sessile *Burkholderia cepacia* complex bacteria. Journal of Antimicrobial Chemotherapy, 64(4), 801–809. https://doi.org/10.1093/jac/dkp253

Pita, T., Feliciano, J. R., & Leitão, J. H. (2020). Extracellular RNAs in bacterial infections: from emerging key players on Host-Pathogen interactions to exploitable biomarkers and therapeutic targets. International Journal of Molecular Sciences, 21(24), 9634. https://doi.org/10.3390/ijms21249634

Pita, T., Feliciano, J. R., & Leitão, J. H. (2023). Identification of *Burkholderia cenocepacia* non-coding RNAs expressed during *Caenorhabditis elegans* infection. Applied Microbiology and Biotechnology, 107(11), 3653–3671. https://doi.org/10.1007/s00253-023-12530-3

Poirel, L., Rodriguez-Martinez, J., PléSiat, P., & Nordmann, P. (2008). Naturally Occurring Class A ß-Lactamases from the *Burkholderia cepacia* Complex. Antimicrobial Agents and Chemotherapy, 53(3), 876–882. https://doi.org/10.1128/aac.00946-08

Pope, C. F., Gillespie, S. H., Pratten, J. R., & McHugh, T. D. (2007). Fluoroquinolone-Resistant Mutants of *Burkholderia cepacia*. Antimicrobial Agents and Chemotherapy, 52(3), 1201–1203. https://doi.org/10.1128/aac.00799-07

Quinlivan, E. P., McPartlin, J., Weir, D. G., & Scott, J. (2000). Mechanism of the antimicrobial drug trimethoprim revisited. The FASEB Journal, 14(15), 2519–2524. https://doi.org/10.1096/fj.99-1037com

Ramos, J. L., Martínez-Bueno, M., Molina-Henares, A. J., TeráN, W., Watanabe, K., Zhang, X., Gallegos, M. T., Brennan, R., & Tobes, R. (2005). The TETR family of transcriptional repressors. Microbiology and Molecular Biology Reviews, 69(2), 326–356. https://doi.org/10.1128/mmbr.69.2.326-356.2005

Rhodes, K. A., & Schweizer, H. P. (2016). Antibiotic resistance in *Burkholderia* species. Drug Resistance Updates, 28, 82–90. https://doi.org/10.1016/j.drup.2016.07.003

Richards, D., & Brogden, R. (1985). Ceftazidime. Drugs, 29(2), 105–161. https://doi.org/10.2165/00003495-198529020-00002

Roier, S., Zingl, F., Cakar, F., & Schild, S. (2016). Bacterial outer membrane vesicle biogenesis: a new mechanism and its implications. Microbial Cell, 3(6), 257–259. https://doi.org/10.15698/mic2016.06.508

Saeed, M., Rasheed, F., Jamil, I., Khurshid, M., Rasool, M. H., Saba, N., Ahmad, M., Wazeer, A., & Waheed, A. (2024). *Burkholderia cepacia*: Understanding Pathogenicity, Virulence Factors, and Therapeutic Strategies. Journal of Islamabad Medical & Dental College, 13(1). https://doi.org/10.35787/jimdc.v13i1.1183

Saiman, L., Waters, V., LiPuma, J. J., Hoffman, L. R., Alby, K., Zhang, S. X., Yau, Y. C., Downey, D. G., Sermet-Gaudelus, I., Bouchara, J., Kidd, T. J., Bell, S. C., & Brown, A. W. (2024). Practical Guidance for Clinical Microbiology Laboratories: Updated guidance for processing respiratory tract samples from people with cystic fibrosis. Clinical Microbiology Reviews, 37(3). https://doi.org/10.1128/cmr.00215-21

Saldías, M. S., Lamothe, J., Wu, R., & Valvano, M. A. (2008). *Burkholderia cenocepacia* Requires the RpoN Sigma Factor for Biofilm Formation and Intracellular Trafficking within Macrophages. Infection and Immunity, 76(3), 1059–1067. https://doi.org/10.1128/iai.01167-07

Saldías, M. S., Ortega, X., & Valvano, M. A. (2009). *Burkholderia cenocepacia* O antigen lipopolysaccharide prevents phagocytosis by macrophages and adhesion to epithelial cells. Journal of Medical Microbiology, 58(12), 1542–1548. https://doi.org/10.1099/jmm.0.013235-0

Sánchez-Encinales, V., Álvarez-Marín, R., Pachón-Ibáñez, M. E., Fernández-Cuenca, F., Pascual, A., Garnacho-Montero, J., Martínez-Martínez, L., Vila, J., Tomás, M. M., Cisneros, J. M., Bou, G.,

Rodríguez-Baño, J., Pachón, J., & Smani, Y. (2017). Overproduction of outer membrane protein A (OmpA) by *Acinetobacter baumannii* is a risk factor for nosocomial pneumonia, bacteremia and mortality increase. The Journal of Infectious Diseases, jix010. https://doi.org/10.1093/infdis/jix010

Sanders, C. C. (1988). Ciprofloxacin: *in vitro* activity, mechanism of action, and resistance. Clinical Infectious Diseases, 10(3), 516–527. https://doi.org/10.1093/clinids/10.3.516

Sass, A. M., & Coenye, T. (2020). Low iron-induced small RNA BrrF regulates central metabolism and oxidative stress responses in *Burkholderia cenocepacia*. PLoS ONE, 15(7), e0236405. https://doi.org/10.1371/journal.pone.0236405

Sass, A. M., & Coenye, T. (2023). The Small RNA NcS25 Regulates Biological Amine-Transporting Outer Membrane Porin BCAL3473 in *Burkholderia cenocepacia*. mSphere, 8(2). https://doi.org/10.1128/msphere.00083-23

Sass, A. M., De Waele, S., Daled, S., Devreese, B., Deforce, D., Van Nieuwerburgh, F., & Coenye, T. (2019). Small RNA NcS27 co-regulates utilization of carbon sources in *Burkholderia cenocepacia* J2315. Microbiology, 165(10), 1135–1150. https://doi.org/10.1099/mic.0.000848

Sass, A., Kiekens, S., & Coenye, T. (2017). Identification of small RNAs abundant in *Burkholderia cenocepacia* biofilms reveal putative regulators with a potential role in carbon and iron metabolism. Scientific Reports, 7(1). https://doi.org/10.1038/s41598-017-15818-3

Schaefers, M. M. (2020). Regulation of virulence by Two-Component systems in pathogenic *Burkholderia*. Infection and Immunity, 88(7). https://doi.org/10.1128/iai.00927-19

Schaefers, M. M., Liao, T. L., Boisvert, N. M., Roux, D., Yoder-Himes, D., & Priebe, G. P. (2017). An Oxygen-Sensing Two-Component System in the *Burkholderia cepacia* Complex Regulates Biofilm, Intracellular Invasion, and Pathogenicity. PLoS Pathogens, 13(1), e1006116. https://doi.org/10.1371/journal.ppat.1006116

Schwarz, C., Taccetti, G., Burgel, P., & Mulrennan, S. (2022). Tobramycin safety and efficacy review article. Respiratory Medicine, 195, 106778. https://doi.org/10.1016/j.rmed.2022.106778

Scoffone, V. C., Chiarelli, L. R., Trespidi, G., Mentasti, M., Riccardi, G., & Buroni, S. (2017). *Burkholderia cenocepacia* Infections in Cystic Fibrosis Patients: Drug Resistance and Therapeutic Approaches. Frontiers in Microbiology, 8. https://doi.org/10.3389/fmicb.2017.01592

Scoffone, V. C., Trespidi, G., Barbieri, G., Irudal, S., Perrin, E., & Buroni, S. (2021). Role of RND efflux pumps in drug resistance of cystic fibrosis pathogens. Antibiotics, 10(7), 863. https://doi.org/10.3390/antibiotics10070863

Scott, M., Gunderson, C. W., Mateescu, E. M., Zhang, Z., & Hwa, T. (2010). Interdependence of cell growth and gene expression: Origins and consequences. Science, 330(6007), 1099–1102. https://doi.org/10.1126/science.1192588

Sfeir, M. M. (2018). *Burkholderia cepacia* complex infections: More complex than the bacterium name suggest. Journal of Infection, 77(3), 166–170. https://doi.org/10.1016/j.jinf.2018.07.006

Shabalin, I. G., Gritsunov, A., Hou, J., Sławek, J., Miks, C. D., Cooper, D. R., Minor, W., & Christendat, D. (2019). Structural and biochemical analysis of *Bacillus anthracis* prephenate dehydrogenase reveals an unusual mode of inhibition by tyrosine via the ACT domain. FEBS Journal, 287(11), 2235–2255. https://doi.org/10.1111/febs.15150

Shmarina, G., Pukhalskaya, D., Shmarin, V., Semykin, S., Avakyan, L., Krasovsky, S., Goryainova, A., Kostyuk, S., Zinchenko, R., & Kashirskaya, N. (2024). *Burkholderia cepacia* in cystic fibrosis children and adolescents: overall survival and immune alterations. Frontiers in Cellular and Infection Microbiology, 14. https://doi.org/10.3389/fcimb.2024.1374318

Shukla, A., Rodriguez, S., & Brennan-Krohn, T. (2024). Activity of antibiotics against *Burkholderia cepacia* complex in artificial sputum medium. Journal of Antimicrobial Chemotherapy, 79(11), 2867–2876. https://doi.org/10.1093/jac/dkae299

Sjöstedt, E., Zhong, W., Fagerberg, L., Karlsson, M., Mitsios, N., Adori, C., Oksvold, P., Edfors, F., Limiszewska, A., Hikmet, F., Huang, J., Du, Y., Lin, L., Dong, Z., Yang, L., Liu, X., Jiang, H., Xu, X., Wang, J., . . . Mulder, J. (2020). An atlas of the protein-coding genes in the human, pig, and mouse brain. Science, 367(6482). https://doi.org/10.1126/science.aay5947

Song, T., Mika, F., Lindmark, B., Liu, Z., Schild, S., Bishop, A., Zhu, J., Camilli, A., Johansson, J., Vogel, J., & Wai, S. N. (2008). A new *Vibrio cholerae* sRNA modulates colonization and affects release of outer membrane vesicles. Molecular Microbiology, 70(1), 100–111. https://doi.org/10.1111/j.1365-2958.2008.06392.x

Sousa, S. A., Morad, M., Feliciano, J. R., Pita, T., Nady, S., El-Hennamy, R. E., Abdel-Rahman, M., Cavaco, J., Pereira, L., Barreto, C., & Leitão, J. H. (2016). The *Burkholderia cenocepacia* OmpA-like protein BCAL2958: identification, characterization, and detection of anti-BCAL2958 antibodies in serum from *B. cepacia* complex-infected Cystic Fibrosis patients. AMB Express, 6(1). https://doi.org/10.1186/s13568-016-0212-1

Sousa, S., Feliciano, J., Pita, T., Guerreiro, S., & Leitão, J. (2017). *Burkholderia cepacia* Complex Regulation of Virulence Gene Expression: A Review. Genes, 8(1), 43. https://doi.org/10.3390/genes8010043

Stanton, B. A. (2021). Extracellular vesicles and Host–Pathogen interactions: A review of Inter-Kingdom signaling by small noncoding RNA. Genes, 12(7), 1010. https://doi.org/10.3390/genes12071010

Stevanovic, M., Boukéké-Lesplulier, T., Hupe, L., Hasty, J., Bittihn, P., & Schultz, D. (2022). Nutrient gradients mediate complex Colony-Level antibiotic responses in structured microbial populations. Frontiers in Microbiology, 13. https://doi.org/10.3389/fmicb.2022.740259

Stevens, M. P., Friebel, A., Taylor, L. A., Wood, M. W., Brown, P. J., Hardt, W., & Galyov, E. E. (2003). A *Burkholderia pseudomallei* Type III secreted protein, BOPE, facilitates bacterial invasion of epithelial cells and exhibits guanine nucleotide exchange factor activity. Journal of Bacteriology, 185(16), 4992–4996. https://doi.org/10.1128/jb.185.16.4992-4996.2003

Stubben, C. J., Micheva-Viteva, S. N., Shou, Y., Buddenborg, S. K., Dunbar, J. M., & Hong-Geller, E. (2014). Differential expression of small RNAs from *Burkholderia thailandensis* in response to varying environmental and stress conditions. BMC Genomics, 15(1). https://doi.org/10.1186/1471-2164-15-385

Subramoni, S., & Sokol, P. A. (2012). Quorum sensing systems influence *Burkholderia cenocepacia* virulence. Future Microbiology, 7(12), 1373–1387. https://doi.org/10.2217/fmb.12.118

Suppiger, A., Schmid, N., Aguilar, C., Pessi, G., & Eberl, L. (2013). Two quorum sensing systems control biofilm formation and virulence in members of the *Burkholderia cepacia* complex. Virulence, 4(5), 400–409. https://doi.org/10.4161/viru.25338

Thomas, M. S. (2007). Iron acquisition mechanisms of the *Burkholderia cepacia* complex. BioMetals, 20(3–4), 431–452. https://doi.org/10.1007/s10534-006-9065-4

Tilly, K., Bestor, A., & Rosa, P. A. (2016). Functional Equivalence of OspA and OspB, but Not OspC, in Tick Colonization by *Borrelia burgdorferi*. Infection and Immunity, 84(5), 1565–1573. https://doi.org/10.1128/iai.00063-16

Tomich, M., Griffith, A., Herfst, C. A., Burns, J. L., & Mohr, C. D. (2003). Attenuated Virulence of a *Burkholderia cepacia* Type III Secretion Mutant in a Murine Model of Infection. Infection and Immunity, 71(3), 1405–1415. https://doi.org/10.1128/iai.71.3.1405-1415.2003

Tseng, S., Tsai, W., Liang, C., Lin, Y., Huang, J., Chang, C., Tyan, Y., & Lu, P. (2014). The Contribution of Antibiotic Resistance Mechanisms in Clinical *Burkholderia cepacia* Complex Isolates: An

Emphasis on Efflux Pump Activity. PLoS ONE, 9(8), e104986. https://doi.org/10.1371/journal.pone.0104986

UniProt. (n.d.-b). https://www.uniprot.org/uniprotkb/Q92925/entry

UNKL unk like zinc finger [Homo sapiens (human)]. (n.d.). NCBI. https://www.ncbi.nlm.nih.gov/gtr/genes/64718/

Van Acker, H., Sass, A., Bazzini, S., De Roy, K., Udine, C., Messiaen, T., Riccardi, G., Boon, N., Nelis, H. J., Mahenthiralingam, E., & Coenye, T. (2013). Biofilm-Grown *Burkholderia cepacia* Complex Cells Survive Antibiotic Treatment by Avoiding Production of Reactive Oxygen Species. PLoS ONE, 8(3), e58943. https://doi.org/10.1371/journal.pone.0058943

Van Den Driessche, F., Vanhoutte, B., Brackman, G., Crabbé, A., Rigole, P., Vercruysse, J., Verstraete, G., Cappoen, D., Vervaet, C., Cos, P., & Coenye, T. (2017). Evaluation of combination therapy for *Burkholderia cenocepacia* lung infection in different *in vitro* and in vivo models. PLoS ONE, 12(3), e0172723. https://doi.org/10.1371/journal.pone.0172723

Van Kessel, J. C., Rutherford, S. T., Cong, J., Quinodoz, S., Healy, J., & Bassler, B. L. (2014). Quorum Sensing Regulates the Osmotic Stress Response in *Vibrio harveyi*. Journal of Bacteriology, 197(1), 73–80. https://doi.org/10.1128/jb.02246-14

Vandenbussche, I., Sass, A., Pinto-Carbó, M., Mannweiler, O., Eberl, L., & Coenye, T. (2020). DNA Methylation Epigenetically Regulates Gene Expression in *Burkholderia cenocepacia* and Controls Biofilm Formation, Cell Aggregation, and Motility. mSphere, 5(4). https://doi.org/10.1128/msphere.00455-20

Vergunst, A. C., Meijer, A. H., Renshaw, S. A., & O'Callaghan, D. (2010). *Burkholderia cenocepacia* Creates an intramacrophage replication niche in zebrafish embryos, followed by bacterial dissemination and establishment of systemic infection. Infection and Immunity, 78(4), 1495–1508. https://doi.org/10.1128/iai.00743-09

Vinion-Dubiel, A. D., & Goldberg, J. B. (2003). Review: Lipopolysaccharide of *Burkholderia cepacia* complex. Journal of Endotoxin Research, 9(4), 201–213. https://doi.org/10.1177/09680519030090040101

Wadhwa, N., & Berg, H. C. (2021). Bacterial motility: machinery and mechanisms. Nature Reviews Microbiology, 20(3), 161–173. https://doi.org/10.1038/s41579-021-00626-4

Winsor, G. L., Khaira, B., Van Rossum, T., Lo, R., Whiteside, M. D., & Brinkman, F. S. L. (2008). The *Burkholderia* Genome Database: facilitating flexible queries and comparative analyses. Bioinformatics, 24(23), 2803–2804. https://doi.org/10.1093/bioinformatics/btn524

Witzel, M., Petersheim, D., Fan, Y., Bahrami, E., Racek, T., Rohlfs, M., Puchałka, J., Mertes, C., Gagneur, J., Ziegenhain, C., Enard, W., Stray-Pedersen, A., Arkwright, P. D., Abboud, M. R., Pazhakh, V., Lieschke, G. J., Krawitz, P. M., Dahlhoff, M., Schneider, M. R., . . . Klein, C. (2017). Chromatin-remodeling factor SMARCD2 regulates transcriptional networks controlling differentiation of neutrophil granulocytes. Nature Genetics, 49(5), 742–752. https://doi.org/10.1038/ng.3833

Xie, Y., Li, X., & Ge, J. (2019). Cyclophilin A–FoxO1 signaling pathway in endothelial cell apoptosis. Cellular Signalling, 61, 57–65. https://doi.org/10.1016/j.cellsig.2019.04.014

Yang, Y., Pan, D., Tang, Y., Li, J., Zhu, K., Yu, Z., Zhu, L., Wang, Y., Chen, P., & Li, C. (2022). H3-T6SS of *Pseudomonas aeruginosa* PA14 contributes to environmental adaptation via secretion of a biofilm-promoting effector. Stress Biology, 2(1). https://doi.org/10.1007/s44154-022-00078-7

Yu, Q., Zhou, B., Zhang, Y., Nguyen, E. T., Du, J., Glosson, N. L., & Kaplan, M. H. (2011). DNA methyltransferase 3a limits the expression of interleukin-13 in T helper 2 cells and allergic airway inflammation. Proceedings of the National Academy of Sciences, 109(2), 541–546. https://doi.org/10.1073/pnas.1103803109

Yurchenko, V., Zybarth, G., O'Connor, M., Dai, W. W., Franchin, G., Hao, T., Guo, H., Hung, H., Toole, B., Gallay, P., Sherry, B., & Bukrinsky, M. (2002). Active site residues of cyclophilin A are crucial for its signaling activity via CD147. Journal of Biological Chemistry, 277(25), 22959–22965. https://doi.org/10.1074/jbc.m201593200

Zavan, L., Fang, H., Johnston, E. L., Whitchurch, C., Greening, D. W., Hill, A. F., & Kaparakis-Liaskos, M. (2023). The mechanism of *Pseudomonas aeruginosa* outer membrane vesicle biogenesis determines their protein composition. PROTEOMICS, 23(10), e2200464. https://doi.org/10.1002/pmic.202200464

Zhang, H., Zhang, Y., Song, Z., Li, R., Ruan, H., Liu, Q., & Huang, X. (2019). sncRNAs packaged by *Helicobacter pylori* outer membrane vesicles attenuate IL-8 secretion in human cells. International Journal of Medical Microbiology, 310(1), 151356. https://doi.org/10.1016/j.ijmm.2019.151356

Zhang, Y., Zhao, X., Wang, J., Liao, L., Qin, H., Zhang, R., Li, C., He, Y., & Huang, S. (2024). VmsR, a LuxR-Type Regulator, Contributes to Virulence, Cell Motility, Extracellular Polysaccharide Production and Biofilm Formation in *Xanthomonas oryzae* pv. *oryzicola*. International Journal of Molecular Sciences, 25(14), 7595. https://doi.org/10.3390/ijms25147595

Zhou, G., Wang, Q., Wang, Y., Wen, X., Peng, H., Peng, R., Shi, Q., Xie, X., & Li, L. (2023). Outer membrane porins contribute to antimicrobial resistance in Gram-Negative bacteria. Microorganisms, 11(7), 1690. https://doi.org/10.3390/microorganisms11071690

Zlosnik, J. E. A., Mori, P. Y., To, D., Leung, J., Hird, T. J., & Speert, D. P. (2014). Swimming Motility in a Longitudinal Collection of Clinical Isolates of *Burkholderia cepacia* Complex Bacteria from People with Cystic Fibrosis. PLoS ONE, 9(9), e106428. https://doi.org/10.1371/journal.pone.0106428

6. Supplementary Materials

Supplementary Table 6.1: Bacterial target predictions for nc5U55 using TargetRNA3 and CopraRNA.

Locus ID	Gene name	Product description	TargetRNA	CopraRNA
BCAM0647	-	putative ring-hydroxylating subunit beta	2|34(0.00025831721144808917)	-111|34(0.00802353714433813)
BCAL1727	cobL	precorrin-6Y C5,15-methyltransferase (decarboxylating)	-16|24(0.0002943308821813373)	-125|20(0.00176591289583615)
BCAL2114	-	uracil DNA glycosylase superfamily protein	50|87(0.001189297707868131)	-54|87(0.00981322891200345)
BCAM2149	-	subfamily M20A metallopeptidase	-77|-42(0.0016250456947893843)	-183|-41(0.015937828645244)
BCAL2953	-	putative prephenate dehydrogenase	-113|-95(0.0017929892288085503)	-162|-132(0.00870561756416333)
BCAM2255	-	putative OmpA/MotB family outer membrane protein	-28|-3(0.0019269718993241147)	-147|-2(0.0219560019204432)
BCAL0726	-	putative lipoprotein	-66|-27(0.0024658037818036105)	-181|-33(0.00161490631863807)
BCAL0052	-	putative oxidoreductase	-100|-66(0.040434986417607344)	-149|-66(0.0363075934949675)
BCAL0262	cutA	putative divalent-cation tolerance protein CutA	39|68(0.0436280487450863)	-73|69(0.0108949243382764)
BCAL0423a	rpmH	50S ribosomal protein L34	-189|-155(0.04574292596889473)	-199|-167(0.0133875861641464)
BCAL2812	-	putative Fur family transcriptional regulator	-116|-78(0.03767070647362858)	-139|-77(0.0305267907210116)
BCAM1977	-	putative amino acid permease	64|98(0.03917838891587566)	16|98(0.0105544432995813)
BCAS0487	-	short chain dehydrogenase	-147|-131(0.03366321867028721)	-199|-130(0.00556514423598234)
BCAL0023	-	putative branched-chain amino acid ABC transporter ATP-binding protein	-29|9(0.0025939891657396075)	54|80(0.0141415832489472)
BCAM2050	bcscK	type III secretion system protein	-20|-8(0.00026286817300169574)	-
BCAM2045	bcscU	type III secretion system protein	74|79(0.0011242492434725415)	-
BCAL1695	orbE	ornibactin biosynthesis ABC transport protein	-164|-133(0.007714914192003097)	-
BCAS0634	-	putative manganese transport protein, NRAMP family	42|73(0.0011309979428766326)	-
BCAS0104	fliD2	A-type flagellar hook-associated protein 2 (HAP2)	-112|-94(0.005907452085631371)	-
BCAM2140	-	transporter system transport protein	-16|24(0.0024963956402427323)	-
BCAM0731	-	MarR family regulatory protein	-111|-74(0.002782971315359095)	-

Locus ID	Gene name	Product description	TargetRNA	CopraRNA
BCAL0563	flgA	flagellar basal body P-ring biosynthesis protein FlgA	7|40(0.021236671041647948)	-
BCAL0140	flhB	flagellar biosynthesis protein FlhB	-128|-107(0.045362868936163925)	-
BCAL0527	fliS	flagellar protein FliS	-40|-32(0.03861495764732248)	-
BCAM1767	hipB	putative regulatory protein	-146|-121(0.01778043922416561)	-
BCAL0066	-	AraC family regulatory protein	43|73(0.0014530843642022173)	-
BCAL1735	-	LuxR superfamily regulatory protein	-2|36(0.009612961792474284)	-
BCAM1193	-	SpoVT/AbrB family regulatory protein	-82|-63(0.021076498959834433)	-
BCAL2693	-	LysR family regulatory protein	-2|6(0.013577537673285844)	-
BCAS0722	-	putative patatin-like phospholipase	75|86(0.0016286663248813449)	-
BCAM2186	-	putative macrolide-specific efflux system transport protein	-54|-26(0.034883373328169376)	-
BCAM2017	-	ABC transporter ATP-binding protein	-34|6(0.0022825364638940915)	-
BCAS0340	-	ABC transporter ATP-binding protein	-13|25(0.003088854593666035)	-
BCAS0289	-	putative multidrug resistance transporter protein	-108|-73(0.03215324723786872)	-
BCAM1259	sigJ	RNA polymerase sigma factor	2|25(0.03032476053362987)	-
BCAL3302	recG	ATP-dependent DNA helicase RecG	-70|-66(0.022975319864755095)	-
BCAM2528	-	putative ABC transporter permease	14|50(0.00394820620439984)	-
BCAM2035	-	putative gycosyltransferase	-25|-9(0.041440747540474776)	-
BCAM0296	phbB	acetoacetyl-CoA reductase	21|52(0.004799500972129445)	-
BCAL0129	cheA	chemotaxis two-component sensor kinase CheA	-26|5(0.041440747540474776)	-
BCAL0774	-	ornithine cyclodeaminase	-101|-95(0.012034625635446772)	-
BCAL1328	wecB	UDP-N-acetylglucosamine 2-epimerase	-20|2(0.02264966540702562)	-
BCAM2163	-	putative monooxygenase	-75|-56(0.0011668508522215681)	-
BCAM1798	-	putative oxidoreductase	-34|-7(0.001575914628343611)	-
BCAL1243	-	putative malonate decarboxylase gamma-subunit	-47|-40(0.00196957411299159)	-

Locus ID	Gene name	Product description	TargetRNA	CopraRNA
BCAM0450	copD	CopD	-63|-38(0.0021746124037099746)	-
BCAS0447	-	putative GNAT family acetyltransferase	-63|-29(0.003955961489588877)	-
BCAL0530	-	putative export system protein	-25|11(0.0022687365542353177)	-
BCAL0139	-	putative 3-demethylubiquinone-9 3-methyltransferase	-54|-16(0.002373740001517022)	-
BCAL2374	-	permease	30|63(0.002523286841940253)	-
BCAM0364	-	putative lipoprotein	44|82(0.002405139357983699)	-
BCAM1696	-	putative lipoprotein	64|83(0.0022094918096140503)	-
BCAM1714	-	putative amidohydrolase	-2|35(0.003088854593666035)	-
BCAS0273	-	urea amidolyase allophanate hydrolase subunit	-68|-30(0.003268653710593039)	-
BCAL1246	-	putative malonyl CoA-acyl carrier protein transacylase	-15|12(0.003088854593666035)	-
BCAL1729	cobK	cobalt-precorrin-6x reductase	-6|30(0.00394820620439984)	-
BCAM0940A	-	putative methyltransferase	10|45(0.00394820620439984)	-
BCAL1413	glnS	glutaminyl-tRNA synthetase	-36|-11(0.009034210730899161)	-
BCAL3278	glnE	bifunctional glutamine-synthetase adenylyltransferase/deadenyltransferase	-67|-35(0.014500053699643689)	-

Supplementary Table 6.2: Bacterial target predictions for RIT17b using TargetRNA3 and CopraRNA.

Locus ID	Gene name	Product description	TargetRNA	CopraRNA
BCAM0764	-	LacI family regulatory protein	44|74(0.00807853121937896)	-74|74(0.00178425226895715)
BCAM2350	-	ABC transporter ATP-binding protein	70|82(0.011691245881061518)	-3|82(0.00214342503152927)
BCAL2984	-	family C26 cysteine peptidase	49|72(0.012894045404617138)	-9|72(0.0118824360358138)
BCAM1330	-	putative polysaccharide export protein	41|79(0.013977119896880108)	33|79(0.011204781981872)
BCAL0696	cpdB	putative 2',3'-cyclic-nucleotide 2'-phosphodiesterase	45|72(0.014545233814753034)	-20|73(0.0242713265549406)
BCAL0351	tssM	type VI secretion system protein TssM	26|48(0.01459195611006836)	-18|48(0.00625909289361836)
BCAL2693	-	LysR family regulatory protein	-87|-57(0.014716208998147073)	-101|-59(0.021063256743653)

Locus ID	Gene name	Product description	TargetRNA	CopraRNA
BCAL0200	-	putative lipoprotein	-93|-86(0.01540164551023182)	-179|-126(0.0242366851738121)
BCAL0375	hemA	glutamyl-tRNA reductase	-113|-80(0.030414481645754887)	-105|-78(0.0190742997096313)
BCAL0399	trpE	anthranilate synthase component I	-65|-37(0.025664234842245226)	27|98(0.019819217739075)
BCAL0667	bioA	adenosylmethionine--8-amino-7-oxononanoate transaminase	-174|-138(0.031864121095630527)	-195|-137(0.00176356518686393)
BCAM1833	acnB	bifunctional aconitate hydratase 2/2-methylisocitrate dehydratase	-156|-126(0.023782132171217385)	-99|1(0.0174133660380797)
BCAM1973	-	putative ABC transporter substrate-binding protein	43|72(0.025050294583367383)	-15|73(0.0235847695124824)
BCAL2212	folD	bifunctional 5,10-methylene-tetrahydrofolate dehydrogenase/ 5,10-methylene-tetrahydrofolate cyclohydrolase	55|72(0.022694698674844416)	-17|75(0.008414022239754)
BCAM0065	-	putative transporter-LysE family	78|99(0.01862334535075194)	18|99(0.0230103685923122)
BCAL0903	glyS	glycyl-tRNA synthetase subunit beta	27|59(0.02778117982527306)	-28|61(0.0209403700514086)
BCAL1043	gudD	glucarate dehydratase	21|45(0.019158218601282084)	-13|34(0.019302168418649)
BCAL1949	gcl	glyoxylate carboligase	-74|-37(0.021350520183806343)	-83|-36(0.0014752793900481)
BCAM0131	hchA	chaperone protein HchA	-57|-26(0.023529749072972894)	-97|-25(0.0210161652674034)
BCAM0459	-	cysteine desulfurase	24|50(0.02408586156582193)	-194|-118(0.0238219695559059)
BCAM0630	-	putative dehydrogenase	-61|-49(0.021181787645875083)	-196|-48(0.0250827317191983)
BCAM1411	-	putative short-chain dehydrogenase	-25|8(0.03170982520130805)	-81|8(0.0185271289451198)
BCAL1695	orbE	ornibactin biosynthesis ABC transport protein	47|60(0.008144595050751269)	-
BCAS0104	fliD2	A-type flagellar hook-associated protein 2 (HAP2)	-146|-118(0.005341727537710561)	-
BCAL0526	fliE	flagellar hook-basal body complex protein FliE	66|98(0.010899543373089293)	-
BCAM2186	-	putative macrolide-specific efflux system transport protein	-43|-7(0.018117662862857764)	-
BCAL1081	mdtA	multidrug resistance protein MdtA	24|42(0.020528019173208012)	-
BCAL1927	-	aminotransferase AlaT	-53|-33(0.016941792025760627)	-
BCAL0140	flhB	flagellar biosynthesis protein FlhB	26|57(0.024023577912217098)	-
BCAL2812	-	putative Fur family transcriptional regulator	-95|-57(0.014159982343788124)	-
BCAL1182	-	TetR family regulatory protein	30|66(0.008870564421438187)	-

Locus ID	Gene name	Product description	TargetRNA	CopraRNA
BCAS0768	-	AraC family regulatory protein	-100|-68(0.007975954742285851)	-
BCAM0133	-	LuxR superfamily regulatory protein	5|25(0.01794827562783674)	-
BCAM0966	-	GntR family regulatory protein	-35|-12(0.014294622351142983)	-
BCAL0042	putA	trifunctional transcriptional regulator/proline dehydrogenase/pyrroline-5-carboxylate dehydrogenase	41|77(0.015555709387535366)	-
BCAL2360	ecfD	RNA polymerase factor sigma-70	-190|-159(0.013147023737576036)	-
BCAM0581	dfsA	diffusible factor synthase A	57|72(0.02911900362456432)	-
BCAL0079	rep	ATP-dependent DNA helicase Rep	-29|-13(0.014266536723144818)	-
BCAL0075	gcvT	glycine cleavage system aminomethyltransferase T	-14|16(0.02318218683532547)	-
BCAM0958	-	ArsR family regulatory protein	-10|18(0.009595402535561237)	-
BCAL0731	gshA	glutamate-cysteine ligase	21|46(0.016473595414054354)	-
BCAM1485	-	ornithine cyclodeaminase	-97|-61(0.0030775823676805203)	-
BCAL3473	-	putative outer membrane porin	-58|-31(0.005551115387359085)	-
BCAL3122	wbiF	glycosyltransferase	-125|-93(0.02794567842618989)	-
BCAL0216	paaA	phenylacetate-CoA oxygenase subunit PaaA	-124|-101(0.029280903884267073)	-
BCAL1327	-	putative glycosyltransferase	76|85(0.00766140684522465)	-
BCAL1328	wecB	UDP-N-acetylglucosamine 2-epimerase	-123|-100(0.0118048128057896)	-
BCAL1831	-	putative betaine aldehyde dehydrogenase	11|37(0.021664859509396228)	-
BCAL0650	-	2-oxoacid ferredoxin oxidoreductase	33|61(0.019758499661805318)	-
BCAL2224	glnA	glutamine synthetase	-93|-84(0.020112783363614772)	-
BCAL2359	ilvI	acetolactate synthase 3 catalytic subunit	55|74(0.015782548134063212)	-
BCAL2718	nadA	quinolinate synthetase	-64|-32(0.02685962756172422)	-
pBCA095	-	putative ligase	85|100(0.007714125746570932)	-
BCAL3373	leuS	leucyl-tRNA synthetase	-19|15(0.024034778939685753)	-
BCAL3429	-	ribonucleotide-diphosphate reductase subunit alpha	-106|-72(0.01622805839029795)	-

Locus ID	Gene name	Product description	TargetRNA	CopraRNA
BCAL3442	rplU	50S ribosomal protein L21	-17|13(0.026645616413461304)	-
BCAM0909	-	exodeoxyribonuclease VII small subunit	-101|-63(0.02502870765384979)	-
BCAM2468	-	putative aldehyde dehydrogenase family protein	-91|-58(0.01388733663890318)	-
BCAL2739	fusA	elongation factor G	1|19(0.012264069779797326)	-

Supplementary Table 6.3: Complete list of the predicted human targets of *B. cenocepacia* small RNAs nc5U55 and RIT17b. Human mRNA targets were computationally predicted for *Burkholderia cenocepacia* sRNAs identified in EVs. EV-associated small RNAs were aligned with the NCBI human reference sequences within the Human G+T database using the algorithm BLASTN 2.16.0. Functional role descriptions were taken from the NCBI Gene Database (https://www.ncbi.nlm.nih.gov/gene/). Expression of the predicted target genes in human cells was demonstrated by Sjöstedt *et al.* (2020).

sRNA	Alignment (Features)	GeneID	Function	Expression (Tissue profile; Tissue specificity/expression cluster; Single cell type specificity/expression cluster)
ncS06	Pre-mrna-processing factor 40 homolog a isoform 11 (NM_001365603.4); pre-mrna-processing factor 40 homolog a isoform 4 (NM_001365596.4)	55660	Enables RNA binding activity. Involved in several processes, including cytoskeleton organization; regulation of cell shape; and regulation of cytokinesis. Located in nuclear matrix and nuclear speck.	Ubiquitous nuclear expression. Low tissue specificity. Low cell type specificity.
ncRNA7	Pre-mrna-processing factor 40 homolog a isoform 11 (NM_001365603.4); pre-mrna-processing factor 40 homolog a isoform 4 (NM_001365596.4)	55660	Enables RNA binding activity. Involved in several processes, including cytoskeleton organization; regulation of cell shape; and regulation of cytokinesis. Located in nuclear matrix and nuclear speck.	Ubiquitous nuclear expression. Low tissue specificity. Low cell type specificity.

sRNA	Alignment (Features)	GeneID	Function	Expression (Tissue profile; Tissue specificity/expression cluster; Single cell type specificity/expression cluster)
	Ankyrin repeat domain-containing protein 7 (NM_019644.4)	56311	Predicted to act upstream of or within blastocyst hatching. Located in centrosome and nucleoplasm.	Localized to the Nucleoplasm. Tissue enriched (Testis - Spermatid development). Single cell type group enriched: early spermatids, spermatocytes (mainly spermatogenesis), late spermatids.
IG1_901672	Potassium voltage-gated channel subfamily D member 2 isoform x1 (XM_047420346.1)	3751	Voltage-gated potassium (Kv) channels represent the most complex class of voltage-gated ion channels from both functional and structural standpoints. Their diverse functions include regulating neurotransmitter release, heart rate, insulin secretion, neuronal excitability, epithelial electrolyte transport, smooth muscle contraction, and cell volume. This gene encodes a member of the shal-related subfamily, which forms A-type potassium ion channels and mediates a rapidly inactivating outward potassium current.	Cytoplasmic expression and synaptic positivity in brain. Tissue enriched: brain (cerebellum - nervous system development). Cell type group enriched: oligodendrocyte precursor cells, inhibitory neurons, excitatory neurons); Neurons - Neuronal signaling.

sRNA	Alignment (Features)	GeneID	Function	Expression (Tissue profile; Tissue specificity/expression cluster; Single cell type specificity/expression cluster)
IG1_2538832	POLG alternative reading frame (NM_001430120.1)	125316803	This gene shares its transcript with POLG but initiates translation from a CUG start codon in an alternative reading frame, producing a distinct 260-amino-acid protein.Unlike POLG isoforms, the POLGARF protein may interact with P32, a mitochondrial matrix protein involved in mitochondrial gene expression. POLGARF may bind and sequester P32 in the nucleolus, potentially affecting its function. Interestingly, some disease-causing mutations previously attributed to POLG may instead involve POLGARF.	Not available; not detected
	Rh family C glycoprotein (NM_001321041.2)	51458	Enables ammonium transmembrane transporter activity; ankyrin binding activity; and identical protein binding activity. Involved in ammonium transmembrane transport; cellular ion homeostasis; and transepithelial ammonium transport. It is an integral membrane protein, localized to both the apical and basolateral plasma membranes.	Selective basolateral membrane expression in renal tubules with membranous and cytoplasmic expression in squamous epithelia. Tissue enhanced: Esophagus (Squamous epithelium - Innate immune response), Vagina. Single cell type group enriched: suprabasal keratinocytes, squamous epithelial cells.
nc5U30	Major facilitator superfamily domain containing 14B: hippocampus abundant transcript 1(NM_032558.3) and isoform x2 (XM_047423972.1)	84641	Predicted to enable transmembrane transporter activity. Predicted to be involved in transmembrane transport. Predicted to be integral component of membrane.	Low tissue specificity: expression cluster - parathyroid gland (vesicular transport). Low cell type specificity: expression cluster - **monocytes (innate immune response)**.
nc5U36	Transmembrane protein 178b (NM_001195278.2) and isoform x2 (XM_017011636.2)	100507421	Predicted to be integral component of membrane. Predicted to be active in membrane.	Selective cytoplasmic expression; localized to the vesicles in addition localized to the nucleoli. Tissue enhanced: brain, heart muscle, parathyroid gland, tongue. Single cell type group enriched: excitatory neurons, inhibitory neurons, oligodendrocyte precursor cells, astrocytes.

sRNA	Alignment (Features)	GeneID	Function	Expression (Tissue profile; Tissue specificity/expression cluster; Single cell type specificity/expression cluster)
nc5U37	Ceramide synthase 3 isoform 2 (NM_001290342.2)	204219	This gene encodes a ceramide synthase involved in the production of ultra-long-chain ceramides (ULC-Cers), which are crucial for epidermal barrier function. It also plays a role in lipid remodeling during spermatogenesis. Mutations have been linked to male infertility and skin disorders such as ichthyosis. Multiple isoforms are produced through alternative splicing	Cytoplasmic expression in several tissues, mainly in testis and squamous epithelial cells. Tissue enhanced: esophagus, skin, vagina. Cell type enhanced: suprabasal keratinocytes, squamous epithelial cells, basal squamous epithelial cells, basal keratinocytes, spermatocytes, early spermatids, late spermatids.
ncS27	MTSS I-BAR domain containing 1: isoform x21 (XM_006716706.3) and isoform x15 (XM_006716703.3)	9788	This gene encodes a protein involved in actin monomer binding, protein-protein interactions, and receptor binding. It is predicted to regulate processes such as response to fluid shear stress, epithelial cell proliferation, and urogenital development, and may play roles in actin polymerization, adherens junction stability, and magnesium ion homeostasis. Localized to the actin cytoskeleton, it may contribute to cancer progression and metastasis through cytoskeletal interactions.	Cytoplasmic expression of variable levels in most tissues: localized to the plasma membrane, cytosol. Low tissue specificity. Cell type enhanced: monocytes, oligodendrocyte precursor cells, inhibitory neurons.

sRNA	Alignment (Features)	GeneID	Function	Expression (Tissue profile; Tissue specificity/expression cluster; Single cell type specificity/expression cluster)
nc5U52	Synaptophysin-like protein 1: isoform g (NM_001381915.1) and isoform d (NM_001381911.1)	6856	Predicted to be involved in chemical synaptic transmission. Located in extracellular exosome.	Ubiquitous cytoplasmic expression. Low tissue specificity: expression cluster - thyroid gland. Cell type enhanced: early spermatids, spermatocytes. Single cell type expression cluster: **B-cells - B-cell function**.
	mucin-2-like(XM_047432049.1)	124903407	Unknown.	Unknown
	Iodothyronine deiodinase 3: thyroxine 5-deiodinase (NM_001362.4)	1735	This intronless gene encodes a selenoprotein from the iodothyronine deiodinase family that inactivates thyroid hormones by removing iodine from their inner ring. It converts T4 to reverse T3 (rT3) and T3 to T2, thereby regulating thyroid hormone activity. Highly expressed in the pregnant uterus, placenta, and fetal tissues, it helps protect the developing fetus from excess thyroid hormones. It is essential for fetal development and thyroid hormone homeostasis, with gene knockouts linked to developmental and reproductive abnormalities. The protein contains a selenocysteine (Sec) residue, encoded by a UGA codon and directed by a specialized SECIS element in the 3′ UTR.	Localized to the Vesicles. Tissue enhanced: cervix, placenta. Cell type enriched: Syncytiotrophoblasts. Single cell type expression cluster: connective tissue cells - ECM organization.

sRNA	Alignment (Features)	GeneID	Function	Expression (Tissue profile; Tissue specificity/expression cluster; Single cell type specificity/expression cluster)
IG2_1885142	ISL LIM homeobox 2: insulin gene enhancer protein ISL-2 (NM_145805.3)	64843	Enables sequence-specific double-stranded DNA binding activity. Predicted to be involved in axonogenesis; neuron fate specification; and regulation of transcription by RNA polymerase II. Predicted to act upstream of or within negative regulation of neuron differentiation and neuron differentiation. Predicted to be part of chromatin. Predicted to be active in nucleus.	Localized to the Rods & Rings. Tissue enhanced: pituitary gland, prostate, vagina (epithelium - extracellular exosomes). Cell type enriched: cone photoreceptor cells.
nc5U55	Unk like zinc finger: transcript variant X14, misc_RNA (XR_007064901.1); transcript variant X12, mRNA (XM_047434490.1)	64718	This gene encodes a RING finger protein that may function in Rac signaling. It can bind to Brg/Brm-associated factor 60b and can promote its ubiquitination. Alternative splicing of this gene results in multiple transcript variants.	Cytoplasmic and membranous expression in several different tissue types; localized to the cytosol. Low tissue specificity. Cell type enhanced: Oocytes.
	Unk like zinc finger: transcript variant X14, misc_RNA (XR_007064901.1); transcript variant X12, mRNA (XM_047434490.1)	64718	This gene encodes a RING finger protein that may function in Rac signaling. It can bind to Brg/Brm-associated factor 60b and can promote its ubiquitination. Alternative splicing of this gene results in multiple transcript variants.	Cytoplasmic and membranous expression in several different tissue types; localized to the cytosol. Low tissue specificity. Cell type enhanced: Oocytes.
	BICRA like chromatin remodeling complex associated protein: transcript variant X7, misc_RNA (XR_007059228.1); transcript variant X6, mRNA (XM_047418547.1); variant X5, mRNA (XM_047418545.1); variant X4 (XM_047418544.1); variant X3 (XM_047418543.1); variant X2 (XM_047418542.1); variant 1 (NM_001318819.2).	23506	Predicted to be involved in positive regulation of transcription, DNA-templated. Part of SWI/SNF complex.	General nuclear expression with additional cytoplasmic expression in several tissues. Low tissue specificity. Cell type enhanced: oligodendrocytes, inhibitory neurons, excitatory neurons, microglial cells.
	Unk like zinc finger: isoform x1 (XM_011522610.2)	64718	This gene encodes a RING finger protein that may function in Rac signaling. It can bind to Brg/Brm-associated factor 60b and can promote its ubiquitination. Alternative splicing of this gene results in multiple transcript variants.	Cytoplasmic and membranous expression in several different tissue types; localized to the cytosol. Low tissue specificity. Cell type enhanced: Oocytes.

sRNA	Alignment (Features)	GeneID	Function	Expression (Tissue profile; Tissue specificity/expression cluster; Single cell type specificity/expression cluster)
nc5U55	DNA methyltransferase 3 alpha: DNA (cytosine-5)-methyltransferase 3A isoform c (NM_001320892.2)	1788	This gene encodes DNMT3A, a DNA methyltransferase involved primarily in de novo DNA methylation, a key epigenetic mechanism important for embryonic development, genomic imprinting, and X-chromosome inactivation. Its expression is developmentally regulated, and the protein localizes to both the cytoplasm and nucleus. DNMT3A plays a crucial role in **regulating immune responses**, such as Il13 gene expression, and in limiting T helper 2-mediated inflammation. Additionally, the protein has been linked to scaffolding functions in the dystrophin-associated protein complex (DPC), interacting with dystrophin (DMD) and syntrophins in muscle and epithelial tissues. It may also contribute to synaptic regulation, particularly in the maturation and function of inhibitory synapses, and possibly acts as a transcriptional repressor during neural differentiation.	Ubiquitous nuclear expression, localized to the nucleoplasm. Low tissue specificity. Single cell type group enriched: cardiomyocytes, rod photoreceptor cells.
	Dystrobrevin beta: isoform 28 (NM_001351394.2)	1838	This gene encodes dystrobrevin beta, a component of the dystrophin-associated protein complex (DPC). The DPC consists of dystrophin and several integral and peripheral membrane proteins, including dystroglycans, sarcoglycans, syntrophins and dystrobrevin alpha and beta. The DPC localizes to the sarcolemma and its disruption is associated with various forms of muscular dystrophy. Dystrobrevin beta is thought to interact with syntrophin and the DP71 short form of dystrophin.	Cytoplasmic and membranous expression in several tissues.
	BICRA like chromatin remodeling complex associated protein	23506	Predicted to be involved in positive regulation of transcription, DNA-templated. Part of SWI/SNF complex.	General nuclear expression with additional cytoplasmic expression in several tissues. Low tissue specificity. Cell type enhanced: oligodendrocytes, inhibitory neurons, excitatory neurons, microglial cells). Low immune cell specificity; **immune cells expression cluster: neutrophils.**

sRNA	Alignment (Features)	GeneID	Function	Expression (Tissue profile; Tissue specificity/expression cluster; Single cell type specificity/expression cluster)
nc5U65	Coiled-coil domain containing 71 like (NM_175884.6)	168455	Predicted to be involved in cellular lipid metabolic process and positive regulation of fat cell differentiation.	Cytoplasmic expression in most tissues; localized to the golgi apparatus, actin filaments and the cytosol. Low tissue specificity and smooth muscle tissue as the expression cluster. Cell type enhanced: **granulocytes**, endometrial stromal cells, mesothelial cells, serous glandular cells); cell type expression cluster: **monocytes (innate immune response)**.
	Phosphatidylinositol-4,5-bisphosphate 3-kinase catalytic subunit gamma (NM_001282426.2)	5294	This gene encodes a phosphoinositide 3-kinase (PI3K) that phosphorylates PIP2 to produce PIP3, a key lipid mediator that activates signaling pathways involved in cell growth, survival, proliferation, migration, and morphology. It links G-protein coupled receptor signaling to PIP3 production and plays **major roles in immune and inflammatory responses by regulating leukocyte, dendritic cell, T cell, B cell, and neutrophil functions**. It also contributes to platelet aggregation and thrombosis, and modulates cardiac contractility through both lipid kinase activity and protein–protein interactions. Additionally, it is involved in angiogenesis, cardiac hypertrophy under stress, and may function as a scaffold protein with serine/threonine kinase activity.	Cytoplasmic and membranous expression in several different tissue types, including lymphoid tissues; localized to the plasma membrane and cytosol. Tissue group enriched: bone marrow, lymphoid tissue; Brain expression cluster: **macrophages and microglia**. Cell type enhanced: d**endritic cells, monocytes**, plasma cells, **macrophages, NK-cells, B-cells.**
Bc_KC_sr7	Hippocampus abundant transcript 1 protein (NM_032558.3)and isoform x2 (XM_047423972.1)	84641	Predicted to enable transmembrane transporter activity. Predicted to be involved in transmembrane transport. Predicted to be integral component of membrane.	Low tissue specificity: expression cluster - parathyroid gland (vesicular transport). Low cell type specificity: expression cluster - **monocytes (innate immune response)**.

sRNA	Alignment (Features)	GeneID	Function	Expression (Tissue profile; Tissue specificity/expression cluster; Single cell type specificity/expression cluster)
RIT17b	Phospholipase A2 group IVA	5321	This gene encodes a cytosolic phospholipase A2 enzyme that hydrolyzes membrane phospholipids to release arachidonic acid, leading to the production of eicosanoids such as prostaglandins and leukotrienes, which regulate inflammation, vascular tone, and other cellular processes. It also generates lysophospholipids, precursors of platelet-activating factor. The enzyme is activated by calcium and phosphorylation, triggering its relocation to perinuclear membranes. Multiple transcript variants exist due to alternative splicing.	General cytoplasmic expression, most abundant in parathyroid gland and seminal vesicle tissues. Cell type enhanced: microglial cells, basal prostatic cells, secretory cells; Cell type enriched: fibroblasts (adrenal gland, kidney, pituitary gland, thyroid gland) and mitotic cells (skin). Immune cell specificity: group enriched - **intermediate monocyte, eosinophil, myeloid DC, classical monocyte, non-classical monocyte, plasmacytoid DC.**
	BMP/retinoic acid-inducible neural-specific protein 3 isoform 1 precursor (NM_199051.3)	339479	This gene shows altered expression in various diseases: it is overexpressed in pituitary tumors and underexpressed in tongue squamous cell carcinoma, ulcerative colitis, and peri-implantitis. Increased expression due to polymorphisms is linked to vascular inflammation and myocardial infarction. Hypermethylation may serve as a biomarker for gastric cancer. Two transcript variants encode different isoforms.	Cytoplasmic expression in several tissues. Tissue enhanced: brain and intestine. Cell type enhanced: oligodendrocyte precursor cells, excitatory neurons, astrocytes, inhibitory neurons.
	Pogo transposable element derived with ZNF domain: isoform 1 (NM_015100.4)	23126	Involved in mitotic cell cycle progression, including kinetochore assembly, chromatid cohesion, and chromosome segregation. Regulates AURKB activation and promotes DNA double-strand break repair via homologous recombination. Functions in DNA binding, cell division, and genome stability.	General nuclear expression; localized to the nucleoplasm and basal body, cytosol. Low tissue specificity: neuronal. Cell type enhanced: oligodendrocytes.
	Tudor domain-containing protein 15 (NM_001306137.2)	100129278	TDRD15 is an uncharacterized Tudor domain-containing protein that contains seven Tudor domains. The Tudor domain binds to proteins with dimethylated arginine or lysine residues, and may also bind methylated histone tails to facilitate protein-protein interactions. Diseases associated with TDRD15 include Phosphoglycerate Kinase 1 Deficiency.	Tissue enriched: Testis. Cell type enhanced: spermatocytes, late spermatids, spermatogonia, early spermatids.
	Kelch-like protein 29 (NM_052920.2)	114818	Predicted to enable ubiquitin-like ligase-substrate adaptor activity. Predicted to be involved in proteasome-mediated ubiquitin-dependent protein catabolic process. Predicted to be part of Cul3-RING ubiquitin ligase complex. Predicted to be active in cytoplasm.	Cytoplasmic expression in most tissues. Low tissue specificity. Cell type group enriched: excitatory neurons, inhibitory neurons.

sRNA	Alignment (Features)	GeneID	Function	Expression (Tissue profile; Tissue specificity/expression cluster; Single cell type specificity/expression cluster)
RIT17b	NEDD4 binding protein 2 isoform x3 (XM_047415953.1)	55728	Encodes a protein with a polynucleotide kinase domain and Smr domain, involved in ATP binding and hydrolysis. Interacts with BCL-3 and Nedd4, may act as a 5'-polynucleotide kinase and ubiquitylation substrate. Potential role in transcription-coupled DNA repair or recombination. Multiple isoforms exist due to alternative splicing.	General cytoplasmic expression. Tissue enhanced: lymphoid tissue; expression cluster: **thymus (adaptive immune response)**. Cell type enhanced: dendritic cells (antigen presentation).
	Peptidylprolyl isomerase A: peptidyl-prolyl cis-trans isomerase a isoform x1 (XM_047420536.1)	5478	Encodes a peptidyl-prolyl isomerase involved in protein folding and cyclosporin A-mediated immunosuppression. Interacts with HIV proteins and is essential for virion formation. **Promotes leukocyte chemotaxis and endothelial cell activation via MAPK and NF-κB pathways.** Modulates apoptosis under oxidative stress and regulates MAP3K5/ASK1 activity.	Cytoplasmic expression in most tissues. Low tissue specificity. Low cell type specificity. Secreted to blood.
	H2A.Z variant histone 2: isoform 2 (NM_138635.3)	94239	Encodes a variant histone H2A that replaces conventional H2A in specific nucleosomes, contributing to chromatin structure and function. Plays roles in transcription regulation, DNA repair and replication, and chromosome stability. May also be involved in heterochromatin formation and chromosome segregation during cell division.	Ubiquitous nuclear expression. Low tissue specificity. Cell type enhanced: early spermatids; Immune cell expression cluster: eosinophils (protein ubiquitination).
	TBC1 domain family member 13 isoform x2 (XM_005252060.3)	54662	Predicted to enable GTPase activator activity. Predicted to be involved in activation of GTPase activity and intracellular protein transport. Predicted to be located in cytosol and membrane.	Cytoplasmic and nuclear expression in all cells. Low tissue specificity. Cell type enhanced: oligodendrocytes; expression cluster: **langerhans cells (innate immune response)**. Immune cells specificity: I**mmune cell enhanced (basophil)**.
	Endonuclease g mitochondrial precursor (NM_004435.2)	2021	The protein encoded by this gene is a nuclear encoded endonuclease that is localized in the mitochondrion. The encoded protein is widely distributed among animals and cleaves DNA at GC tracts. This protein is capable of generating the RNA primers required by DNA polymerase gamma to initiate replication of mitochondrial DNA.	General cytoplasmic expression. Tissue enhanced: skeletal muscle. Cell type enhanced: late spermatids, ciliated cells.

sRNA	Alignment (Features)	GeneID	Function	Expression (Tissue profile; Tissue specificity/expression cluster; Single cell type specificity/expression cluster)
RIT17b	Zinc finger protein 709 (NM_152601.4)	163051	Predicted to enable DNA-binding transcription factor activity, RNA polymerase II-specific and RNA polymerase II transcription regulatory region sequence-specific DNA binding activity. Predicted to be involved in regulation of transcription by RNA polymerase II. Predicted to be active in nucleus.	Localized to the nucleoplasm. Tissue enriched: testis; tissue expression cluster: spermatids (flagellum assembly). Cell type enhanced: early spermatids, late spermatids, oligodendrocyte precursor cells, inhibitory neurons, excitatory neurons.
	Zinc finger protein 564 (NM_144976.4)	163050	Predicted to enable DNA-binding transcription factor activity and RNA polymerase II cis-regulatory region sequence-specific DNA binding activity. Predicted to be involved in regulation of transcription by RNA polymerase II. Predicted to be located in nucleus.	Localized to the Golgi apparatus. Low tissue specificity: kidney and intestine. Cell type enhanced: microglial cells, oligodendrocyte precursor cells.
	Aristaless related homeobox, protein arx (NM_139058.3)	170302	This gene encodes a homeobox-containing transcription factor involved in brain development. It plays a key role in neuronal proliferation, migration, and differentiation during embryonic forebrain development. It is primarily expressed in the nervous system. Mutations, including polyalanine tract expansions, are linked to X-linked intellectual disability and epilepsy.	Tissue group enriched: ovary, skeletal muscle. Cell type enhanced: leydig cells, ovarian stromal cells, peritubular cells, inhibitory neurons, enteroendocrine cells.
	MAGE family member B18: melanoma-associated antigen b18 (NM_173699.4)	286514	Tumor antigen. Predicted to be involved in negative regulation of transcription by RNA polymerase II. May enhance ubiquitin ligase activity of RING-type zinc finger-containing E3 ubiquitin-protein ligases. Proposed to act through recruitment and/or stabilization of the Ubl-conjugating enzyme (E2) at the E3:substrate complex.	Nuclear expression in seminiferous ducts. Cell type enriched: spermatocytes. Cell line expression cluster: Myeloma - Immunoglobulins.

Supplementary Table 6.4: IntaRNA results for all predicted sRNA-mRNA interactions. Due to limitations of the program, target mRNA sequences had to be divided into different parts. Particularly strong candidates regarding total interaction energy results have been highlighted. The weakest candidates were excluded based on the same criteria (total interaction energy > -9).

Target	Target (start)	Target (end)	Target seed region start	Target seed region end	Accessibility energy (sRNA)	sRNA	sRNA (start)	sRNA (end)	sRNA seed region start	sRNA seed region end	Accessibility energy (target mRNA)	Total interaction energy	Hybridization energy	Total (nt)
RPF40A_isoform11_part1	188	217	211	217	6.36	ncS06	48	80	48	54	4.58	-9.41	-20.35	1986
PRPF40A_isoform11_part1	320	332	320	326	3.8	ncS06	223	233	227	233	2.75	-9.11	-15.66	1986
PRPF40A_isoform11_part2	236	254	248	254	6.47	ncS06	62	79	62	68	3.79	-10.66	-20.92	1041
PRPF40A_isoform4_part1	596	605	596	602	1.89	ncS06	144	153	147	153	3.69	-9.07	-14.65	1971

Target	Target (start)	Target (end)	Target seed region start	Target seed region end	Accessibility energy (sRNA)	sRNA	sRNA (start)	sRNA (end)	sRNA seed region start	sRNA seed region end	Accessibility energy (target mRNA)	Total interaction energy	Hybridization energy	Total (nt)
PRPF40A_isoform4_part2	378	396	390	396	6.47	ncS06	62	79	62	68	3.79	-10.66	-20.92	1183
UNKL_isoform X12	**1386**	**1534**	**1497**	**1503**	**50.89**	**nc5U55**	**57**	**204**	**85**	**91**	**54.88**	**-36.56**	**-142.33**	**1896**
UNKL_isoform X12	1580	1608	1593	1599	18.95	nc5U55	224	253	232	238	13.14	-12.92	-45.01	1896
BICRAL_isoform X6_part1	**94**	**218**	**148**	**154**	**64.2**	**nc5U55**	**105**	**254**	**194**	**200**	**60.29**	**-27.71**	**-152.2**	**1875**
BICRAL_isoform X6_part2	1525	1538	1525	1531	5.65	nc5U55	127	140	134	140	3.58	-12.8	-22.03	1909
BICRAL_isoform X6_part2	1441	1454	1441	1447	2.71	nc5U55	247	258	252	258	2.44	-9.65	-14.8	1909
BICRAL_isoform X6_part2	1721	1727	1721	1727	0.53	nc5U55	38	44	38	44	4.56	-9.1	-14.19	1909
BICRAL_isoform X5_part1	**219**	**343**	**273**	**279**	**64.43**	**nc5U55**	**105**	**254**	**194**	**200**	**60.29**	**-27.48**	**-152.2**	**1950**
BICRAL_isoform X5_part2	1575	1588	1575	1581	5.65	nc5U55	127	140	134	140	3.58	-12.8	-22.03	1959
BICRAL_isoform X5_part2	1491	1504	1491	1497	2.71	nc5U55	247	258	252	258	2.44	-9.65	-14.8	1959
BICRAL_isoform X4_part1	**188**	**312**	**242**	**248**	**64.43**	**nc5U55**	**105**	**254**	**194**	**200**	**60.29**	**-27.48**	**-152.2**	**1950**
BICRAL_isoform X4_part2	1544	1557	1544	1550	5.65	nc5U55	127	140	134	140	3.58	-12.8	-22.03	1928
BICRAL_isoform X3_part1	**264**	**388**	**318**	**324**	**64.43**	**nc5U55**	**105**	**254**	**194**	**200**	**60.29**	**-27.48**	**-152.2**	**1956**

Target	Target (start)	Target (end)	Target seed region start	Target seed region end	Accessibility energy (sRNA)	sRNA	sRNA (start)	sRNA (end)	sRNA seed region start	sRNA seed region end	Accessibility energy (target mRNA)	Total interaction energy	Hybridization energy	Total (nt)
BICRAL_isoformX3_part2	**1850**	**1974**	**1904**	**1910**	**64.4**	**nc5U55**	**105**	**254**	**194**	**200**	**60.29**	**-27.51**	**-152.2**	**1998**
BICRAL_isoformX2_part1	**264**	**388**	**318**	**324**	**64.43**	**nc5U55**	**105**	**254**	**194**	**200**	**60.29**	**-27.48**	**-152.2**	**1956**
BICRAL_isoformX2_part2	1614	1627	1614	1620	5.65	nc5U55	127	140	134	140	3.58	-12.8	-22.03	1998
BICRAL_isoformX2_part2	1530	1543	1530	1536	2.71	nc5U55	247	258	252	258	2.44	-9.65	-14.8	1998
BICRAL_isoformX2_part2	1810	1816	1810	1816	0.53	nc5U55	38	44	38	44	4.56	-9.1	-14.19	1998
BICRAL_isoform1_part2	1308	1321	1308	1314	5.65	nc5U55	127	140	134	140	3.58	-12.8	-22.03	1692
BICRAL_isoform1_part2	1504	1510	1504	1510	0.53	nc5U55	38	44	38	44	4.56	-9.1	-14.19	1692
UNKL_isoformX1_part1	27	49	42	48	11.16	nc5U55	231	259	232	238	10.54	-19.3	-41	1347
UNKL_isoformX1_part1	382	400	391	397	7.04	nc5U55	120	138	123	129	6.84	-16.44	-30.32	1347
UNKL_isoformX1_part1	518	527	521	527	5.92	nc5U55	201	210	201	207	2.32	-14.69	-22.93	1347
UNKL_isoformX1_part1	863	880	866	872	11.29	nc5U55	56	72	64	70	3.48	-14.64	-29.41	1347
UNKL_isoformX1_part1	1020	1039	1021	1027	6.71	nc5U55	54	71	64	70	4.73	-10.73	-22.17	1347
UNKL_isoformX1_part2	**469**	**617**	**580**	**586**	**50.89**	**nc5U55**	**57**	**204**	**85**	**91**	**54.88**	**-36.56**	**-142.33**	**1129**
UNKL_isoformX1_part2	**756**	**776**	**769**	**775**	**10.25**	**nc5U55**	**52**	**72**	**53**	**59**	**5.12**	**-21.57**	**-36.94**	**1129**
UNKL_isoformX1_part2	813	841	826	832	18.96	nc5U55	224	253	232	238	13.14	-12.93	-45.03	1129
DNMT3A_isoform5	**247**	**393**	**386**	**392**	**47.69**	**nc5U55**	**59**	**199**	**60**	**66**	**55.14**	**-23.05**	**-125.88**	**903**
DNMT3A_isoform5	621	632	624	630	4.46	nc5U55	183	194	185	191	6.94	-12.4	-23.8	903
DTNB_isoform28_part1	192	263	257	263	13.27	nc5U55	112	173	112	118	19.19	-16.05	-48.51	825

Target	Target (start)	Target (end)	Target seed region start	Target seed region end	Accessibility energy (sRNA)	sRNA	sRNA (start)	sRNA (end)	sRNA seed region start	sRNA seed region end	Accessibility energy (target mRNA)	Total interaction energy	Hybridization energy	Total (nt)
DTNB_isoform28_part1	29	78	29	35	33.38	nc5U55	199	249	243	249	23.74	-13.96	-71.08	825
DTNB_isoform28_part1	559	568	559	565	4.31	nc5U55	182	191	185	191	6.71	-12.17	-23.19	825
DTNB_isoform28_part2	814	884	835	841	27.1	nc5U55	127	193	167	173	26.41	-13.73	-67.24	1288
DTNB_isoform28_part2	1140	1158	1145	1151	13.31	nc5U55	194	209	198	204	6.15	-9.94	-29.4	1288
CCDC71L	1046	1067	1047	1053	7.24	nc5U65	24	43	36	42	4.72	-12.45	-24.41	1110
cytosolic_phospholipase_a2_part1	200	225	211	217	4.76	RIT17b	134	159	141	147	6.54	-13.13	-24.43	1491
cytosolic_phospholipase_a2_part2	574	586	580	586	0.66	RIT17b	195	208	195	201	3.25	-9.73	-13.64	1010
BRINP3_isoform1_part1	1354	1391	1355	1361	4.53	RIT17b	113	144	137	143	12.27	-10.53	-27.33	1413
POGZ_isoform1_part1	960	1023	1017	1023	14.76	RIT17b	94	151	94	100	16.28	-18.43	-49.47	1266
POGZ_isoform1_part2	168	238	231	237	16.14	RIT17b	84	155	85	91	22.84	-17.09	-56.07	1572
POGZ_isoform1_part2	360	440	434	440	19.09	RIT17b	80	157	80	86	23.79	-15.85	-58.73	1572
POGZ_isoform1_part2	1462	1503	1468	1474	11.39	RIT17b	98	143	129	135	15.51	-12.31	-39.21	1572
POGZ_isoform1_part2	1443	1457	1450	1456	1.93	RIT17b	127	141	128	134	5.21	-10.55	-17.69	1572
POGZ_isoform1_part3	114	151	145	151	5.19	RIT17b	112	142	112	118	12.18	-14.01	-31.38	1797
POGZ_isoform1_part3	328	352	328	334	5.13	RIT17b	131	152	146	152	5.16	-9.97	-20.26	1797
TDRD15_part1	1053	1064	1057	1063	2.57	RIT17b	129	140	130	136	2.56	-13.73	-18.86	1926
TDRD15_part2	1190	1213	1202	1208	3.04	RIT17b	79	101	84	90	9.01	-10.43	-22.48	1989
TDRD15_part3	78	113	93	99	2.93	RIT17b	128	151	137	143	5.64	-12.2	-20.77	1317
TDRD15_part3	127	147	141	147	2.73	RIT17b	111	132	111	117	10.19	-10.11	-23.03	1317
KLHL29_part1	1284	1299	1293	1299	6.15	RIT17b	10	25	10	16	5.06	-15.46	-26.67	1827
KLHL29_part1	1557	1575	1569	1575	6.18	RIT17b	113	132	113	119	9.62	-14.51	-30.31	1827
KLHL29_part1	1435	1453	1444	1450	3.78	RIT17b	128	143	131	137	2.74	-11.14	-17.66	1827
KLHL29_part2	907	932	926	932	4.78	RIT17b	111	133	111	117	10.42	-15.45	-30.65	1203
KLHL29_part2	1084	1128	1121	1127	6.01	RIT17b	97	148	98	104	15.83	-13.2	-35.04	1203
N4BP2_isoform X3_part1	1106	1117	1106	1112	3.18	RIT17b	122	132	126	132	6.2	-10.71	-20.09	1839
N4BP2_isoform X3_part2	867	900	884	890	4.87	RIT17b	116	149	126	132	14.1	-19.09	-38.06	1986
N4BP2_isoform X3_part3	939	959	952	958	6.12	RIT17b	111	132	112	118	10.19	-12.82	-29.13	1590
peptidylprolyl_cistrans_isomerase_a	575	613	590	596	5.92	RIT17b	44	78	59	65	12.71	-10.06	-28.69	720
H2AZ2_isoform 2	99	113	107	113	8.54	RIT17b	8	22	8	14	5.57	-14.04	-28.15	701
H2AZ2_isoform 2	574	654	643	649	20.7	RIT17b	89	159	94	100	23.09	-11.9	-55.69	701

Target	Target (start)	Target (end)	Target seed region start	Target seed region end	Accessibility energy (sRNA)	sRNA	sRNA (start)	sRNA (end)	sRNA seed region start	sRNA seed region end	Accessibility energy (target mRNA)	Total interaction energy	Hybridization energy	Total (nt)
TBC1D13_isoformX2	1155	1228	1222	1228	23.56	RIT17b	87	155	87	93	22.01	-11.81	-57.38	1377
TBC1D13_isoformX2	960	967	961	967	2.17	RIT17b	57	64	57	63	1.98	-9.41	-13.56	1377
ENDOG	630	709	687	693	25.41	RIT17b	64	158	74	80	29.41	-12.33	-67.15	1145
ENDOG	772	781	775	781	3.88	RIT17b	116	125	116	122	5.52	-9.74	-19.14	1145
ZNF709_part1	114	148	128	134	9.6	RIT17b	130	158	141	147	8.57	-12.88	-31.05	762
ZNF564	178	209	178	184	9.2	RIT17b	33	61	55	61	8.81	-12.25	-30.26	2000
ZNF564	1812	1822	1816	1822	3.54	RIT17b	14	24	14	20	3.99	-9.74	-17.27	2000
ARX_part1	81	126	119	125	2.95	RIT17b	69	124	70	76	22.82	-12.85	-38.62	1119
ARX_part1	526	541	535	541	10.01	RIT17b	8	22	8	14	5.57	-12.19	-27.77	1119
ARX_part2	291	320	314	320	4.93	RIT17b	84	118	84	90	15.37	-13.15	-33.45	972
ARX_part2	777	828	777	783	16.21	RIT17b	69	118	112	118	21.55	-10.3	-48.06	972
MAGEB18	1117	1154	1117	1123	10.35	RIT17b	115	155	149	155	16.32	-14.66	-41.33	1420

Supplementary Table 6.5: Orthologous genes of the predicted human targets of *B. cenocepacia* small RNAs nc5U55 and RIT17b identified via Ortholist2.

sRNA	WormBase ID	Common Name	Locus ID	Ensembl ID	HGNC Symbol	No. of Databases	Matched Databases	Ahringer Location
nc5U55	WBGene00016407	-	C34D10.2	ENSG00000059145	UNKL	4	Ensembl Compara 87-89|InParanoid|OrthoInspector|OrthoMCL	X-4I13
	WBGene00001115	dyb-1	F47G6.1	ENSG00000138101	DTNB	6	Ensembl Compara 87-89|Homologene|InParanoid|OMA|OrthoInspector|OrthoMCL	I-1A02
RIT17b	WBGene00000433	ceh-8	ZK265.4	ENSG00000004848	ARX	1	Ensembl Compara 87-89	I-4E11
	WBGene00000440	ceh-17	D1007.1	ENSG00000004848	ARX	1	Ensembl Compara 87-89	I-2A09
	WBGene00044330	alr-1	R08B4.2	ENSG00000004848	ARX	3	Ensembl Compara 87-89|OrthoInspector|OrthoMCL	X-8H23
	WBGene00006778	unc-42	F58E6.10	ENSG00000004848	ARX	1	InParanoid	V-6H06
	WBGene00006744	unc-4	F26C11.2	ENSG00000004848	ARX	1	OrthoMCL	II-7E11
	WBGene00000787	cps-6	C41D11.8	ENSG00000167136	ENDOG	6	Ensembl Compara 87-89|Homologene|InParanoid|OMA|OrthoInspector|OrthoMCL	None
	WBGene00009508	row-1	F37D6.2	ENSG00000143442	POGZ	1	Ensembl Compara 87-89	I-9B22
	WBGene00009726	tbc-13	F45E6.3	ENSG00000107021	TBC1D13	6	Ensembl Compara 87-89|Homologene|InParanoid|OMA|OrthoInspector|OrthoMCL	X-5P12
	WBGene00021201	-	Y17G9B.4	ENSG00000196262	PPIA	1	Ensembl Compara 87-89	IV-2O20

sRNA	WormBase ID	Common Name	Locus ID	Ensembl ID	HGNC Symbol	No. of Databases	Matched Databases	Ahringer Location
RIT17b	WBGene00044705	-	T22F3.12	ENSG00000196262	PPIA	1	Ensembl Compara 87-89	None
	WBGene00000877	cyn-1	Y49A3A.5	ENSG00000196262	PPIA	4	Homologene|InParanoid|OrthoInspector|OrthoMCL	V-16H03
	WBGene00000878	cyn-2	ZK520.5	ENSG00000196262	PPIA	3	InParanoid|OrthoInspector|OrthoMCL	III-6F18
	WBGene00000879	cyn-3	Y75B12B.5	ENSG00000196262	PPIA	3	InParanoid|OrthoInspector|OrthoMCL	V-9P02
	WBGene00000883	cyn-7	Y75B12B.2	ENSG00000196262	PPIA	3	InParanoid|OrthoInspector|OrthoMCL	None
	WBGene00021931	-	Y55F3AM.14	ENSG00000242852	ZNF709	2	InParanoid|OrthoMCL	IV-8N11|IV-9G04
	WBGene00001223	ehn-3	ZK616.10	ENSG00000242852	ZNF709	1	OrthoMCL	None
	WBGene00021931	-	Y55F3AM.14	ENSG00000249709	ZNF564	1	InParanoid	IV-8N11|IV-9G04